Tailored Surface Texture Characterisation of Metal Additive Components for Aerospace Applications

---

Angepasste Oberflächencharakterisierung additiv gefertigter Metallkomponenten für die Luft- und Raumfahrt

Cumulative Dissertation

Approved by the Faculty of Production Engineering of the University of Bremen for the Doctoral Degree in Engineering (Dr.-Ing.)

Genehmigt vom Fachbereich Produktionstechnik der Universität Bremen zur Erlangung des Grades einer Doktorin der Ingenieurwissenschaften (Dr.-Ing.)

Submitted by	Theresa Buchenau, M.Sc.
Reviewers	Prof. Dr. Bernd Mayer (University of Bremen) Prof. Dr. Richard Bibb (Nottingham Trent University)
Topical Advisors	Dr. Marc Amkreutz Dr. Hauke Brüning

Date of the public defence / Tag der mündlichen Prüfung: 18.07.2024

"Nothing in life is to be feared, it is only to be understood.
Now is the time to understand more, so that we may fear less."

Marie Curie

Declaration of Authorship

In accordance with § 65 (5) BremHG, I, Theresa Buchenau, declare under oath, that the work presented in this doctoral thesis was carried out without any unauthorised third party assistance. No other sources or aids than the ones specified have been used. The sources of works and text passages which have been included word by word or by content are indicated.

The submitted electronic version is identical with the submitted paper version and may be checked with qualified plagiarism detection software.

Bremen, March 2024

Theresa Buchenau

Abstract

In the past decades, additive manufacturing (AM) has been evolving from a rapid prototyping technology towards a mature manufacturing process with significant advantages for lightweight design and the potential of fulfilling requirements for highly demanding and specialised applications. Surface quality is often of functional importance and hence critical for the qualification of metal AM parts, particularly for load-bearing aerospace applications.

Surface quality resulting from a laser powder bed fusion (LPBF) AM process is typically characterised by agglomerations of attached powder particles, spatter, weld or layer tracks. The specific features depend on the used material, powder properties, build direction and further influencing factors.

This work contributes to a more comprehensive understanding and an improved, more holistic description of surface quality from LPBF, its formation, characterisation, and role in part functionality. This will be achieved by taking novel approaches to tailored surface texture characterisation of metal AM parts from LPBF, employing state-of-the-art optical measurement techniques and areal surface texture characterisation.

The results of this thesis are presented in three parts: “Measurement and Data Post-processing”, “Surface Texture and Mechanical Properties” and “Areal Surface Features”.

Part one, “Measurement and Data Post-processing”, discusses the application of optical measurements and related method-specific challenges in regard to as-built and post-processed LPBF surfaces. The current practice for surface texture characterisation in industry is based on stylus contact measurements, resulting 2D profiles and corresponding parameters. However, the characterisation based on individually measured profile lines is hardly representative of the complex surface structure generated in LPBF processes. By means of a systematic, user-centred and application-based comparison of confocal microscopy, fringe projection and stylus profilometry, it is demonstrated that areal measurements do have considerable advantages regarding representative surface coverage, reproducibility and inhibition of surface damage (i.e. contact vs. non-contact measurements). In conclusion, the transition from 2D to 3D parameters for surface texture characterisation and, correspondingly, from contact stylus to non-contact optical methods is proposed. This is an important first step towards enabling a holistic description of AM surfaces by providing adequate and comprehensive data.

Part two, “Surface Texture and Mechanical Properties”, suggests a description of AM surfaces related to part functionality. Specifically, the use of surface texture parameters from the material ratio curve in the context of fatigue performance is introduced, as opposed to the typically used 2D profile extreme value, the maximum height difference Rt, and the arithmetic mean of the roughness profile Ra. These parameters fail to capture the specific nature of LPBF surfaces which is often dominated by powder particle agglomerations and layer or weld tracks. Additionally, they are sensitive to outliers and hence largely influenced by the measured location and measurement artefacts. Even their areal equivalents Sz and Sa are affected by these disadvantages. The material ratio curve is less effected by local irregularities, as it is derived from the entire surface height distribution. The reduced valley depth Svk is one of the parameters that are derived from that curve. Rather than an individual extreme value, it represents the size of the valley population within the measured surface region. As fatigue failure for as-built LPBF parts often occurs from multiple crack initiation locations on the surface, Svk relates particularly well to this observed failure mode. The use of Svk in conjunction with fatigue of LPBF parts is an outstanding example of an adapted and functionality-based approach to surface texture characterisation. Furthermore, it is demonstrated that the optimisation of processing parameters can lead to surface and mechanical properties competitive with surface post-processed and conventionally manufactured properties. This finding shows the potential to eliminate the

surface post-processing step from the LPBF value chain, reducing overall process duration and cost.

Part three, “Areal Surface Features”, introduces the development of process-related characterisation of surface texture and will take the concept of a functionality-based description one step further. The measurement of areal surface data enables the extraction and quantification of process-specific surface features, such as the aforementioned particle attachments or weld tracks. The presented work on surface feature characterisation focusses on the determination of appropriate pruning thresholds. The ISO 25178 standard on areal surface texture characterisation proposes to define the threshold in terms of the extreme value Sz. It is demonstrated that this approach is unfit to obtain meaningful feature segmentations on as-built LPBF surfaces. The suggested solution is to base pruning thresholds on the particle size distribution of the used metal powder. These defined thresholds are then applied to predefined surface feature parameters from ISO 25178 and for the detection of the LPBF-specific particle attachment features. While height-based ISO 25178 parameters are based on (extreme values of) height variations and deviations from the mean profile line/area, feature characterisation provides insights on various physical properties of topography elements, such as shapes, quantity, and size distribution. Height pruning strongly affects the numerical results on those properties. This novel approach of connecting the definition of pruning thresholds to the knowledge on materials and processing variables is introduced for the first time. It will pave the way for future advancements of tailored surface texture characterisation concepts. Feature-based characterisation has great potential for defining functionality-based requirements on surface texture and to obtain the most accurate description achievable with data from modern measurement instruments. It will continuously evolve with improved metrology systems and significantly advance the comprehension of process-structure-property correlations of AM components. As a result, AM will become more accessible and sustainable. The range of application of AM technologies will be broadened across various sectors with specialised functionality requirements.

Kurzfassung

In den letzten Jahrzehnten hat sich die additive Fertigung (AM) von einer Rapid-Prototyping-Technologie zu einem ausgereiften Fertigungsverfahren entwickelt, welches erhebliche Vorteile für den Leichtbau bietet und das Potenzial hat, Anforderungen für sehr anspruchsvolle und spezialisierte Anwendungen zu erfüllen. Die Oberflächenqualität ist oftmals von funktionaler Bedeutung und daher entscheidend für die Qualifizierung von AM-Metallteilen, insbesondere derer für hoch belastete Luft- und Raumfahrtanwendungen.

Die Oberflächenqualität, die aus einem Laser Powder Bed Fusion (LPBF) AM-Prozess resultiert, ist typischerweise durch Ansammlungen von anhaftenden Pulverpartikeln, Spritzern, Schweiß- oder Schichtspuren gekennzeichnet. Die spezifischen Merkmale hängen von den verwendeten Materialien, Pulvereigenschaften, Baurichtung und weiteren Einflussfaktoren ab.

Die vorliegende Arbeit trägt zu einem umfassenderen Verständnis und einer verbesserten Beschreibung der Oberflächenqualität von LPBF, ihrer Entstehung, Charakterisierung und Rolle in der Funktionalität von Bauteilen bei. Dieses Verständnis wird durch neuartige Ansätze zur angepassten Charakterisierung der Oberflächentextur von Metall-AM-Bauteilen aus LPBF unter Verwendung modernster optischer Messsysteme und flächenhafter Oberflächentexturcharakterisierung erreicht.

Die Ergebnisse dieser Arbeit werden in drei Teilen vorgestellt: “Measurement and Data Post-processing” (Messung und Datennachbearbeitung), “Surface Texture und Mechanical Properties” (Oberflächentexture und mechanische Eigenschaften) and “Areal Surface Features” (Flächenbezogene Oberflächenmerkmale).

Teil eins, “Measurement and Data Post-processing” (Messung und Datennachbearbeitung), behandelt die Anwendung optischer Messungen und damit verbundene methodenspezifische Herausforderungen im Hinblick auf as-built und nachbearbeitete LPBF-Oberflächen. Die derzeitige Praxis zur Charakterisierung der Oberflächentextur in der Industrie basiert auf Tastschnittmessungen, daraus resultierenden 2D-Profilen und entsprechenden Parametern. Die Charakterisierung auf Basis von einzeln gemessenen Profillinien ist jedoch in Anbetracht der komplexen Oberflächenstruktur, die bei LPBF-Prozessen entsteht, nur wenig repräsentativ. Anhand eines systematischen, nutzerzentrierten und anwendungsbezogenen Vergleichs von Konfokalmikroskopie, Streifenlichtprojektion und Tastschnittmessung wird gezeigt, dass flächenhafte Messungen erhebliche Vorteile bei der repräsentativen Oberflächenabdeckung, der Reproduzierbarkeit und der Vermeidung von Oberflächenbeschädigungen haben (berührende vs. berührungslose Messungen). Zusammenfassend wird der Übergang von 2D- zu 3D-Parametern für die Charakterisierung der Oberflächentextur und dementsprechend von berührenden Tastschnittgeräten zu berührungslosen optischen Methoden vorangetrieben. Dies ist ein wichtiger erster Schritt in Richtung einer ganzheitlichen Beschreibung von AM-Oberflächen durch Bereitstellung der erforderlichen Daten.

Teil zwei, "Surface Texture and Mechanical Properties" (Oberflächentextur und mechanische Eigenschaften), schlägt eine Beschreibung von AM-Oberflächen auf der Grundlage der Teilefunktionalität vor. Insbesondere wird die Verwendung von Oberflächentexturparametern aus der Materialverhältniskurve im Zusammenhang mit der Ermüdungsleistung eingeführt, im Gegensatz zu den typischerweise verwendeten 2D-Profilextremwerten, der maximalen Höhendifferenz Rt und dem arithmetischen Mittelwert des Rauheitsprofils Ra. Diese Parameter werden der typischen Beschaffenheit von LPBF-Oberflächen nicht gerecht, die häufig von Pulverpartikelagglomerationen und Schicht- oder Schweißspuren geprägt sind. Darüber hinaus sind sie empfindlich gegenüber Ausreißern und werden daher stark von der Messstelle und Messartefakten beeinflusst. Auch ihre flächenbezogenen Äquivalente Sz und Sa sind mit diesen Nachteilen behaftet. Die Materialverhältniskurve wird durch lokale Unregelmäßigkeiten weniger beeinflusst, da sie aus

der gesamten Oberflächenhöhenverteilung abgeleitet wird. Die reduzierte Taltiefe Svk gehört zu den Parametern, die aus dieser Kurve abgeleitet werden. Sie ist kein einzelner Extremwert, sondern repräsentiert die Größe der Talpopulation innerhalb der gemessenen Oberflächenregion. Da Ermüdungsversagen bei LPBF-Bauteilen im as-built Zustand häufig von mehreren Rissinitiierungsstellen an der Oberfläche ausgeht, lässt sich Svk besonders gut mit dieser beobachteten Versagensart in Verbindung bringen. Die Verwendung von Svk in Verbindung mit der Ermüdung von LPBF-Bauteilen ist ein hervorragendes Beispiel für einen angepassten und funktionsbasierten Ansatz zur Charakterisierung der Oberflächentextur. Außerdem wird gezeigt, dass die Optimierung der Verarbeitungsparameter zu verbesserten Eigenschaften in Bezug auf Oberfläche und mechanisches Verhalten führen kann, die mit den Eigenschaften nachbearbeiteter und konventionell hergestellter Oberflächen konkurrenzfähig sind. Dieses Ergebnis ermöglicht potenziell, den Oberflächennachbearbeitungsschritt aus der LPBF-Wertschöpfungskette zu eliminieren, was die Gesamtprozessdauer und -kosten reduzieren würde.

Teil drei, “Areal Surface Features” (Flächenbezogene Oberflächenmerkmale), führt in die Entwicklung der prozessbezogenen Charakterisierung der Oberflächentextur ein und wird das Konzept einer funktionsbasierten Beschreibung weiterentwickeln. Die Messung von flächenhaften Oberflächendaten ermöglicht die Extraktion und Quantifizierung von prozessspezifischen Oberflächenmerkmalen, wie z.B. die bereits erwähnten Partikelanhaftungen oder Schweißspuren. Die vorgestellten Arbeiten zur Charakterisierung von Oberflächenmerkmalen konzentrieren sich auf die Bestimmung geeigneter Prunenschwellwerte. Die Norm ISO 25178 zur flächenhaften Charakterisierung von Oberflächentexturen schlägt vor, die Schwellwerte über den Extremwert Sz zu definieren. Es wird gezeigt, dass dieser Ansatz nicht geeignet ist, um aussagekräftige Oberflächensegmentierungen auf LPBF-Oberflächen im as-built Zustand zu erhalten. Die hier vorgeschlagene Lösung basiert auf der Partikelgrößenverteilung des verwendeten Metallpulvers als Schwellenwert für das Pruning. Diese so definierten Schwellenwerte werden dann auf "Feature Parameters" (Elementparameter) aus der ISO 25178 und zur Detektion der LPBF-spezifischen Partikelanhaftungsmerkmale angewendet. Während die höhenbasierten ISO 25178-Parameter auf Höhenvariationen und Abweichungen von der mittleren Profillinie/-fläche beruhen, liefert die merkmalbasierte Charakterisierung Erkenntnisse über verschiedene Eigenschaften wie Formen, Menge und Größenverteilung von physischen Topographieelementen. Die Wahl des Schwellwertes wirkt sich wesentlich auf die numerischen Ergebnisse zu diesen Eigenschaften aus. Der neuartige Ansatz, die Definition von Prunenschwellwerten mit dem Wissen über Materialien und Prozessvariablen zu verbinden, wird hier erstmalig vorgestellt. Dieser Ansatz kann wegweisend sein für zukünftige Weiterentwicklungen von angepassten Konzepten zur Charakterisierung von Oberflächentextur. Die merkmalsbasierte Charakterisierung hat großes Potenzial für die Definition von funktionsbasierten Anforderungen an die Oberflächentextur und deren möglichst genaue Beschreibung, die mit Daten von Messsystemen nach dem neuesten Stand der Technik erreicht werden kann. Sie wird sich mit verbesserten Messsystemen kontinuierlich weiterentwickeln und das Verständnis von Prozess-Struktur-Eigenschafts-Korrelationen von AM-Bauteilen fördern. Infolgedessen werden AM-Technologien zugänglicher und nachhaltiger werden. Die Einsatzbereiche von AM-Bauteilen können so in diversen Industriezweigen mit spezialisierten Funktionsanforderungen erweitert werden.

Nomenclature

Abbreviations

AM	Additive Manufacturing
ASTM	American Society for Testing and Materials
CAD	Computer Aided Design
CM	Confocal Microscopy
CrediT	Contributor Roles Taxonomy
CSI	Coherence Scanning Interferometry
DED	Directed Energy Deposition
EBPBF	Electron Beam Powder Bed Fusion
FoV	Field of View
FP	Fringe Projection
FV	Focus Variation
ISO	International Organisation for Standardisation
LPBF	Laser Powder Bed Fusion
LSCM	Laser Scanning Confocal Microscopy
NMP	Non Measured Points
PBF	Powder Bed Fusion
QA	Quality Assurance/ Quality Assessment
SEM	Scanning Elelctron Microscopy
UTS	Ultimate Tensile Strength
VED	Volume Energy Density
xCT	X-ray Computed Tomography

Parameters and Variables

d_{max}	Average maximum particle diameter
$d10$	10% of particles have a smaller diameter than d10
$d50$	50% of particles have a smaller diameter than d50
$d90$	90% of particles have a smaller diameter than d90
h	Hatch spacing
N_L	Endurance limit (number of cycles)
P	Laser power
σ_L	Stress at endurance limit
σ_{max}	Maximum stress
σ_{min}	Minimum stress
σ_{mean}	Mean stress
σ_{ult}	Ultimate tensile strength (UTS)
v	Scan speed
z_{max}	Average maximum particle z-height

Surface Texture Parameters (ISO 21920 and ISO 25178)

Ra	Arithmetic mean height of 2D profile
Rq	Root mean square height of 2D profile
Rt	Maximum total height of 2D profile
Rz	Mean maximum 2D profile height (from five profile sections)
Rk	2D core height
Rvk	2D reduced valley depth
Rpk	2D reduced peak height
Sa	Arithmetic mean height of 3D profile
Sq	Root mean square height of 3D profile
Sz	Maximum total height of 3D profile
Sv	Maximum valley depth
Sp	Maximum peak height
Sk	3D core height
Svk	3D reduced valley depth
Spk	3D reduced peak height
$Smr1$	Peak material ratio
$Smr2$	Valley material ratio
Ssk	Skewness of the surface height distribution
Sku	Kurtosis of the surface height distribution
Sda	Mean dale area
Sdd	Mean local dale depth
$Sded$	Mean dale equivalent diameter
Sdv	Mean dale volume
Shh	Mean local hill height
Spc	Mean peak curvature
Spd	No. of peaks per unit area
Svd	No. of valleys per unit area
$S5v$	Five point average dale depth

Contents

Declaration of Authorship V
Abstract VII
Kurzfassung IX
Nomenclature XI

1. Introduction **3**

2. Motivation and Objective **11**

3. Review of Related Theory, Practice and Literature **13**
3.1. Additive Manufacturing for Aerospace Applications 13
3.1.1. Process and Part Quality 13
3.1.2. Materials 15
3.2. Surface Texture Characterisation for Metal Additive Manufacturing 16
3.2.1. Measurement Systems for Areal Characterisation 16
3.2.2. Height-based Areal Field Parameters 17
3.2.3. Feature-based Characterisation 18
3.3. Mechanical Properties of LPBF-processed AlSi Alloys 21

4. Measurement and Data Post-processing **23**
Summary – Measurement and Data Post-Processing 24

5. Surface Texture and Mechanical Properties **29**
Summary – Surface Texture and Mechanical Properties 30

6. Areal Surface Features **35**
Summary – Areal Surface Features 36

7. Synthesis – Conclusions and Future Prospects **45**
7.1. Main Results 45
7.2. Contributions to the State of the Art 47
7.3. Implementation in Industrial Practice 49
7.4. Limitations and Future Work 49
7.5. Future Prospects – The Big Picture 51

A. Full-length Publications **52**
A.1. Publication 1 – Surface Texture Characterisation for Industrial Applications[1] . . 52
A.2. Publication 2 – Post-processing of Areal Surface Topography Data[2] 71
A.3. Publication 3 – Influence of Contour Scan Variation[3] 79
A.4. Publication 4 – Surface Texture and High Cycle Fatigue[4] 95
A.5. Publication 5 – Surface Feature Parameters[5] 103
A.6. Publication 6 – Process-specific Surface Features[6] 109

B. Author Contributions and Selection of Publication Media for Publications 1 to 6 **117**

C. List of Publications and Public Presentations **121**

D. Acknowledgements **125**

Bibliography **127**

1. Introduction

Over the last decades, various additive manufacturing (AM) processes and their outcomes became popular research topics and resulted in an improved understanding of process parameters, material properties and suitability for applications with challenging requirements. Additive manufacturing technologies facilitate lightweight, tailored-for-purpose design and development of biomimetic structures. They contribute to the reduction of material waste and process duration [1, 2]. According to a study from 2018, AM can reduce the world energy consumption by up to 25% by 2050 [3] and consequently lower global greenhouse emissions.

AM technology has come a long way since its first commercialisation in the 1980s. It is referred to as a "revolution in manufacturing" [4] and is generally perceived as a game-changing technology [1, 2, 5–7]. Various materials and material classes can be processed by AM, tailoring parts for all kinds of purposes. The manufacturing technique is able to achieve part quality suitable for specialised applications, though the surface finish often presents a challenge.

Currently, one of the most popular AM processes for aerospace applications is laser-based metal powder bed fusion (LPBF) [2, 7]. LPBF is a layer-based technique, where individual powder layers are combined by laser melting and ultimately yielding a three-dimensional (3D) part. The process is illustrated by Figure 1: A powder layer, typically of thickness between 20 µm and 100 µm, is applied to a vertically movable build platform using an automated coater. The laser melts the powder and as the melt pool solidifies, a two-dimensional (2D) slice of the object to be manufactured is produced. The powder supply is moved upward while the build platform moves downward by one layer thickness and the coater applies another layer of powder to the build platform. Again, the layer is molten and combined with the previous layers by the laser. The process is repeated until all layers are stacked to form the final 3D part [5].

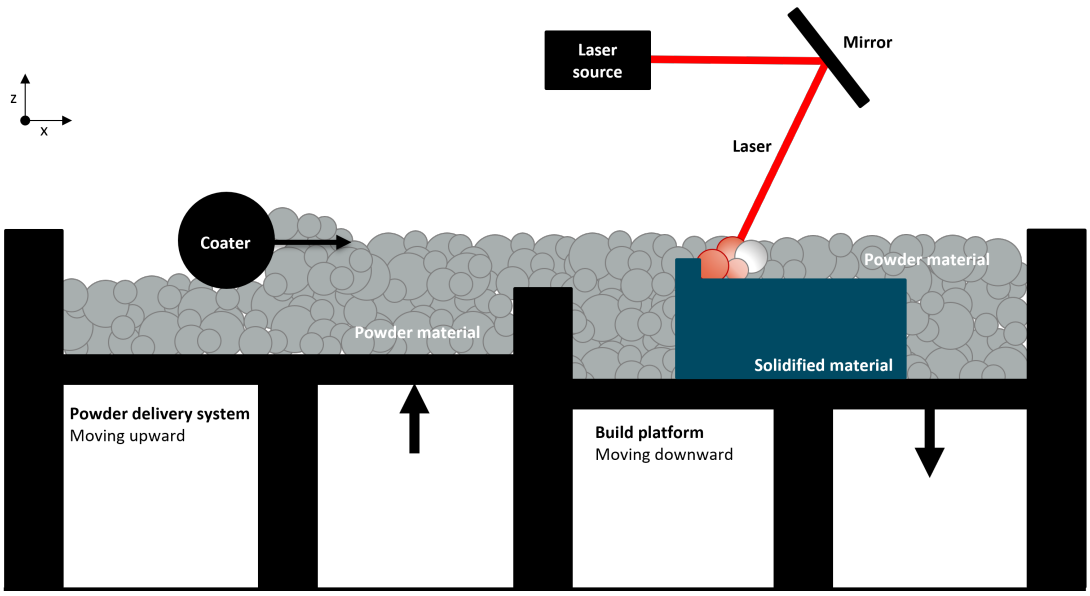

Figure 1.: Schematic overview of the LPBF process

Influencing Factors on LPBF Part Quality

The part quality resulting from the LPBF process and related post-treatment steps depends on numerous influencing factors [1, 8–10].

Selected key groups of factors are summarised in Figure 2. The diagram includes properties of the powder material, the build environment, the build job itself, energy input (including scan strategy), and influence of post-treatment, such as mechanical and chemical surface processing or heat treatment. The "build environment" refers to general machine-related properties and settings such as temperature (build chamber and powder bed) and type of coater. "Build job" means in this case, factors related to the part to be manufactured, like geometry (including shapes and build angles), positioning on the platform, slicing of the CAD file, etc. The most common process parameters investigated in literature are related to the energy input, namely laser power P, hatch spacing h (spacing of parallel laser exposure tracks), layer thickness t and scan speed v. These parameters can be combined into the volume energy density (VED).

All of these aspects have a considerable impact on the properties of the final part, production time and cost. The listed key groups and stated process parameters and their contributions to the part quality are addressed more elaborately in Section 3.1.1.

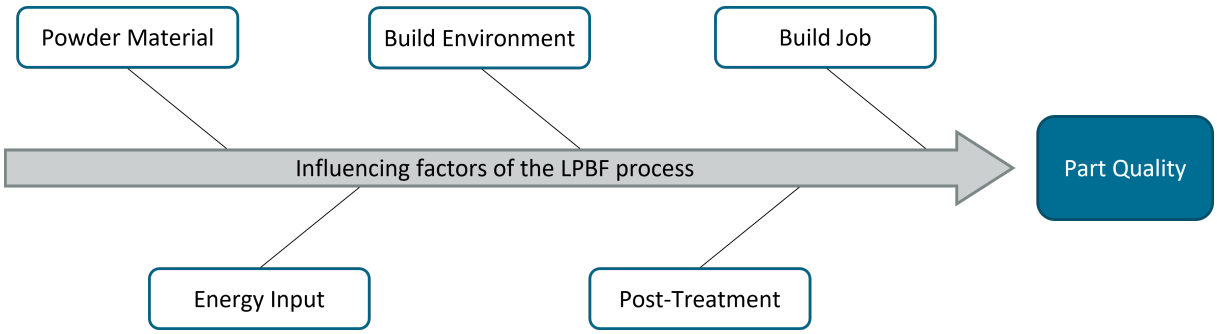

Figure 2.: Selected key groups of influencing factors on LPBF part quality

Surface Quality from LPBF

Parts manufactured by LPBF typically exhibit agglomerated, partially melted powder particles of different sizes (Figure 3), re-entrant features (Figure 4), as well as waviness from layers and weld tracks. All of these may add up to a coarse surface quality in as-built condition. Size and quantity of those charactersitic features depend on the material, geometry and processing, as briefly introduced previously.

An LPBF aluminium alloy surface in as-built condition with clearly visible powder particle attachments and a total height variation on the surface of up to 100 μm within the measured area is shown in Figure 3.

Among the influencing factors leading to an increased number of particle agglomerations on the surface are the application of high VED, slow heat dissipation of the used material (e.g. titanium vs. aluminium) and build angle. This is illustrated in Figure 5, showing the heat flow during

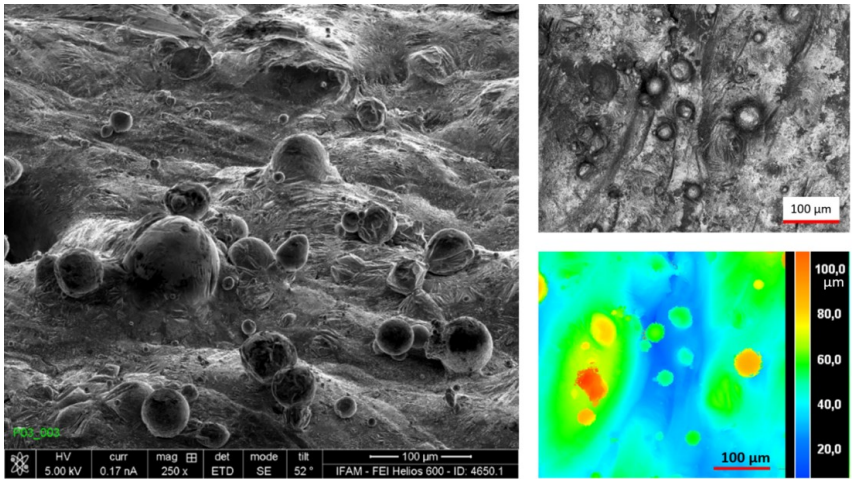

Figure 3.: Micrograph (SEM) showing agglomerations of partially melted powder particles of different sizes on the sample surface in as-built condition *(left)*, micrograph (LSCM) and corresponding height representation *(right)*

the process for two different build angles and its effect on the side surfaces. For a horizontal build, the heat can largely move through the solidified material, melting and attaching only a few particles to the surface (grey particles with blue contour in the figure). When manufacturing parts with downskin faces, more severe agglomerations occur. This increased attachment of powder particles for downskin surfaces is called the "staircase effect". This effect is due to part of the layer being build on loose powder. The heat dissipates through the loose powder and melts neighbouring particles onto the surface. The surface topography of thin-walled structures is influenced more severely due to less solid material being available to accommodate the heat flow [11].

The surface is the region of interaction between a part and its surroundings (i.e. gas, fluids, other parts). The surface and its quality are often of functional importance. This is the case when looking at components subjected to cyclic loading, corrosion resistance, application of coatings or adhesive bonding.

Regarding the application of LPBF in load-bearing aerospace systems, the definition of standards for part certification and quality assurance is still pending. Hence, the use in critical parts

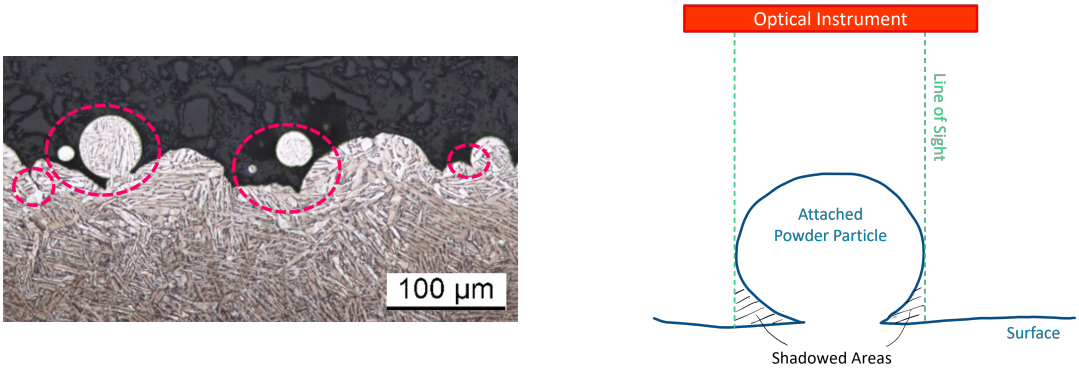

Figure 4.: Cross-section micrograph: Re-entrant features (pink dashed markers) caused by agglomerated powder particles *(left)*, line-of-sight and shadowed areas from re-entrant features *(right)*

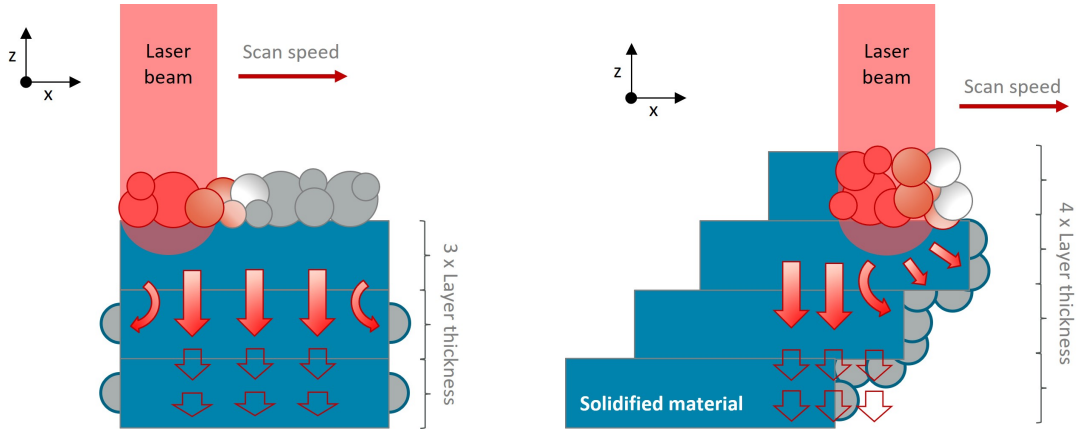

Figure 5.: Particle attachments due to heat flow for horizontal *(left)* and 45° downskin *(right)*, *based on [12]*

is currently still restricted [7, 13]. Mechanical or chemical post-processing may be required for certain applications [14, 15], causing additional processing steps and increasing time and cost. Some post-processing technologies also restrict the geometrical freedom. Thus, when post-processing is required, a number of AM advantages are diminished. Adjustment of the identified influencing factors (detailed in Section 3.1.1) helps improving part quality and has potential to reduce the required post-processing significantly.

Measurement of Surface Topography

The term “surface topography” describes the deviation of a surface from a perfectly flat plane. It includes the full geometric information of a surface, such as shape or form, waviness of different scales and surface texture. According to ISO 25178-2, “surface texture” is defined as the surface irregularities that are left after removing form by applying an F-operation, waviness (i.e. low frequency lateral components) by means of an L-filter and high frequency components (i.e. smaller than instrument resolution) using an S-filter, from the primary surface. It is also referred to as “S-L-surface” or “roughness” [16].

The surface characteristics observed on LPBF parts differ significantly from those manufactured in traditional processes, such as machining, rolling or casting. Therefore, new challenges are imposed on methods and measurement instruments for surface texture characterisation.

The established (2D) contact stylus method remains popular with users across academia and industry. It is based on a contact measurement using a diamond tip moving across the surface of interest. However, also optical measurement systems enabling areal surface texture characterisation are increasingly implemented. Examples for such systems are fringe projection (FP), confocal microscopy (CM), focus variation (FV) and coherence scanning interferometry (CSI). This allows for an areal, more representative depiction of a surface using (almost) 3D data.

"Almost" – because even though various methods can cover large areas on the part to be measured, optical measurements are limited to line-of-sight. This means that re-entrant features (see Figure 4), as frequently caused by the typical powder particle agglomerations, cannot be detected. Resulting shadowing effects may, depending on the method, cause measurement artefacts. Measurement with focus on AM parts is covered in Section 3.2.1 and Chapter 4.

Surface Texture Characterisation

The stylus method is associated with 2D height based surface texture parameters, the most common ones being *Ra* (arithmetic mean profile height), *Rz* (average maximum profile height) and *Rt* (total maximum profile height). Nowadays, also their areal equivalents *Sa* (arithmetic mean height, equivalent to *Ra*) and *Sz* (total maximum height, equivalent to *Rt*) are generally well known. However, as these parameters are simply calculated from height variations, very different surface structures can be represented by the same value [17], as visualised in Figure 6.

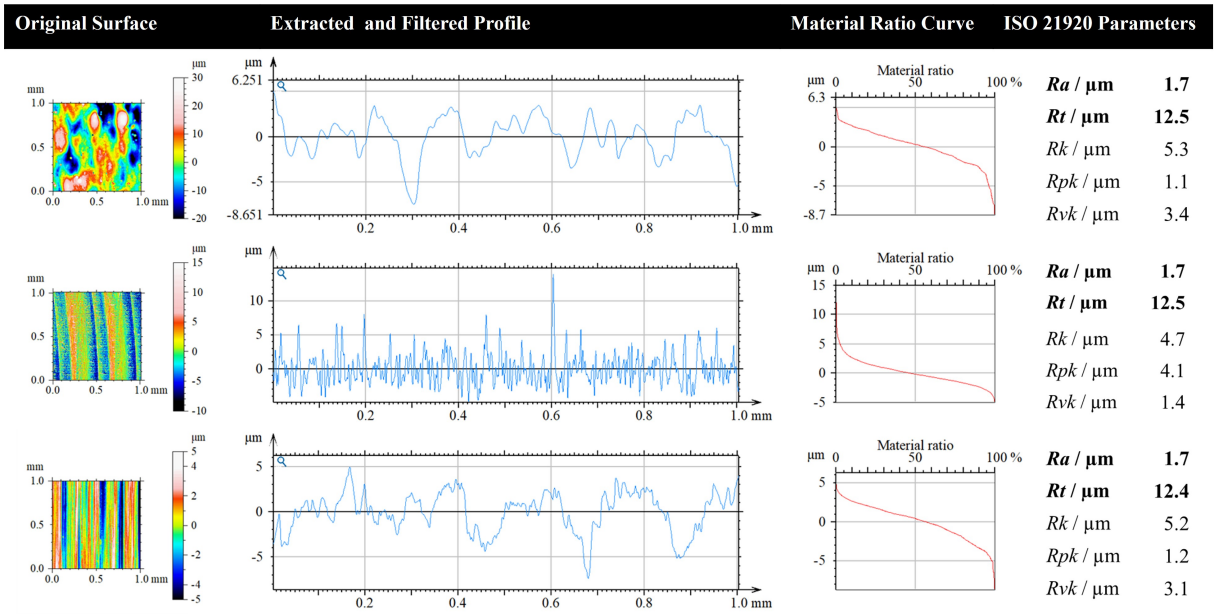

Figure 6.: Surface height maps from different manufacturing processes, extracted and filtered profiles, corresponding material ratio curves and resulting ISO 21920 parameters *(left to right)*: Visually, the surface characteristics and profiles differ drastically, while they are characterised by similar *Ra* and *Rt*. The 2D Material ratio curve parameters *Rk*, *Rpk* and *Rvk* are similar for the top and bottom profiles, but can differentiate the middle profile.

Figure 6 highlights two major issues of current surface texture characterisation practice:

1. The common parameters *Ra* and *Rt* are unable to distinguish profiles exhibiting obvious visual differences which suggest differences in functionality.

2. Extracted 2D profiles are (mostly) not representative of 3D surfaces.

These issues are illustrated by means of extracted profiles from an LPBF surface, a milled surface and a turned surface (Figure 6, top to bottom). While the three extracted and filtered surfaces

have very different appearances, all of them have the same $Ra = 1.7$ µm and $Rt = 12.5 \pm 0.1$ µm. The 2D material ratio curves and corresponding parameters are able to distinguish the middle profile from the other two. Regarding the top and bottom profiles, they show similar lateral spacings and height distributions and have hence similar material ratio curves and parameters. However, considering the original surfaces they are extracted from, it is misleading, that those very different surface finishes can be characterised by the same 2D parameters.

This emphasises the need for 3D characterisation of functional surfaces. Looking at the ISO 25178 on areal (i.e. 3D) surface characterisation, numerous options besides Sa and Sz are available. A more robust, though still height based, description is offered by parameters from the (3D) material ratio curve, Sk (core height), Svk (reduced valley depth) and Spk (reduced peak height). The corresponding parameter definitions are covered in more detail in Section 3.2.2.

A rather novel approach is the characterisation of surface features. While this concept is not yet established in industrial applications, hill-and-dale-based feature detection and parameters representing a variety of their geometric properties are included in the ISO 25178 standard [16]. Feature-based characterisation opens up opportunities to correlate part function, such as crack propagation under cyclic loading or adhesion of protective coatings, to certain shapes present on a part's surface. Beyond hills and dales, the detection of process-specific features is also possible. Looking at LPBF parts in particular, particle agglomerations, spatter or weld tracks may be of interest [18, 19].

Figure 7 shows extracted features from an LBPF surface: two powder particles attached to the surface. Depending on the applied method for feature analysis, they can be classified as hill features or as process-specific particle features.

Selected literature on feature-based characterisation is summarised in Section 3.2.3, the related concepts are explained in Chapter 6.

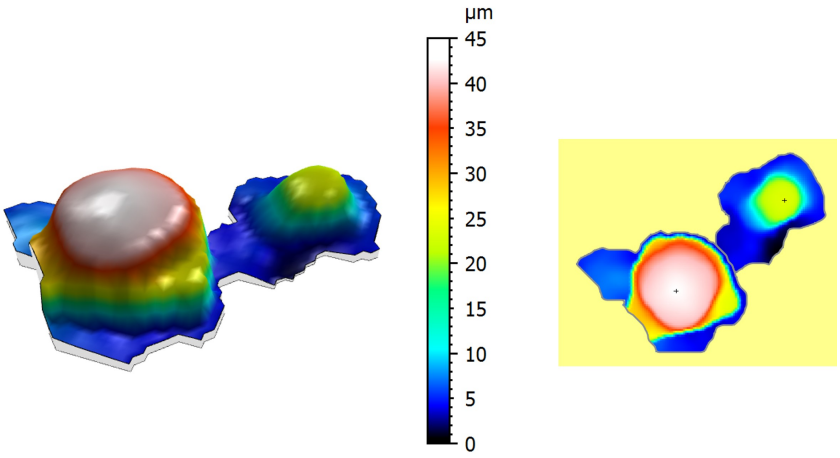

Figure 7.: Attached particle features on LPBF surface: 3D view (left), top view (right)

Document Structure

This thesis is written in cumulative format and the results presented are subdivided into six publications: four articles, published in peer-reviewed journals, one peer-reviewed conference paper and one article preprint, that was also presented at a conference. The publications in full length are included in Appendix A. Full bibliographic details and co-author contributions, as well as the selection criteria for the publication media are included in Appendix B. A full list of publications and presentations generated during my time as doctoral candidate at Fraunhofer IFAM is enclosed in Appendix C.

The structure of the thesis framework document is as follows:

This Chapter 1 gave a brief introduction to the concepts and technologies relevant to follow the upcoming elaborations.

The motivation and objective of the presented work are outlined in Chapter 2.

In Chapter 3, literature in the context of the topics is reviewed, starting with materials for AM in aerospace, metal AM surface texture characterisation and mechanical properties (incl. the relationship of mechanical properties and surface texture). Where found appropriate, related concepts and definitions are explained. Chapter 3 presents complementary information to the literature reviews included in the respective publications.

After the introductory part in Chapters 1-3, the results are presented in Chapters 4-6, each covering another aspect of LPBF part quality assessment:

- Chapter 4: Measurement and Data Post-processing
  - Publication 1: *Surface Texture Characterisation for Industrial Applications*
  - Publication 2: *Post-processing of Areal Surface Topography Data*
- Chapter 5: Surface Texture and Mechanical Properties
  - Publication 3: *Influence of Contour Scan Variation*
  - Publication 4: *Surface Texture and High Cycle Fatigue*
- Chapter 6: Areal Surface Features
  - Publication 5: *Surface Feature Parameters*
  - Publication 6: *Process-specific Surface Features*

Each chapter covers two publications and includes a summary of the main results and conclusions.

Chapter 7 gives a summary and synthesis of the work done, knowledge gained and conclusions drawn. This work's contributions to the state of the art are highlighted and an outline of upcoming work and future prospects conclude the final chapter.

2. Motivation and Objective

The main objective of the presented doctoral research project is the adaption of novel approaches to tailored surface texture characterisation of metal AM parts from LPBF, employing state-of-the-art optical measurement technology and areal surface texture characterisation, and thus, to contribute to the overarching goal of gaining a more comprehensive understanding of LPBF manufactured surfaces and their process-structure-property correlations. This improved understanding will expand the range of application of AM technologies in various sectors with specialised functionality requirements.

During my master thesis work on wet-chemical surface post-processing of metal additive parts between November 2017 and June 2018, I realised that there is a gap between available state-of-the-art measurement technology for surface texture characterisation and the current practice in industry and research applications. With the intention of bridging that gap, the concept of this doctoral research project was developed.

In recent years, optical measurement systems have been increasingly used for surface texture characterisation, especially in research. The technologies are constantly evolving, facilitating faster, more precise data acquisition of large regions, depicting diverse surface structures on complex geometries. To utilise the advantages of optical measurement systems for part qualification processes in industry, it is necessary to understand the differences and advantages with regard to the established stylus method and the corresponding 2D characterisation. A distinct benefit is the opportunity to use areal data for surface texture characterisation, allowing for a more statistically representative evaluation. Especially for the stochastic, inhomogeneous metal PBF surfaces, evaluation of areal data is advantageous when aiming for a comprehensive understanding of their surface quality. However, due to the differences in physical interaction of different optical instruments and measured surfaces and prerequisites for adequate operation, there is a need for a user-oriented analysis. Every method has their specific requirements regarding part positioning, instrument settings or data processing in order to minimise the influence of measurement artefacts on the resulting surface data and calculation of texture parameters. Especially as-built LPBF surfaces, but also post-processed surface conditions, impose challenges on measurement systems, which are addressed in the context of the following first key question:

“Under which conditions do surface texture measurement systems based on different physical working principles produce reliable, representative and comparable data for metal AM surfaces from LPBF?”

Regarding the interaction of fatigue performance and surface quality of metal PBF parts, current research is still focussed on 2D data and using profile mean height and individual extreme values. This approach is hardly representative of typical as-built metal PBF fracture modes with a tendency toward crack initiation from multiple (near-)surface defects. The use of areal data to describe metal PBF parts allows for a more realistic and representative surface description, as these surfaces are typically irregular, exhibiting inhomogeneous individual or clustered, often

(part-) spherical particle agglomerations of various sizes. Alternative concepts, taking into account the process-specific features of metal PBF parts, are to be explored. In order to accommodate the integration into existing part qualification processes, as a first step, areal surface texture parameters included in the ISO 25178 standard are investigated, aiming at answering the second key question:

“How can the interaction between processing, resulting part quality and part functionality for metal AM parts from LPBF and their surfaces be described?”

The utilisation of areal data obtained from optical measurement instruments does not only allow for generating more statistically representative surface texture parameters, but also for the evaluation, extraction and quantification of characteristic surface features. A novel approach employing the knowledge of the LPBF manufacturing process and material has the potential to gain an even more authentic description of the resulting surface quality. This motivates the third key question:

“Can the description of metal PBF surfaces be improved by using process-related inputs to surface texture characterisation?”

3. Review of Related Theory, Practice and Literature

This chapter gives an overview of relevant concepts and recent work on the topics related to this thesis. It is meant to complement the state-of-the-art reviews of the published works (summarised in Chapters 4, 5 and 6, full-length publications in Appendix A), which are referred to where appropriate.

The opening of this chapter is Section 3.1 on AM for aerospace applications with focus on part quality influencing factors and materials selection, followed by an introduction to surface texture characterisation, Section 3.2, with common methods and parameters and their application to metal additive surfaces. Furthermore, the section comprises a review of recent work on feature-based surface texture characterisation in 3.2.3. The chapter concludes with Section 3.3, presenting a brief summary of studies on mechanical properties of LPBF-processed AlSi alloys and additional relevant work.

3.1. Additive Manufacturing for Aerospace Applications

The most popular metal additive process for aerospace components is LPBF, which was already shown in Figure 1 (Chapter 1). Amongst other high requirements, lightweight construction with extraordinary mechanical performance is vital for many applications. This calls for high quality parts and specialised materials [1, 7]. Related factors are briefly introduced in this upcoming section.

3.1.1. Process and Part Quality

AM part quality is affected by various influencing factors, summarised in Figure 8. This overview is by no means complete and is meant to illustrate the large number of influencing factors in an LPBF process and their interconnection [1, 8–10].

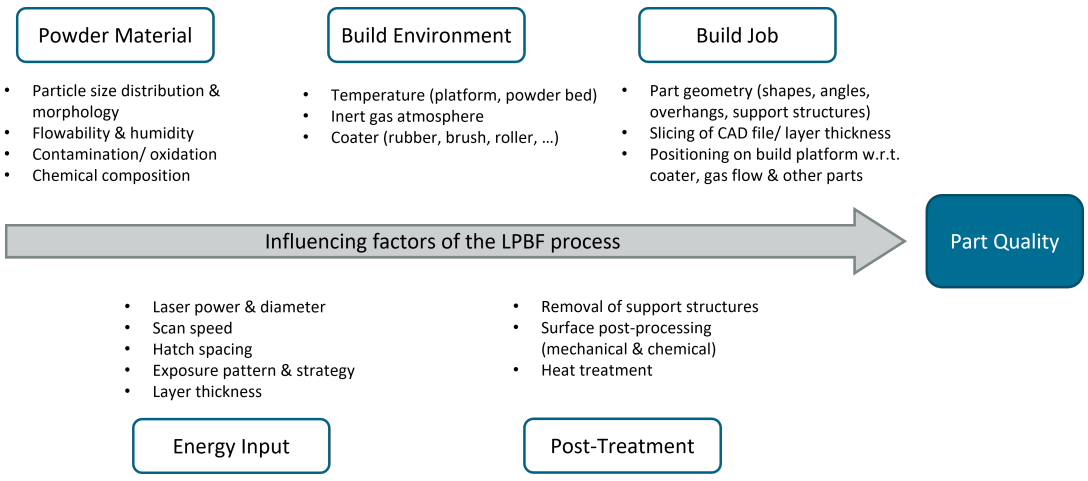

Figure 8.: Selected influencing factors on LPBF part quality

The characteristics of the used powder material affect the process and its outcome. Particle size distribution, morphology and powder humidity have an impact on flowability, hence on the application of the powder layer and ultimately on the resulting part density. Powder contaminations of various types influence the microstructure, leading to reduced part performance. The chosen alloy and its chemical composition, usually based on the desired application, will partly determine the selection of manufacturing parameters and process handling.

Factors attributed to the build environment, like the temperatures of powder bed, build chamber and build platform, manipulate the heat flow. This has an effect on the formation of part microstructure and surface texture. The gas flow and its fine tuning in combination with other process parameters regulates the transportation of process-related by-products (e.g. reaction products, evaporating gases). Properties of the coater, such as shape, material or coating speed, in interaction with the powder material are additional contributing factors towards the quality of the powder layer application.

The geometry of the part to be manufactured and its placement within the build chamber defines the need of support structures, stair step effects (Figure 5) and the influence of gas flow and coating direction. Also the packing density on the platform (i.e. parts per area) contributes to part quality. These factors are summarised in the category "build job".

The most frequently discussed machine settings in literature are those relevant to define the volume energy density (VED):

$$VED = \frac{P}{v \cdot h \cdot t} \tag{3.1}$$

P is the laser power, v is the scan speed, h is the hatch spacing and t represents the layer thickness. These parameters are also visualised in Figure 9. The energy input is relevant for proper melting and fusion of the powder. Too little energy will lead to keyhole porosities, resulting from an unstable melt pool. Often, loose powder is enclosed in these pores. Too much energy input may lead to metallurgical pores with entrapped gas from the build environment or evaporation from alloying elements. In both cases, part density and mechanical properties are compromised. The suitable amount of energy and appropriate exposure strategy depend on the used powder material (alloy, size distribution), desired properties and production time [20–22].

Although many studies are found that are based on the optimisation of the volume energy density, it is important to note that this approach is flawed. It fails to include factors like exposure patterns/hatch strategy, beam shape, laser angle/deformation or remelting of entire layers or parts of it (e.g. the contour), which contribute significantly to the overall energy input into the material [1, 22]. A few existing studies address processing and effects of remelting of individual and multiple layers in bulk and contour for different materials [22–25].

The final group of factors of interest in Figure 8 is related to post-processing, which includes removal of support structures (process-related) as well as mechanical or chemical surface processing and heat treatment (property-related). Especially property-related post-processing activities have

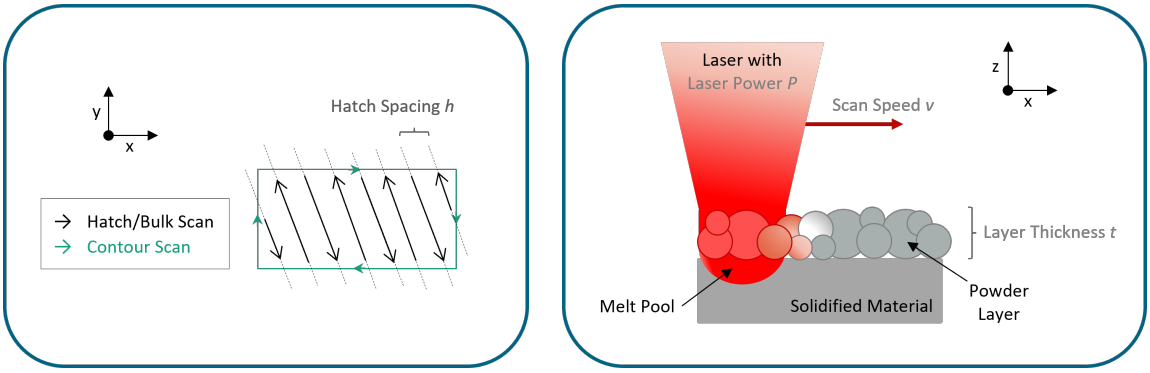

Figure 9.: Visualisation of selected LPBF process parameters

been addressed in literature, aiming at improved performance tailored to specific applications [24, 26–38].

3.1.2. Materials

An extensive number of studies on Ti-64 [8, 39–41], Inconel 718 [22, 42, 43] and 316L steel [44–47] exist in literature. According to various review papers, those are the most common research materials in metal PBF. The LPBF processing of aluminium (Al) alloys, however, only became increasingly important during the last decade [9, 20, 48–52].

Al alloy powders show low flowability (impacting recoating of layers) and are susceptible to oxidation (causing porosity) due to the high reactivity of Al and the powders' large overall surface area. Added to this are the materials' high reflectivity and low absorption of the typical LPBF process laser wavelength range and its high thermal conductivity, resulting in high required laser power. Those specified properties contribute to the processing of aluminium alloys by LPBF being particularly challenging. However, Al alloys are of interest for LPBF in lightweight construction applications. They are lightweight, strong, corrosion resistant (i.e. for finished parts, the oxide layer acts as a shield, as opposed to the powder material, where oxidation causes contaminations in the final part) and highly weldable. In combination with the geometrical freedom of LPBF processing, they have high potential for tailoring parts to numerous applications within automotive, aerospace and other industries [20]. The best processable aluminium alloys by LPBF are aluminium-silicon-based. The most commonly studied one is AlSi10Mg, but also AlSi12 and AlSi7Mg show good processability [1, 51, 53].

While aluminium itself has great lightweight design potential with a density of 2.7 g/cm^3, alloying elements play an essential role in improving and defining material properties and processing. The silicon phase in the solidified LPBF material inhibits crack initiation and propagation and reduces the overall weight of the manufactured part with its density of 2.4 g/cm^3. Silicon as alloying element improves hardness and reduces shrinkage [1, 51, 53]. The addition of magnesium improves corrosion resistance and weldability [54].

Over the last few years, work has been done on tailoring and adapting alloys to the process- and application-specific needs of additive manufacturing, rather than using those developed

for traditional (i.e. subtractive) processes, as Clare et al. stated in their recent review [55]. Examples of tailored Al alloys for LPBF are Scalmalloy®, Scancromal® and Custalloy [54, 56].

3.2. Surface Texture Characterisation for Metal Additive Manufacturing

This section comprises an overview on methods, parameters and approaches to surface texture characterisation and its application to metal additive surfaces. The first two subsections 3.2.1 and 3.2.2 are complementary to the state-of-the-art review included in Publication 1. The final subsection 3.2.3 presents an overview of relevant work on the characterisation of areal surface features.

3.2.1. Measurement Systems for Areal Characterisation

Areal surface texture characterisation has been gaining acceptance in recent years. Methods used in literature in conjunction with metal additive surfaces are confocal microscopy (CM) [57–61], fringe projection (FP) [22, 62, 63] focus variation (FV) microscopy [58–60, 64, 65], coherence scanning interferometry (CSI) [58–60, 66] and X-ray computed tomography (xCT) [22, 59, 60, 67]. The first four are included in the ISO 25178-6 standard on areal surface characterisation. They are optical systems and therefore restricted to line-of-sight measurements. Compared to the well-known and established stylus method, all of them offer better representation of the evaluated surfaces by means of 3D depiction. Line-of-sight measurements, due to their inability to detect re-entrant features, are sometimes referred to as 2.5D measurements [68]. The working principles of those methods listed above are briefly described subsequently.

In **Confocal Microscopy (CM)**, the same location is measured with different focus depths, with only the in-focus z-portion exposed to the light source. Layering of the in-focus z-data results in a height map. The most commonly used light sources are lasers. A resolution in the range of several hundred nanometres can be achieved [57, 69, 70].

Fringe Projection (FP) uses fringe patterns of different sizes that are projected onto a surface. A detector captures the projected patterns and their deviation from the original projection is determined. From this deviation, the 3D (line-of-sight) surface is reconstructed [63, 71]. In addition to surface texture, the method is often used for form measurement at different scales [71–74] and, in the context of metal AM, for in-process powder bed monitoring [75–78].

Focus Variation (FV) microscopy measures the same x-y-location with different focus depths with the entire measured region being exposed to light. The method uses contrast to determine the in-focus surface position. It is well suited for rough surfaces and surfaces with high slope angles but is mostly inadequate for very smooth surfaces [64, 79].

In **Coherence Scanning Interferometry (CSI)**, the position of the surface w.r.t. a detector is determined using the changes of an interference signal. The surface is detected where the constructive interference signal is the strongest. Similarly to FV and CM, a given z-range is scanned for each position and obtained information is layered to reconstruct the surface height representation. Often, white light is used as light source in CSI [80].

X-ray Computed Tomography (xCT) is a method to create a 3D representation of an object (not just its surface). This is done by means of x-ray scanning around a rotational axis. The method is well known in medical applications. Only during the last decade, it was successfully shown to reach appropriate resolutions to measure surface texture of metal AM parts. In addition, xCT offers the data to gain a complete description of investigated samples, including re-entrant features, sub-surface flaws and bulk material porosities. Also measurement of internal surfaces is possible [67]. However, it is the most complex, time-consuming and expensive among the presented methods.

3.2.2. Height-based Areal Field Parameters

Height-based parameters have been used in surface texture characterisation since the middle of the 20th century. Especially prominent in engineering applications are the arithmetic mean profile height (Ra/Sa), root mean square profile height (Rq/Sq) and maximum profile height (Rt/Sz) [6, 81]. However, the ISO 25178 standard on areal surface texture characterisation contains many more parameters [16, 82]. This subsection includes a brief overview of parameters applied to metal AM surfaces and definitions of selected areal parameters. For more details, refer to the literature sections of Publications 1 to 4.

Application to Metal AM Surfaces

In 2017, Todhunter et al. conducted a survey on the use of profile and areal surface texture parameters in both research and industry. The study found that Ra and Rt were commonly utilised, particularly in automotive, aerospace, and product manufacturing. These parameters have also been applied in recent publications on metal additive manufacturing surface texture, sometimes in conjunction with their areal equivalents. Also the root mean square height Rq/Sq is often used [38, 83–86]. Other height-based parameters appearing in conjunction with metal AM surfaces are skewness Ssk and kurtosis Sku [58, 87–91]. These parameters are properties of the surface topography's height distribution and relate to its symmetry and spread, respectively.

Definitions – Height-based Areal Parameters

The areal (i.e. 3D) equivalents to Ra (arithmetic mean profile height), Rq (root mean square profile height), Rz (mean maximum profile height) and Rt (absolute maximum profile height) are Sa (arithmetic mean profile height), Sq (root mean square profile height), Sz (absolute

maximum profile height - equivalent to Rt). These areal parameters have been increasingly applied due to the expanding adoption of optical measurement systems, mostly in academic research [6, 16, 81, 82].

Ra or Sa are calculated from the height distribution of data points across the measured profile or area. It is the mean of the absolute distance between the mean line and those data points, represented by

$$Sa = \frac{1}{N}\sum_{i=1}^{N}|z_i - \bar{z}| \ . \tag{3.2}$$

Similarly, Rq and Sq are determined from the root mean square of the profile deviation from the mean line and can be computed using

$$Sq = \sqrt{\frac{1}{N}\sum_{i=1}^{N}(z_i - \bar{z})^2} \ . \tag{3.3}$$

Rt and its areal equivalent Sz are the height difference between the lowest and the highest point within the measured profile or area. They can also be calculated from the sum of the absolute values of the depth of the deepest valley Sv and the height of the highest peak Sp:

$$Sz = \max(z_i) - \min(z_i) = Sp + Sv \ . \tag{3.4}$$

More information on the surface texture and its distribution, even though still height-based, is offered by the material ratio curve, shown in Figure 10. It is created from the profile z-data and indicates which percentage of the profile is above a certain height. The parameters Sk (core height), Spk (reduced peak height) and Svk (reduced valley depth), $Smr1$ and $Smr2$ (peak and valley material ratio) are calculated from that curve as indicated in Figure 10. Core height Sk is defined as the height difference of the intersections of the main slope tangent (dotted red line) with vertical axes at 0% and 100%. The reduced peak height Spk and reduced valley depth Svk represent the size of peaks or valleys outside (i.e. above or below) the core portion of the profile. They are the height of a right-angled triangle (purple) enclosing an area of equal size to the peak portion below and valley portion above the curve delimited by Smr1 and Smr2, respectively. The material ratios $Smr1$ and $Smr2$ mark the transition point between core region and peak or valley region, respectively. It is known that the material ratio curve provides means of distinguishing surfaces where mean and maximum roughness parameters fail to (see also Figure 6) [17].

3.2.3. Feature-based Characterisation

In contrast to parameters solely based on height variations, those parameters based on the extraction of areal surface features can provide insights on present features shapes, feature size distribution or feature count. This can be especially interesting when looking into part functionality, like mechanical performance, corrosion resistance or adhesion. ISO 25178 comprises feature parameters specifying various geometric properties of hills and dales, such as roundness,

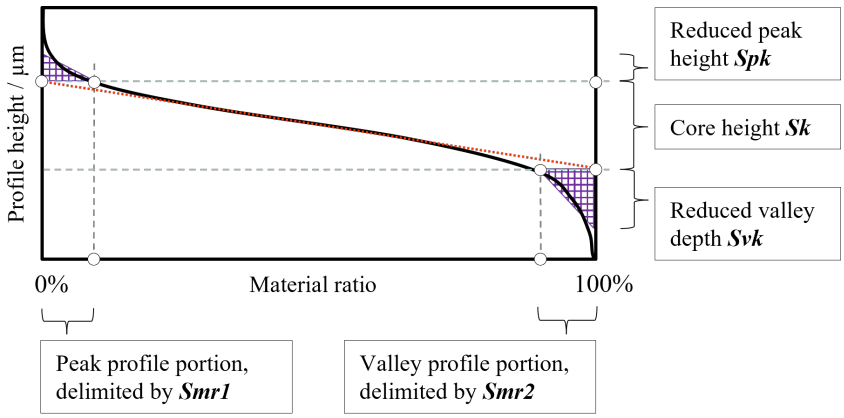

Figure 10.: Material ratio curve

aspect ratio, equivalent diameter, projected area or enclosed volume [6, 16, 18, 19, 82, 92]. Following is an overview of relevant literature. Note that the extraction of features and related methods and definitions are covered in Chapter 6.

The extraction of surface features (e.g. hills, dales, agglomerated particles, weld tracks, milling tracks) and the characterisation of surface texture based on the properties of those features has been developed and applied in different engineering research disciplines over the course of the past 20 years. Examples are the characterisation of surfaces for and from micro electronics, biomedical and conventional/subtractive manufacturing [93–96].

Wang et al. investigated biomedical grade titanium with tailored surface texture for implants [94]. Amongst others, they used feature characterisation to circumvent the impact of measurement noise on the parameters commonly used in the context of cellular attachment. Tian et al. examined wear particles occurring in the synovial joint due to degeneration from osteoarthritis [95]. They demonstrated that feature parameters have the capability of describing functional properties of the wear particle surface texture.

In recent years, feature characterisation became a research topic in regard to metal additive surfaces [18, 19, 65, 97–104]. Selected work is summarised subsequently.

Zou et al. investigated a metal additive surface manufactured by direct energy deposition (DED), where parts are fabricated in a layer-based approach using a metal feedstock (in this case, powder) and an energy source (e.g. laser or electron beam) [97]. For DED surfaces, they identified the weld tracks as major contributor to surface roughness and stated that particle attachments have a lesser influence. They demonstrated that weld tracks can be extracted by watershed segmentation, combined with Wolf pruning and subsequent merging of adjacent particles in direction of the weld tracks by centroid alignment. They presented images of the segmented surface with $1\%Sz$ and $10\%Sz$ Wolf pruning, stating that their threshold selection is unfit to detect smaller agglomerated particles. They suggested to adjust the pruning threshold to obtain better results. In their work, there are no numerical feature parameter results presented and the pruning is defined in terms of the extreme value Sz.

Newton et al. compared three segmentation approaches and their application to metal PBF

surfaces [98]. They applied an edge detection method, watershed segmentation (according to ISO 25178) and contour stability analysis [100] and investigated their ability to identify spatter and particle agglomerations on the selected surfaces from LPBF and electron beam powder bed fusion (EBPBF) at different build angles. They concluded that none of the methods is superior for all evaluated test cases and state that manual reference segmentation, though necessary due to lack of "perfect" algorithmic segmentation, may introduce bias into the comparison.

In following work, Newton et al. investigated Ti-64 surfaces from EBPBF with varied orientation between 0 deg and 180 deg [65]. They confirmed that larger build angles and especially downskin surfaces, resulted in a higher feature count. They used a pixel-based edge detection method in an iterative process to determine particle boundaries and separate particle features (spatter and agglomerations) from remaining topography and applied height thresholding to isolate the topmost regions of protruding elements. They quantified by means of count, area, height and coverage and did not apply feature parameters specified in ISO 25178. They highlighted that feature-based characterisation requires knowledge of the specific manufacturing process and application in order to identify relevant features and developed a tailored extraction process. Due to the need for application-related inputs, feature-based approaches are referred to as "information-rich" characterisation [100, 104].

Thompson et al. worked on correlating surface features and internal porosities of Ti-64 EBPBF parts [102]. For this purpose, they used surface data from CSI to measure the weld tracks and xCT to identify pores. They linked wider weld tracks to lower porosity.

Struzikiewicz and Sioma [101] applied watershed segmentation with a pruning threshold of $5\%Sz$ (as suggested by the standard) to metal AM samples with machined surface finish. They used the feature parameters Spd (density of peaks), Spc (arithmetic mean peak curvature), $S5v$ (five point pit depth), Sda (mean dale area) and Sdv (mean dale volume) alongside common height-based parameters from ISO 25178. However, they did not use feature characterisation on as-built AM surfaces in this study. They investigated the formation of surface cracks caused by the machining process. Regarding surface texture parameters, they concluded that it is useful to generate multiple parameters and interpret them in context. They further noted that, for their application, parameters from the areal and volumetric material ratio curves contain more useful information than Ra/Sa and Rz/Sz.

Lou et al. applied both, morphological and robust Gaussian regression filters to separate melt tracks on one EPBF and LPBF top surface, each. After, they used watershed segmentation to identify and extract powder particle agglomerations (in their work referred to as "globules"). They generated roughness and waviness parameters from the surfaces after removing attached powder particles as well as the density of extracted particles on the surfaces. In their work, they state that both, traditional and novel characterisation parameters need to be studied in order to link surface properties with AM processing and resulting part functionality. Regarding the characterisation of metal PBF process-specific features, they concluded that research into the definition of appropriate thresholds is indispensable [19].

3.3. Mechanical Properties of LPBF-processed AlSi Alloys

Publication 3 includes a literature review on mechanical performance with focus on LPBF AlSi7Mg0.6 parts. A brief summary of this review is included subsequently, as well as an overview of additional relevant work with focus on the effect of LPBF process parameter modifications.

Especially the alloys AlSi10Mg, AlSi12 and AlSi7Mg are classified as "highly printable" [51]. In as-built condition, ultimate tensile strength (UTS) values between 300 and 450 MPa are found in literature [1, 26, 29, 31, 32, 51, 105–110]. The LPBF-processed AlSi7Mg0.6 alloy was found to exceed the mechanical performance of the material in as-cast condition. This is attributed to the typical fine microstructure resulting from fast cooling rates [1, 51, 53].

With regard to tensile strength of AlSi alloys, the influence of different heat treatment strategies has frequently been investigated [24, 26–32, 37]. However, for many aerospace, automotive, medical and other applications, resistance to periodic loading is required. In their textbook "Materials Science and Engineering", Callister states that about 90% of all metallic failures are related to fatigue [111]. Considering fatigue properties, where surface texture plays an important role [1, 7, 22, 85], the effects of surface post-processing [33–36, 39, 41, 44, 112–114] and positioning on the build platform [37, 38] were studied by various authors. Though, surface post-processing does not necessarily improve fatigue performance, as found by Aboulkhair et al., as milling can open up pores if the subsurface material quality is insufficient [33].

A few additional studies (i.e. not included in Publication 4) focussing on part quality modification by adjusting AM processing parameters are summarised below:

The effect of build orientation and post-processing on fatigue and tensile behaviour was investigated by Beevers et al. [83]. Amongst others, they looked into the effect of as-hatched (i.e. only hatch scan, also "net-shaped") vs. the application of an additional contour scan for AlSi10Mg. However, their focus was on mechanical and microstructural properties and they post-processed both conditions, as-hatched samples and samples with additional contour scan, by vibratory polishing. They found that their as-hatched samples exhibited more near-surface porosities than after an additional contour scan.

Beretta et al. [85] examined the effect of build orientation on rotating bending fatigue for AlSi10Mg. They found that horizontally built specimens show the best fatigue properties among the tested samples and concluded that fatigue life prediction applying the maximum total profile height Rt led to overestimation as compared to experimental data.

Gockel et al. [22] investigated contour scan variations for Inconel 718 material from LPBF and linked decreased values of Sa and Sv with increasing laser power. They attributed this to the larger melt pool. They also observed the tendency of increased fatigue life for decreased Sv and noted that, in their study, Sa did not correlate with fatigue performance. They acknowledged the issue of accessibility for post-processing tools for complex AM geometries and consequently identify internal surface roughness as likely cause for fatigue failure of such parts.

4. Measurement and Data Post-processing

Key Question:

"Under which conditions do surface texture measurement systems based on different physical working principles produce reliable, representative and comparable data for metal AM surfaces from LPBF?"

This chapter is on the measurement and processing of metal additive surface data obtained from optical instruments. In the following, pitfalls during the preparation of data for the generation of surface texture parameters are discussed and a user-oriented approach is taken.

To accommodate accessibility of the results, in Publication 1 *Comparison of Optical and Stylus Methods for Surface Texture Characterisation in Industrial Quality Assurance of Post-Processed Laser Metal Additive Ti-6Al-4V*, optical measurements from laser scanning confocal microscopy (LSCM) and fringe projection (FP) are compared to results from stylus profilometry. The latter is current industrial practice for surface texture measurement. During this first work it became apparent that, due to shadowing effects, LSCM data for the as-built surface condition were the most complex to handle. That is why Publication 2 *Post-processing of Surface Topography Data for As-built Metal Additive Surface Texture Characterisation* covers the data acquisition and post-processing for this method.

Publication 1	*Comparison of Optical and Stylus Methods for Surface Texture Characterisation in Industrial Quality Assurance of Post-processed Metal Additive Ti-6Al-4V*
Type	Peer-reviewed journal article
Status	Published
Submitted to	*Materials*
Publication 2	*Post-processing of Surface Topography Data for As-built Metal Additive Surface Texture Characterisation*
Type	Peer-reviewed journal article
Status	Published
Submitted to	*Journal of Additive Manufacturing Technologies*

Summary – Measurement and Data Post-processing

In Publication 1 *Comparison of Optical and Stylus Methods for Surface Texture Characterisation in Industrial Quality Assurance of Post-processed Laser Metal Additive Ti-6Al-4V*, results from the widely known and industrially established stylus method are compared with results from optical systems. The benefits and drawbacks of fringe projection (FP), laser scanning confocal microscopy (LSCM) and stylus profilometry are discussed and compared with regard to the methods' applicability to metal additive surfaces in as-built and wet-chemically processed conditions. The reasoning behind considering both – as-built and post-processed conditions – is, that for load bearing applications, the surface quality often plays a significant role. Wet-chemical methods are under investigation by big players in the aerospace industry to achieve this desired quality, and hence the need for appropriate methods to investigate those surfaces arises. However, Publication 1 explicitly aims at the evaluation of the applicability of characterisation methods rather than the assessment of the surface-enhancing post-processing methods. The qualitative results of the method comparison are presented in Table 4.1.

Operator-centred Method Comparison

While being the most time consuming and requiring the highest level of operator skill, **Confocal Microscopy** offers high resolution non-contact areal measurement. The method is suitable to evaluate profile as well as areal parameters and the representative areal data acquisition supports the reproducibility of measurements. Quantitative effects of measurement and data processing settings are covered in Publication 2.

The investigated **Fringe Projection** system was easier to operate regarding measurement setup and post-processing. The larger field of view (FoV) of the instrument allowed for covering large areas, simplifying the reproduction of measurements. The resulting mean roughness Ra was lower than for LSCM (approx. -20%) and stylus profilometry (approx. -15%), where the method's larger data point spacing was a contributing factor.

Stylus Profilometry is a commonly known and established method in academia and industry to characterise surface texture. The measurement procedure and instrument characteristics are completely standardised, which is advantageous in quality assurance (QA) and part qualification processes. Furthermore, handheld devices are inexpensive and fairly easy to operate, making the method accessible to a wide range of users. However, the contact measurement might compromise the investigated surface and is limited to profile measurements, which are hardly reproducible.

In conclusion, all three methods under consideration produce valid and comparable results when properly processing optical data and applying the same bandpass filters. However, the process-specific surface features of as-built as well as wet-chemically-processed LPBF surfaces are better represented by areal data. The extensive application of optical systems in research and industry requires education and guidance of users. Considering the selection of parameters, the well-known Ra and Rt as well as their areal equivalents Sa and Sz are hardly capable of characterising those

specific features and might even misrepresent the surface under investigation. More suitable options, standardised and non-standard, are explored in Publications 3 to 6.

Table 4.1.: Summary - Comparison of confocal microscopy, fringe projection and stylus profilometry for metal AM surface texture characterisation

	Confocal microscopy	**Fringe projection**	**Stylus profilometry**
Acquisition time	very long – large z-range required to capture entire evaluation length in one measurement	short – larger FOV, stitching of few images for full evaluation length	long (multiple individual line measurements necessary, restricted tip movement due to surface features)
Lateral / spatial resolution	high	sufficient	sufficient
Representative surface coverage	yes	yes	no
Linear / areal parameters	both	both	linear
Standardisation	listed as suitable method	listed as suitable method	fully standardised (instrument, data processing, parameters)
Physical principle	optical/non-contact; layering of in-focus z-data	optical/non-contact; pattern projection, triangulation	contact measurement
Surface damage	no	no	possible
Detection of re-entrant features	no	no	no
Reproducibility	medium/high – localisation of small area portions is possible but challenging using macroscopic markers	high – large area portions can been measured and located by means of macroscopic markers	low – individual lines unlikely to be located when repeating measurement, surface may be influenced by first (contact) measurement
Measurability	good	good	restriction of tip movement (powder particle agglomerations, craters), limited z-range (handheld devices)
Operator skill	high level of proficiency required to select measurement settings appropriately and perform data processing	medium high level of proficiency required to select measurement settings appropriately and perform data processing	handheld devices are easy to use, process is fully standardised, alignment of multiple (parallel) measurements is highly difficult
Operator effort	medium/low – complex initial setup, automated measurement	low – fairly straightforward initial setup, automated measurement	labor-intensive – every location has to be selected and measured individually (for handheld devices)

Effect of Selected Data Acquisition Settings in LSCM

Publication 2 *Post-processing of Surface Topography Data for As-built Metal Additive Surface Texture Characterisation* focusses on the effect of selected data acquisition and post-processing settings on areal surface texture parameters. Amongst others, the impact of adjusting the measurement's z-range Δz is investigated. This scenario represents a stitched measurement of a curved sample with large Δz across the region of interest, visualised in Figure 11 and 12. It is demonstrated that the Δz variation in fact has an impact on the occurrence of spike artefacts and, consequently on the resulting number of measured points after outlier removal. Furthermore, the effect of interpolating points on calculated areal parameters is investigated.

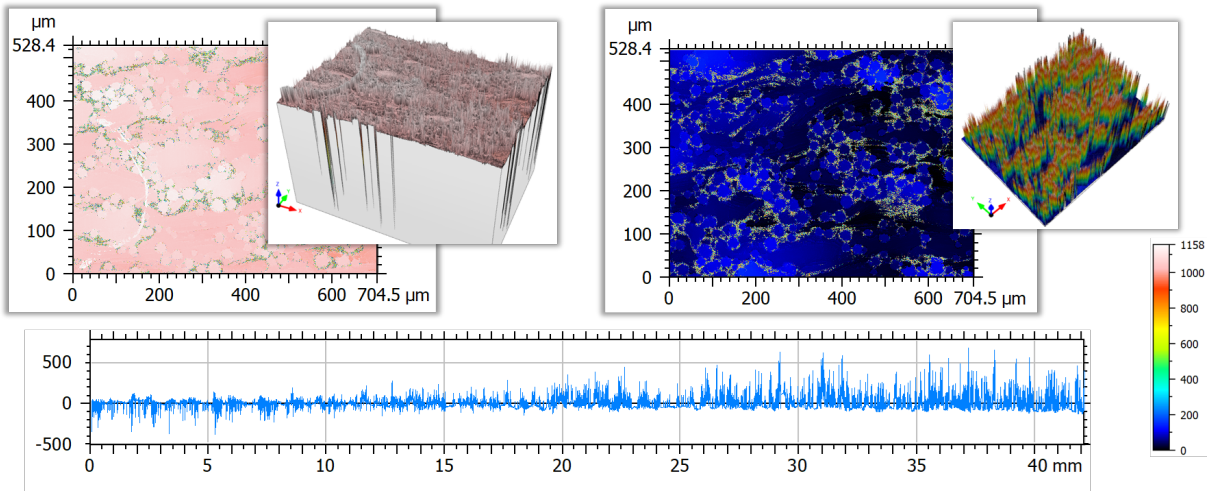

Figure 11.: As-built surface: Height distributions of left (0 mm) and right (42 mm) images from LSCM measurement showing spike artefacts along particle boundaries *(top)*; LSCM profile data after form removal, showing spike size variations along the measured profile for one full evaluation length *(bottom)*

The largest effect amongst the investigated aspects was observed from measuring with different Δz. The reason for addressing this issue is the possibility of large delta z variation across the region of interest for as-built LPBF samples, as demonstrated in Figure 11. Calculating surface texture parameters without data post-processing resulted in a difference in Sq (root mean square height) and Sz (maximum total z-height) of nearly 40%. The parameters from the material ratio curve showed to be more robust against extending the measurement z-range: core height Sk varied by 12%, the reduced valley depth Svk by 4%.

Effect of Selected Data Post-processing Settings in LSCM

The used data evaluation software *MountainsMap® Expert* offers three different outlier removal strength settings - soft, normal and strong - which lead to a ratio of non-measured points (NMP) of roughly 15%, 20% and over 30%, respectively. Considering the $\Delta z = 229$ µm data set, the interpolation of NMP as compared to not filling the NMP results in deviations of up to 11% for Sq, Sk and Svk. The interpolation doesn't affect the extreme value Sz. Contrary to the

other parameters, Svk increases when interpolating points - due to the interpolation, material is added in the core portion of the material ratio curve, resulting in a flattened main slope (i.e. a decreased Sk) and increased extreme values.

This publication highlights the importance of data post-processing and careful consideration of measurement settings when taking optical areal measurements. The interaction of typical LPBF as-built surfaces and optical measurement systems (in this case, LSCM) significantly impacts the raw data results. While optical systems have the clear advantage of providing an areal, more statistically significant representation of a surface as compared to stylus profile measurements, data post-processing requires a higher level of expertise.

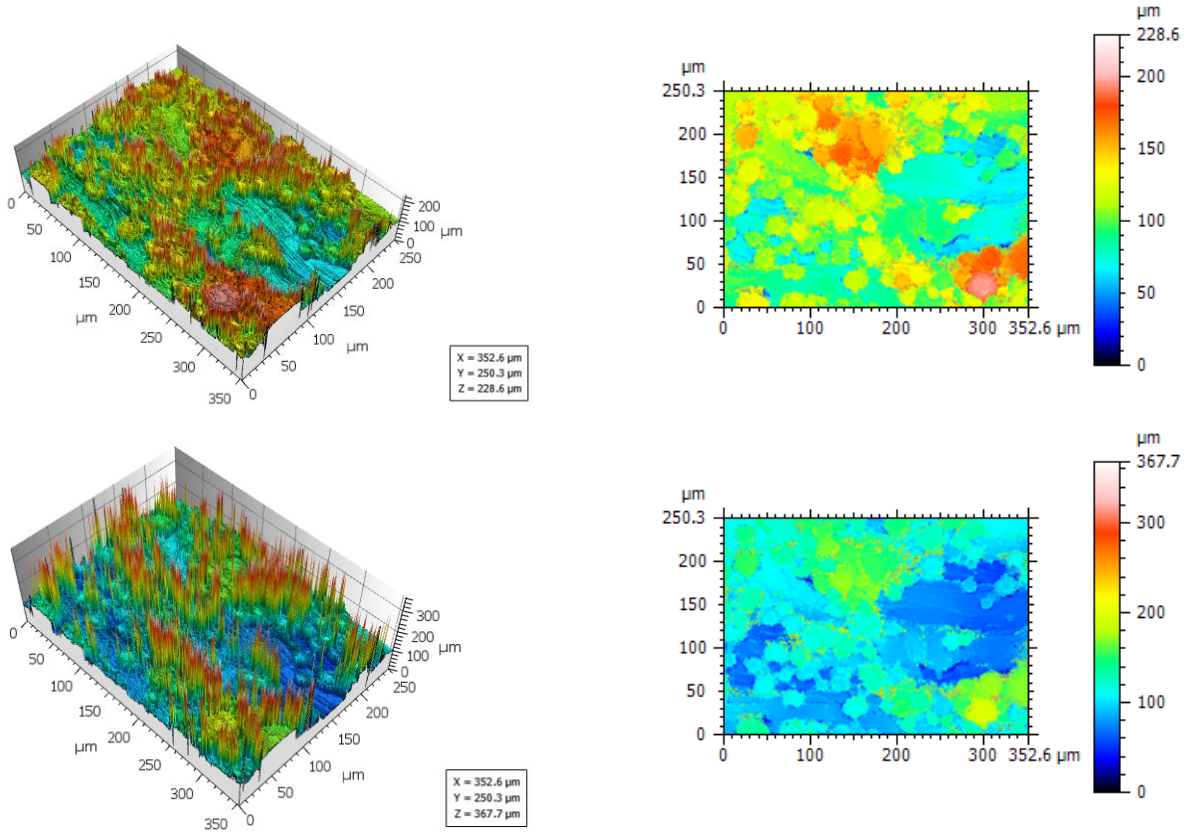

Figure 12.: As-built surface: Spike size with variation of pre-selected measurement z-range from LSCM. $\Delta z = 229\ \mu m$ *(top)* , $\Delta z = 368\ \mu m$ *(bottom)*. Spike size is increased with larger pre-selected z-range

5. Surface Texture and Mechanical Properties

Key Question:

"How can the interaction between processing, resulting part quality and part functionality for metal AM parts from LPBF and their surfaces be described?"

In this following chapter, the creation of distinctive as-built surfaces with consistent bulk material quality (i.e. the bulk material is manufactured with identical hatch scan parameters and combined with different contour scan parameters) is addressed, to investigate the relationship of surface quality and mechanical performance. The results from the previous Chapter 4 were applied by employing the fringe projection (FP) method to obtain surface data and generate surface texture parameters.

Publications 3 *Influence of Contour Scan Variation on Surface, Bulk and Mechanical Properties of LPBF-Processed AlSi7Mg0.6* and Publication 4 *Surface Texture and High Cycle Fatigue of As-built Metal Additive AlSi7Mg0.6* discuss the contour parameter optimisation, the characterisation of resulting surfaces and mechanical testing (tensile and fatigue performance). The focus is on the investigation of the interaction of processing parameters, surface texture and mechanical performance.

Publication 3	*Influence of Contour Scan Variation on Surface, Bulk and Mechanical Properties of LPBF-Processed AlSi7Mg0.6*
Type	Peer-reviewed journal article
Status	Published
Submitted to	*Materials*
Publication 4	*Surface Texture and High Cycle Fatigue of As-built Metal Additive AlSi7Mg0.6*
Type	Peer-reviewed journal article
Status	Published
Submitted to	*Journal of Additive Manufacturing Technologies*

Summary – Surface Texture and Mechanical Properties

The ultimate aim of the study presented in Publications 3 *Influence of Contour Scan Variation on Surface, Bulk and Mechanical Properties of LPBF-Processed AlSi7Mg0.6* and Publication 4 *Surface Texture and High Cycle Fatigue of As-built Metal Additive AlSi7Mg0.6* was to create as-built surfaces performing well enough in fatigue testing to omit additional surface-enhancing processing steps. This is especially significant for inner surfaces, but is just as much a potential time-saver in the metal AM value chain in general. The following chapter presents investigations of specimens from AlSi7Mg0.6 material.

Bulk Properties

After an initial parameter study focussing on material density, the hatch parameter set producing the best density was paired with different contour scans, presented in detail in Publication 3. In the following step, the influence of the variation in contour scan on the bulk material properties was determined by means of Archimede's density measurements and subsequently confirmed by tensile testing. This was necessary as the contour scan also partially remelts the bulk material and dominantly defines the properties of the near-surface zone. The measured **density** values were **above 99%** for all samples.

Regarding tensile strength, the deviation between samples of the same surface condition shows the tendency to be higher for coarser surface structure. A possible explanation is the lower line energy. Due to the fast heat dissipation and high reflectivity of aluminium alloy powder material, the melt pool size is irregular, causing a larger height variation on the surface and thus, a coarser surface texture. However, the seven as-built conditions tested for tensile strength performed equally well as or even better than specimens manufactured of the same material in the same build direction [26, 30, 37, 115], with mean **ultimate tensile strength (UTS) between 374 and 406 MPa**. The results suggest that the tensile strength is largely defined by the hatch scan and is hence a bulk property. The influence of the contour scan on the UTS is considered negligible for this study. However, microstructural properties may be affected. This topic will be subject to future work.

Surface Texture

After confirmation of the negligible impact of varied contour scan on bulk properties, the surface texture was assessed. Initial visual inspection validated that surface texture of varying quality was achieved, visible in Figure 13. The general trend is toward a coarser appearing surface structure for higher scan speed (i.e. lower energy input on the contour). Comparing simple contour scan and pre-sintered (i.e. the contour is pre-scanned with 50% of the chosen laser power, before the actual contour scan at full laser power) conditions, for sets A to F, the pre-sintered conditions seem slightly smoother. Conditions G to J are not distinguishable from purely visual indicators, however, numerically, arithmetic mean height Sa as well as core height Sk are significantly larger (by about 50% on Sa mean values) on I and J surfaces than on the G

and H groups. Also, numerically, pre-sintered and simple scan conditions don't show a significant variation.

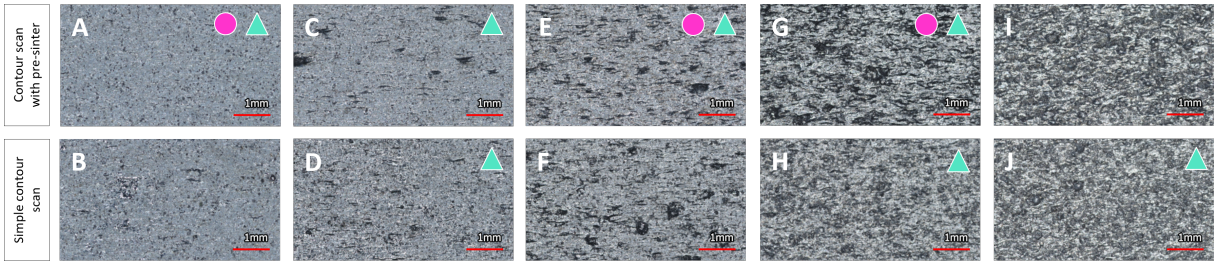

Figure 13.: Microscopic images of samples with resulting surface quality from contour scan variation study, from lowest (left) to highest (right) scan speed; △ denote tensile tested contour parameter sets, ◯ mark fatigue tested sets.

The final selection for mechanical testing surface groups were the following:

- Smooth surface parameter sets A, C (both with additional pre-sinter) and D (simple contour)
- Original parameter set E (additional pre-sinter)
- Coarse surface parameter sets G (additional pre-sinter) and H (simple contour)
- Very coarse surface parameter set J (simple contour)

These were selected to have a large variety of smooth/coarse and pre-sintered/simple contour sets for comparison of the respective effects. Tensile testing was performed on all of the listed groups (UTS between 374 and 406 MPa), fatigue testing was conducted for A, E and G samples (with contour pre-sinter). Fatigue testing and data evaluation on the remaining contour groups will be covered in future work.

Fatigue Testing and Endurance Limit Estimation

As expected, the smoothest surface condition, A or AsB-smooth, achieves the very best fatigue performance (i.e. highest number of cycles to failure) among the tested sets across all tested load levels. The same tendency is reported in studies including post-processed surface conditions [34, 36, 39, 41, 44, 113]. In Figure 14, the increased scatter of number of cycles to failure for the group E (AsB-medium) and G (AsB-rough) samples is visible. A possible interpretation is that for those conditions, the higher load levels are already in the non-linear low-cycle regime, where the logarithmic-linear relationship of load and cycles is no longer valid [116]. This is because the tested load levels were defined in terms of the UTS, which was comparable for the three tested conditions. However, as opposed to the UTS, fatigue performance is heavily affected by the surface quality (i.e. rougher surfaces typically withstand a lower number of cycles to failure than smoother surfaces).

From the tested data, the endurance limit was estimated based on the horizon method, employing a logarithmic-linear equation [116]. The stress at endurance limit σ_L was calculated for $N_{L1} = 10^6$,

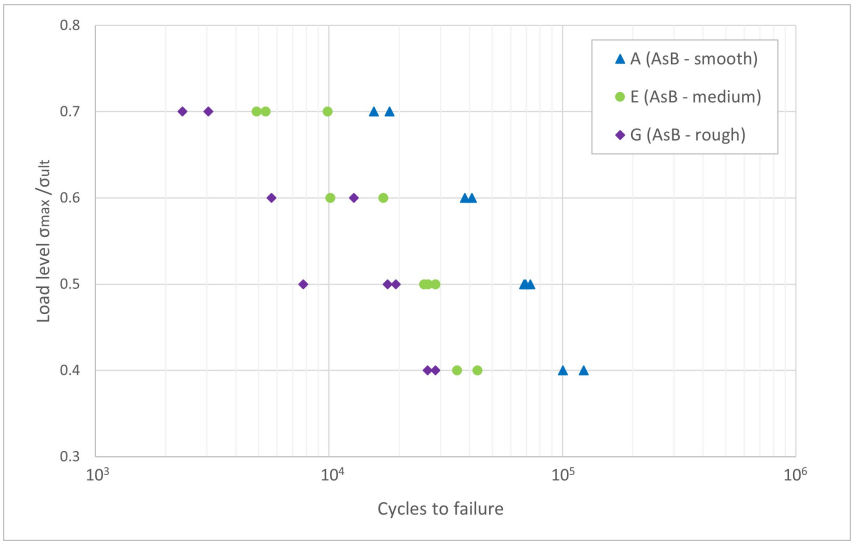

Figure 14.: σ – N curve for surface conditions A (AsB-smooth), E (AsB-medium) and G (AsB-rough), reference stress UTS = 392 MPa

$N_{L2} = 2 \times 10^6$ and $N_{L3} = 10^7$, visualised in Figure 15. The given endurance limits were selected based on literature to facilitate comparison.

With $\sigma_{L2,E}$ = 49 MPa, condition E matched the experimentally determined endurance limit for as-built conditions by Denti and Sola [34], as well as those found by Gatto et al. [36]. The same studies investigated post-processed surfaces. The $\sigma_{L2,A}$ = 68 MPa of condition A corresponds with the limit stresses reached by their laser shot processed and metal shot peened (S70) samples. In comparison to conventionally manufactured AlSi7Mg0.6 material from investment casting with $\sigma_{L1,cast}$ = 73 MPa [117], the group A samples performed 15% better with $\sigma_{L1,A}$ = 84 MPa.

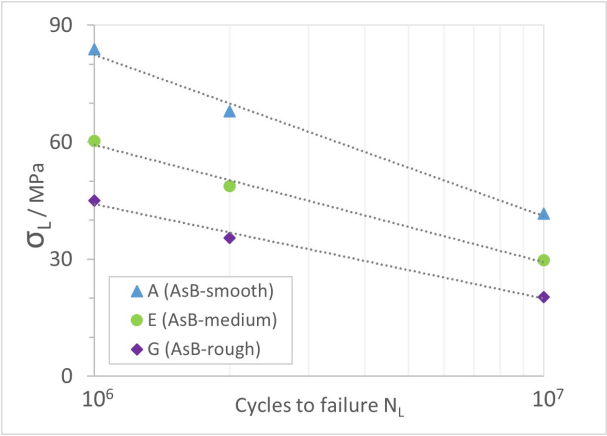

Figure 15.: Estimated stress for different endurance limit values N_L

Surface and Fatigue

In literature on the correlation of surface texture and fatigue performance of metal PBF processed materials, the surface texture parameters generally used are the arithmetic mean profile height

(Ra/Sa), the maximum profile height (Rt/Sz), mean maximum profile height (Rz) and maximum valley depth (Rv/Sv). In Publication 4, it was shown that especially on rougher as-built surfaces (i.e. E and G in this study), crack initiation often starts from multiple locations on the surface (indicated in Figure 16). Note that in contrast to literature, even the rougher surface conditions in this study are comparatively smooth.

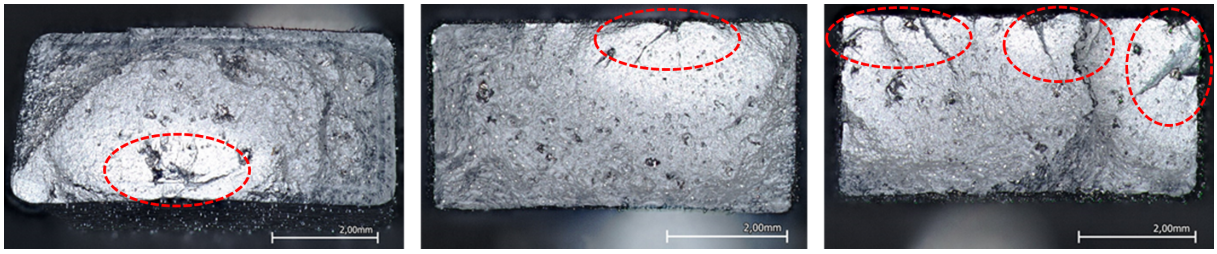

Figure 16.: A / AsB-smooth *(left)*: Crack propagation from bulk defect, E / AsB-medium *(middle)*: Crack propagation from surface defect, G / AsB-rough *(right)*: Crack propagation from multiple surface defects

50% of the tested group E samples and 100% of group G samples experienced crack initiation from multiple surface defects. Only one out of nine group A (AsB-smooth) samples exhibited multi-crack-initiation, and 2 out of 9 samples showed crack propagation from internal defects. This suggests that for general (i.e. non-optimised) LPBF as-built surfaces, crack initiation from multiple surface defects is likely.

Considering the typically stochastic, irregular as-built surface quality of LPBF parts and taking into account the observed failure modes, it seems improper to apply individual extreme values such as Rt/Sz or Rv/Sv to describe surfaces with regard to fatigue prediction. These parameters represent the maximum height difference within the measured region (Rt and Sz) or the maximum valley depth (Sv), respectively. However, it does seem natural that cracks start from valleys (or pits) and hence, the use of surface valley properties would seem reasonable. Therefore, it is suggested to employ the Svk parameter from the material ratio curve. It is a standard parameter from ISO 25178 (with an equivalent 2D parameter definition in ISO 21920) and is, just as

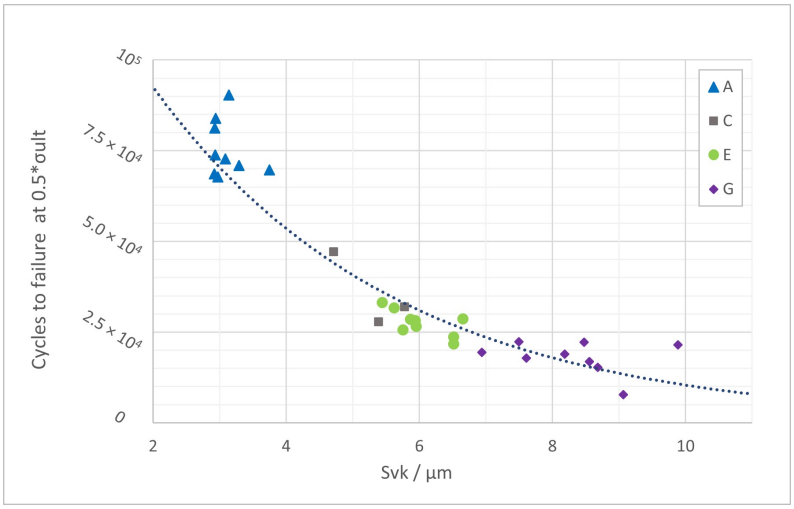

Figure 17.: Exponential fit Svk vs. cycles to failure at $0.5\sigma_{ult}$

those common parameters mentioned previously, based on height variation within the measured surface area. Though, it does comprise information on the entire valley population across the measured area and hence appears to be more suitable to describe as-built LPBF surfaces in regard to fatigue performance, bearing in mind the largely observed multi-surface-crack-initiation mode.

In Publication 4, it is demonstrated that the experimentally determined number of cycles to failure at load level $0.5\sigma_{ult}$ (=0.5UTS) across the investigated surface conditions show a better exponential fit with Svk than with Sv. Figure 17 from Publication 3 displays the exponential fit for all experimental and factorised fatigue data at load level $0.5\sigma_{ult}$.

A surface description taking into account relevant surface features for fatigue prediction will lead to a more accurate indication of failure and will ultimately enable more adapted designs of AM parts. In the spirit of continuous improvement of processes and applications, the use of Svk in already existing fatigue prediction models can be a first step toward the adaption of those models to include a more comprehensive understanding of AM surface quality.

6. Areal Surface Features

Key Question:

"Can the description of metal PBF surfaces be improved by using process-related inputs to surface texture characterisation?"

This Chapter discusses possibilities on improved surface description as compared to Chapter 5, by applying the watershed segmentation method and a circle detection algorithm in attempts to extract LPBF-process-specific surface features. The results are published in Publication 5 *Feature parameters for Metal Additive Surface Texture Characterisation* and Publication 6 *Surface Features of As-built Metal Additive AlSi7Mg0.6.*

The novelties of the research presented in this Chapter are firstly, the application to a batch of multiple specimens from the same processing conditions and secondly, the selection of thresholding values for both, watershed segmentation and circle detection, based upon the powder particle size distribution. The use of process-related inputs to surface texture characterisation has potential to provide an improved surface description, closer to the "real" surface, as compared to surface texture parameters solely based on height variations.

Note that this summary is more elaborate than in the previous chapters. This is due to Publication 5 being published in German.

Publication 5	*Feature parameters for Metal Additive Surface Texture Characterisation*
Type	Peer-reviewed conference paper
Status	Published
Presented at	*40. DGM Werkstoffprüfung, October 2022, Dresden (Germany)*
Publication 6	*Surface Features of As-built Metal Additive AlSi7Mg0.6*
Type	Conference paper, preprint
Status	Preprint
Presented at	*17th ECSSMET, March 2023, Toulouse (France)*

Summary – Areal Surface Features

In the previous parts of this dissertation, surface texture characterisation using parameters based on height variation was discussed in detail. Particularly the parameters derived from the material ratio curve, *Sk* (core height), *Svk* (reduced valley depth) and *Spk* (reduced peak height) proved to be useful in regard to fatigue properties, as presented in Chapter 5.

However, the specific nature of metal additive surfaces from LPBF calls for new approaches to describe surface topography. A promising concept is the characterisation based on areal surface features, as it has the potential to give more comprehensive information on the considered topography required for intended applications [18].

Jiang et al. suggested the following definition of a *surface feature*: *"A point, continuous line or contiguous portion of a surface topography, which bears a particular meaning (i.e. semantic interpretation) of the surface being investigated[18]"*. This definition includes the general categories included in ISO 25178, namely hills and dales (as also used in geography), but also process-specific features (i.e. for metal PBF: Powder or spatter particles, weld tracks, layers, ...).

This following summary will focus on the application of surface feature characterisation to the AlSi7Mg0.6 specimens introduced in Chapter 5.

Important terms in the context of features characterisation are hills, dales, peaks, pits, course lines, ridge lines and saddle points:

- **Hills** are protruding features. The highest point on a hill is called its **peak** and from every point belonging to the hill, there is an upward path toward the respective peak.
- A Hill feature is enclosed by a **course line**, which is where the surface slope changes its direction.
- **Dales** are receding features, **pits** are their lowest points. There is a downward path toward the pit from every point of the dale.
- A dale feature is enclosed by a **ridge line**.
- The intersections of ridge and course line are called **saddle points**.
- The height difference between a peak or pit and its closest saddle point defines the **feature height/depth**, i.e. the difference between the highest saddle point on a course line and the corresponding peak, or between the lowest saddle point on a ridge line and the corresponding pit.

In Publication 5, conventional and feature parameters from ISO 25178 are evaluated for the surface conditions AsB–smooth (A), AsB–medium (E) and AsB–rough (G) to demonstrate the potential of feature-based characterisation and the effect of Wolf pruning (also: height pruning) thresholds.

In order to compute feature parameters, the first step to be taken is the segmentation of the surface. In Publication 5, watershed segmentation is used. Depending on the desired application, segmentation based on hill or dale features can be selected. E.g. hill features may play a role as contact or wear zones, while dale features, depending on shape, may have an impact on crack initiation under cyclic loading. A brief introduction of the necessary steps from segmentation to parameter computation is given subsequently.

Step 1 – Watershed Segmentation Based on Hill or Dale Features:

Based on the hill and dale features described previously, watershed segmentation can be applied. A useful illustration of the process is that of flowing water drops. A drop starting from the peak or any point on the hill will always move downward to a point on the course line. Similarly, from any point on the ridge line and within the dale, water will flow down toward the pit. The depth of a dale is then the height difference between the pit and the lowest point on the ridge line, where the water would flow to the adjacent dale first.

Step 2 – Combination of Small Features by Wolf Pruning:

Considering every single hill or dale by the above definition may lead to over-segmentation, as even the smallest height variations would be detected as individual features. To overcome this issue, Wolf pruning can be applied. The process is explained using the concept of the "change tree", illustrated in Figure 18 (bottom). In a change tree, each saddle point (S) and the peaks (P) and pits (V) of the adjacent hill and dale features are recorded and connected (see Figure 18, bottom). Looking at dale features, the lowest saddle point on the ridge line defines the respective height. Using, again, the water analogy, the lowest saddle point is where a dale being filled with water would overrun first. When selecting a pruning threshold, every feature smaller than this threshold is merged with its neighbouring larger feature, as visualised in Figure 18. Saddle points are eliminated and hills or dales are connected to the next higher order saddle point in the tree. Figure 18 shows the elimination of saddle point S_2, when the pruning threshold exceeds the value of d_1. Subsequently, the pit V is connected to S_3 and the new feature depth d_2 is defined. This process is repeated until all features exceed the given threshold value. The result is a trimmed, or "pruned", change tree (see Figure 18, bottom right).

Step 3 – Computation of Surface Feature Parameters:

Once the surface features on the scale of interest are identified, parameters can be evaluated. For hill and dale features, a number of parameters representing their respective geometric properties are defined in ISO 25178 [16]. These properties include feature height, equivalent diameter, density, shape related parameters and others.

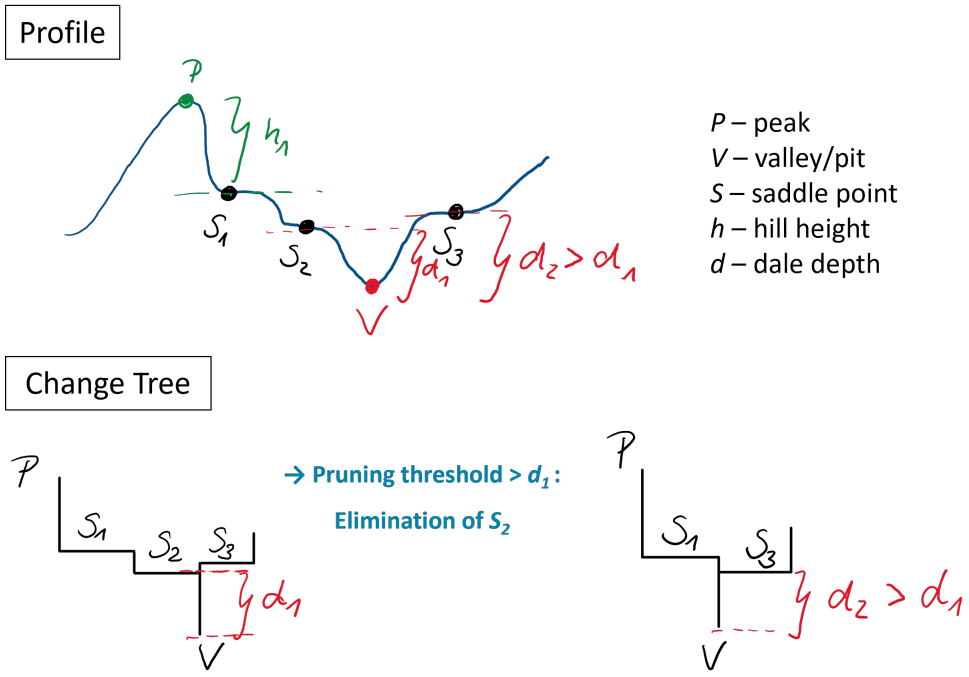

Figure 18.: 2D profile *(top)* and change tree *(bottom)*: Elimination of saddle points by Wolf pruning

Effect of Pruning Threshold on Surface Feature Parameters

After this brief introduction to watershed segmentation and Wolf pruning, an overview of the results presented in Publication 5 will follow subsequently.

The ISO 25178 surface feature parameters considered in Publication 5 are *Svd* (density of pits), *Sdd* (mean local dale depth) and *Sded* (mean equivalent dale diameter). *Svd* simply expresses the number of pits/dale features per unit area. *Sdd* is defined as mean value of the dale depth (height difference between the lowest saddle point and the corresponding pit, as described for the Wolf pruning process) for all dales within the considered region of interest, and *Sded*, the mean diameter of a circular projected feature area of equivalent size for all considered dales.

For reference, *Sa* (arithmetic mean height) and *Sz* (maximum total height) are computed. *Sz* is also relevant since ISO 25178 suggests the pruning threshold to be defined as a percentage of *Sz*.

An obvious and expected observation from the data is that surfaces with a coarser structure are characterised by higher *Sa* and *Sz* values. It is especially notable that *Sa* and *Sz* are similar for the AsB–medium and AsB–rough samples. This is the case specifically for the individual samples evaluated in Publication 5.

The pruning value suggested in the standard is 5% *Sz*. However, it is recommended to adjust the value according to the specific application.

Thus, the effect of 5%*Sz* and 10 %*Sz* pruning value on the selected feature parameters is investigated. For each surface condition, one sample is considered. The parameters and prun-

ing values are visualised in Figure 19 and corresponding numerical values are included in Table 6.1.

Table 6.1.: Results for selected surface feature parameters

Parameter	AsB-smooth		AsB-medium		AsB-rough	
Sz / µm	55.50		125.00		140.00	
Sa / µm	2.74		4.54		5.49	
Pruning	5% Sz	10% Sz	5% Sz	10% Sz	5% Sz	10% Sz
Pruning / µm	2.78	5.55	6.25	12.50	7.00	14.00
Svd / 1/mm²	76.10	25.90	44.30	10.70	40.10	9.82
Sdd / µm	4.71	7.16	9.77	15.40	11.20	18.60
$Sded$ / mm	0.12	0.20	0.16	0.30	0.17	0.32

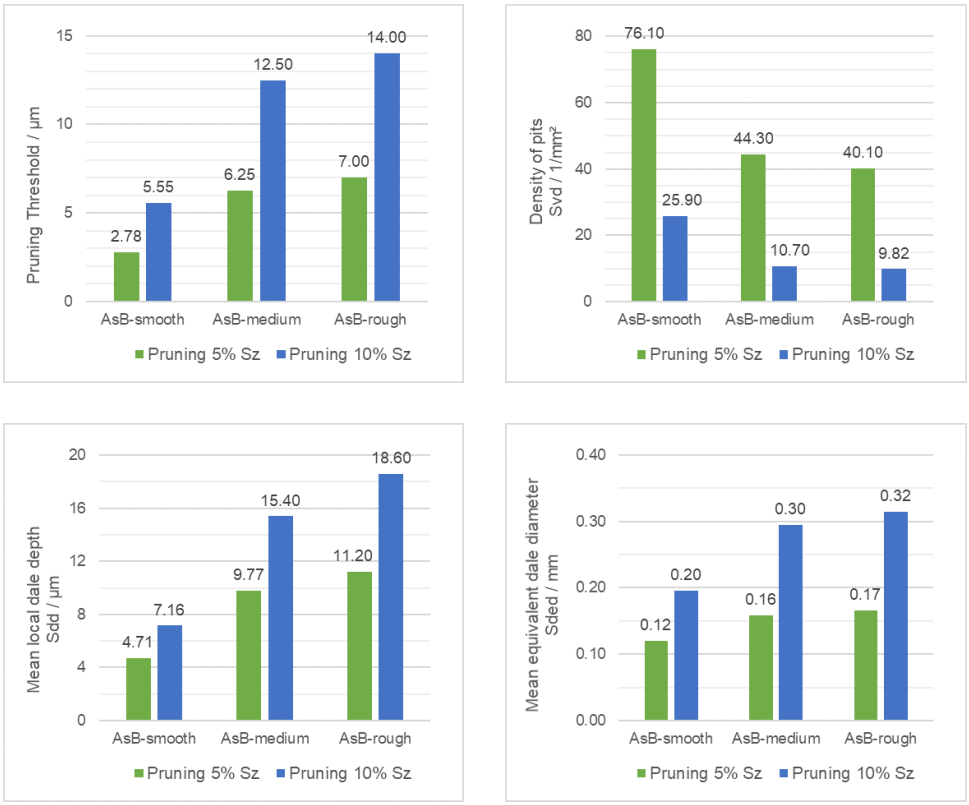

Figure 19.: Variation of pruning threshold *(top left)*, pit density *Svd (top right)*, dale depth *Sdd (bottom left)* and dale diameter *Sded (bottom right)* for three surface conditions

Comparing the resulting parameter values for thresholds 5%Sz and 10%Sz, the pruning threshold's big impact and importance is emphasised: Svd is reduced by about 2/3 for the higher value (i.e. when more features are combined).

The feature parameters are strongly dependent on the applied pruning threshold. It is observed that the pit density Svd (Figure 19, top right) decreases for rougher surfaces for both pruning thresholds (5%Sz and 10%Sz). This is due to the threshold being set depending on the extreme value Sz. The lower Sz value for AsB–smooth causes a higher degree of segmentation. This results in a higher pit density Svd. However, the dale features counted on the AsB–smooth surface are far shallower than for the other surface conditions, as can be recognised by the Sdd values. The larger thresholds (defined w.r.t. %Sz) for coarser surfaces lead to a lower Svd, as

more dales are combined. The dale depth *Sdd* (Figure 19, bottom left) becomes larger for rougher surfaces and is larger for the larger threshold value per surface condition. *Sded* (Figure 19, bottom right) hardly differs for AsB–medium and AsB–rough at the same threshold percentage and is slightly smaller for AsB–smooth in comparison. This suggests that the applied conditions generate feature segmentations with similar lateral size.

Revisiting the fact that the pruning threshold is defined with respect to Sz: The presented results demonstrate a clear disadvantage of Sz and Wolf pruning based on $\%Sz$. The parameter represents one extreme value within the measured area. It may lead to misinterpretation of results and can also be compromised by measurement artefacts, as discussed in Publication 2. Therefore, other options to define more suitable pruning thresholds are to be explored. Also Lou et al. concluded in their work on characterisation of PBF surfaces, that research into the definition of thresholds is needed [19].

Selection of a Pruning Threshold with Physical Relevance

To overcome the $\%Sz$-issue, the search for a physically relevant definition of the pruning threshold began. After analysing potentially relevant material and processing factors, the particle size distribution of the used AlSi7Mg0.6 powder was selected as basis for the threshold definition.

Publication 6 includes results on hill-based and LBPF process-specific feature characterisation, and their comparison with height based parameters from ISO 25178. The investigated samples were manufactured with optimised LPBF parameters (see Publication 3) from AlSi7Mg0.6 material. These samples with the presented surface condition were referred to as *"AsB–smooth"* or *"A"* in previous chapters.

From microscopic visual inspection, particle agglomerations (mostly individual) were identified as the predominant process-specific surface features. This justifies the use of the particle size distribution of the processed powder to define the pruning threshold.

The threshold value is defined based on d10 = 27 µm. The d10 value represents the maximum diameter of the smallest 10% of particles present in the used powder. The pruning threshold applied to the data presented subsequently was set to 13.5 µm, which is equal to half the d10 diameter. This value was selected based on the assumption that an attached particle will mostly have negative impact on mechanical properties if more than half of it is above the surface, causing an undercut (see Chapter 1, Figure 4) and a possible crack initiation location.

Generation of Feature Parameters from ISO 25178 – Hill-based Segmentation

Figure 20 shows the 3 mm by 6 mm region of interest for one sample, segmented applying the watershed method based on hill features. (+)'s indicate the highest point of each segment, colours are used for visual differentiation of the segments. The selected height pruning threshold of

13.5 µm causes segments less high than half the d10 diameter ($d10 = 27\mu m$) to be merged with adjacent hill segments. Table 6.2 lists all surface texture parameters generated in Publication 6 as well as their brief description. Note that the value of $Svd = 0.06$ mm^{-2} in this case is equal for all evaluated samples due to the total valley count of one over the entire (3 × 6) mm^2 area.

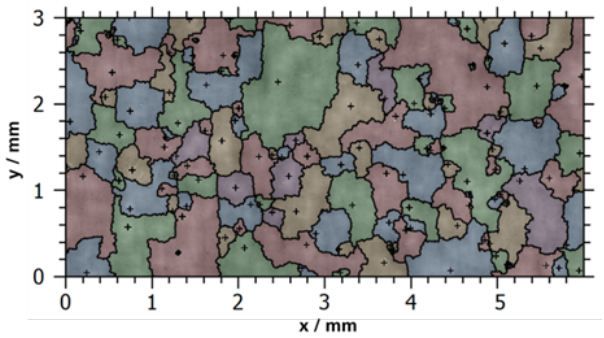

Figure 20.: Example (AsB–smooth sample): Watershed segmentation with height pruning threshold 13.5 µm; (+): highest point per segment.

Table 6.2.: Overview of height-based parameters (L-filter 0.25 mm) and feature-based parameters (height pruning threshold 13.5 µm): Generated values, mean and standard deviation (SD), and description

Parameter / Unit	**Mean**	**SD**	**Description**
Sz/µm	61.74	7.68	Maximum total height of profile
Sa/µm	1.76	0.11	Arithmetic mean height of profile
Sk/µm	4.87	0.23	Core height
Spk/µm	5.21	0.90	Reduced peak height
Svk/µm	2.12	0.13	Reduced valley depth
Spd/mm^{-2}	10.10	3.48	No. of peaks per unit area
Svd/mm^{-2}	0.06	0.00	No. of valleys per unit area
Shh/µm	22.39	1.42	Mean local hill height
d_{max}/µm	27.74	1.87	Average max. particle diameter
z_{max}/µm	33.64	4.19	Average max. particle z-height
Area covered/%	1.35	0.28	Particle coverage
Particle density/mm^{-2}	21.80	5.68	No. of particles per unit area

Generation of LPBF-specific Feature Parameters – Agglomerated Powder Particles

Particle agglomerations in this particular investigated case were detected applying the commercially available software tool *MountainsMap® Expert* for circular feature detection from height data. Diameters between 20 µm and 200 µm, the smaller diameter being of the order of magnitude of d10, the bigger one representing roughly triple the d90 to account for clustered attachments. In analogy with d10, d90 is the largest diameter of 90% of the powder particles. Again, a height pruning value of 13.5 µm is applied so that smaller features are combined. However, this is only the case for adjoining or overlapping features, meaning, features smaller than 13.5 µm are only merged, if in direct contact. This is why also smaller features might be detected.

In preparation of the particle extraction, an L-filter of 0.0055 mm was applied to the surface data from focus variation microscopy (FV), resulting in images like Figure 21. This very small L-filter value is chosen in order to extract sharp edges, such as particle boundaries from "more than half" particles. "Sharp edges" in this case refers to the intersections of the line of sight and the boundary of particles forming re-entrant features, as shown in Figure 4 (left). The "map of particles" detected in this S-L surface (Figure 21, right) was then reapplied to the original height map (after outlier removal, form removal, S-filter).

Various geometric properties and statistics of these properties of detected particles can be calculated. In this particular case, d_{max}, the largest diameter of a detected particle (hence, at its equator = spherical particle diameter), and the z_{max}, the maximum z-value of a particle (i.e. its peak), show mean values about the d10 size. Note that additional data processing steps are specified in Publication 6. All details will be disclosed in an upcoming publication (in preparation).

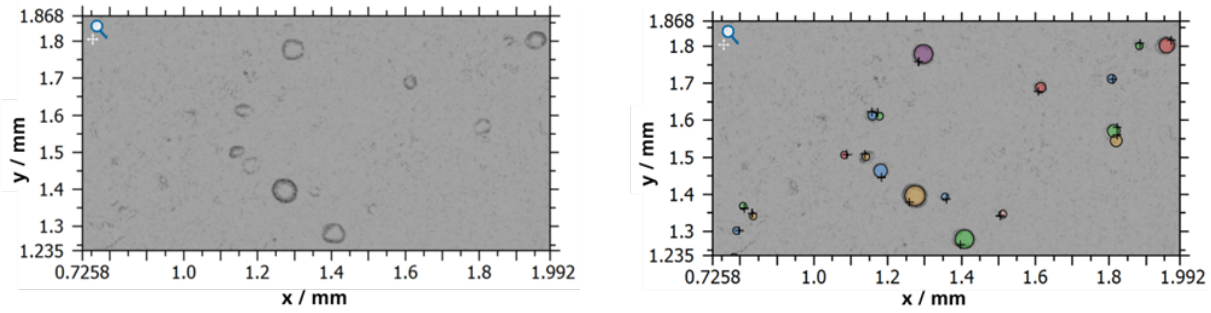

Figure 21.: Example (AsB–smooth sample): Circle detection, min. diameter 20 µm, max. diameter 200 µm; Extracted area with (near) circular features (*left*), Detected circular features (same area, *right*)

Comparison of Selected Feature-based and Height-based Parameters

As mentioned before, the dominant observable features for this surface condition are attached powder particles. These particles are protruding features. Considering the most common surface texture parameters among those investigated, Sa and Sz, this information is not provided, as they only give an average or maximum height value. The material ratio curve, however, includes an Spk approximately twice as high as Svk, clearly indicating the predominance of the protruding surface portion. Hence, the material ratio curve supplies more information than the typical Sa and Sz, although it is also just height-based.

The feature parameters calculated after watershed segmentation also clearly support the visual observation – dale-based vs. hill-based segmentation result in $Svd = 0$ and $Spd \approx 10$, respectively.

Looking at the detection of process-specific features, circular particles with a mean size around the d10 diameter were detected. The limit values were set to $20\ \mu m\ <\ d10$ and $200\ \mu m\ \approx 3 \times d90$. However, the maximum detected feature size was of the order of magnitude of d90, suggesting that, at least for the larger powder particle sizes, individual attachments are formed rather than

clusters. Comparing the maximum particle z_{max} to Sz, it is recognised that both values are very close. E.g. on sample I, $(Sz)_I = 67.71\ \mu m$, $(z_{max})_{I,max} = 67.9\ \mu m$ and $(d_{max})_{I,max} = 70.97\ \mu m$. All three values being very similar confirms again that the particle attachments are dominantly determining of the height variation.

It is also observed that a large portion of the particle attachment sizes are close to the lower limit of the predefined range. This makes sense, as smaller particles require less heat to get attached. E.g. from the size distribution of particles on sample I in Figure 22, it is retrieved that 61% of the detected particles are smaller than $d10 = 27\ \mu m$ and 96% are smaller in diameter than $d50 = 50\ \mu m$. Regarding height, 37% of the particle attachments are below d10 and 91% are smaller in height than d50.

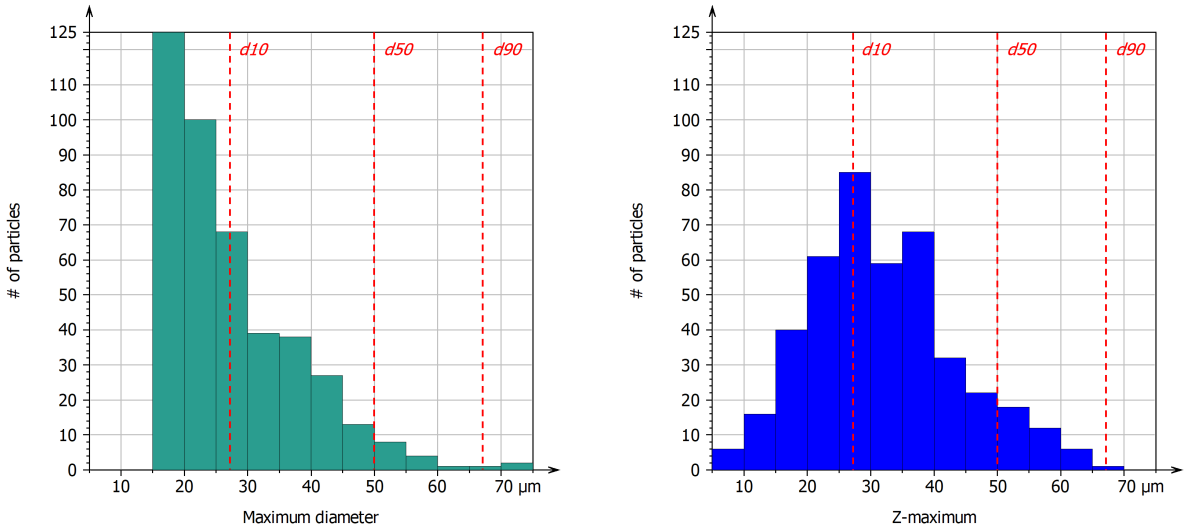

Figure 22.: Distribution of particle sizes (Sample I), represented by d_{max} *(left)* and z_{max} *(right)*, for a total # of particles of 426; red dashed lines mark the $d10$, $d50$ and $d90$ values from the size distribution of the processed powder

Feature-based methods for surface texture characterisation require the most amount of information as input (which is why it is sometimes referred to as "information-rich" [104]), but also delivers the most specific output in regard to the characterisation of process-related features. This is why it will help researchers to gain a deeper understanding of the relationships of used materials, processing parameters and resulting properties. Future work will include the investigation of correlations between feature-based surface texture parameters (ISO 25178 and process-related) and part functionalities, such as fatigue, and the exploration of different process- or material-related inputs to define meaningful pruning thresholds to gain more realistic surface descriptions for various (LPBF-)materials.

7. Synthesis – Conclusions and Future Prospects

The main objective of this thesis is the development of novel approaches to tailored surface texture characterisation of metal AM parts from LPBF and thus to contribute to the overarching goal of gaining a more comprehensive understanding of LPBF manufactured surfaces and their behaviours under cyclic loading. Such surfaces generally exhibit attachments of partially melted powder particles, spatter or weld tracks. The formation of those characteristics is mostly defined by the used powder material and processing conditions (including numerous factors, as discussed in Section 3.1).

The presented work was subdivided into the following key questions:

1. Under which conditions do surface texture measurement systems based on different physical working principles produce reliable, representative and comparable data for metal AM surfaces from LPBF?
2. How can the interaction between processing, resulting part quality and part functionality for metal AM parts from LPBF and their surfaces be described?
3. Can the description of metal PBF surfaces be improved by using process-related inputs to surface texture characterisation?

The coverage of these key questions distinguishes this work from other doctoral research projects. While a lot of remarkable work on the advancement of AM is done across the globe, hardly anyone has access to so many elements of the metal PBF value chain. The immediate access to processing (AM machine and powder material), surface measurement systems, mechanical testing systems and surface texture characterisation, created unique prerequisites for this project, enabling a holistic point of view on AM part quality and its characterisation. A visual summary is provided in Figure 23. The schematic includes title, main activities and generalised outcomes for Chapters 4, 5 and 6, from top to bottom.

This final chapter summarises the main results, contributions to the state of the art, implementation in industrial practice, and limitations and future work. It concludes with an outline of future prospects in a more generalised context.

7.1. Main Results

Chapter 4 *Measurement and Data Post-processing* addresses the first of those questions. The established stylus method and corresponding 2D line profile characterisation are inappropriate to describe the stochastic, inhomogeneous nature of metal AM surfaces from LPBF. This is due to statistical limitations, potential surface damage, and other drawbacks. Using optical systems, such as fringe projection (FP) or confocal microscopy (CM), allows for capturing statistically more relevant portions of surfaces without surface contact (and damage), and enables 3D characterisation. In Chapter 4, it was demonstrated that the extraction of 2D profiles and

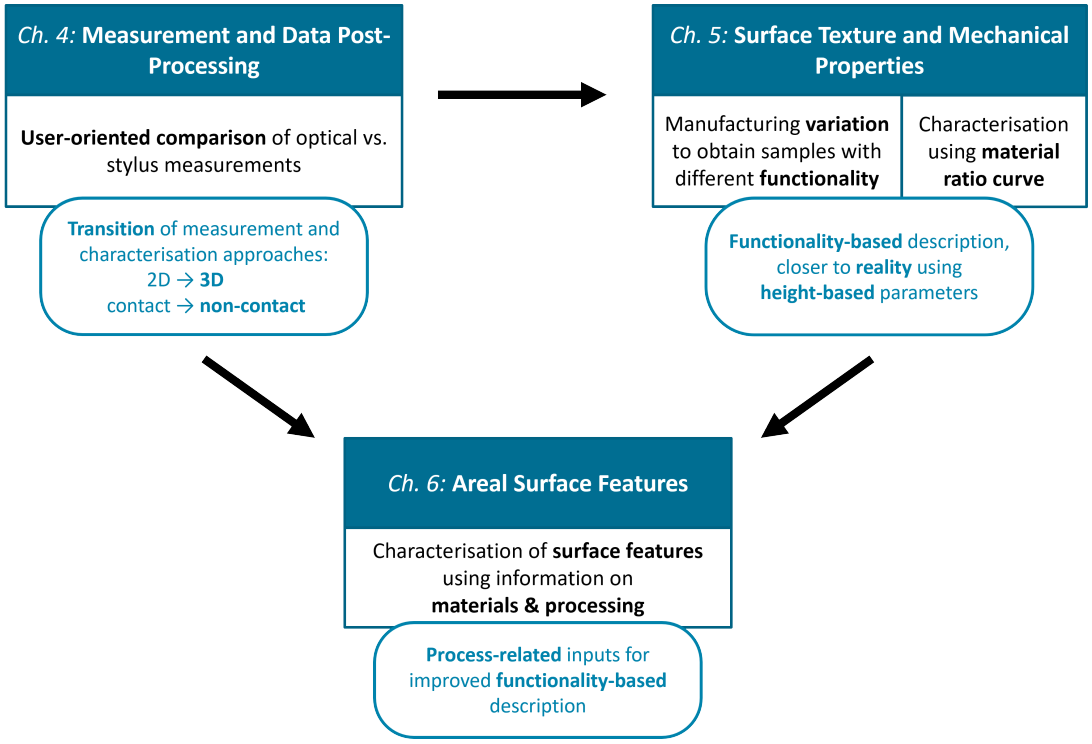

Figure 23.: Schematic overview of the advancements by this thesis: Title, main activities, generalised outcomes *(boxes top to bottom)* and interconnections of Chapters 4 to 6

generation of related surface texture parameters from optical measurement data compares well with stylus results. When data post-processing is performed properly, areal surface data from the two assessed optical methods are reproducible and comparable. Thus, the presented results justify the transition from stylus to optical measurements. Accordingly, the evolution from linear to areal surface texture characterisation is facilitated and its necessity is demonstrated (for metal PBF and selected post-processed surfaces in particular).

Chapter 5 *Surface Texture and Mechanical Properties*, focussing on the second question, revolves around two main topics: The generation of high quality as-built surfaces to omit the surface processing step from the value chain and the exploration of suitable parameters to link surface quality and fatigue performance. As intended, high-quality as-built surfaces were successfully manufactured from the employed AlSi7Mg0.6 material. The produced samples even outperformed surface-processed and conventionally manufactured parts. From fatigue testing, it was confirmed that especially rougher as-built surfaces (while "rougher" in this study is still relatively smooth as compared to surface conditions found in literature) experience crack initiation from multiple surface defects. This failure mode is well described by the *Svk* (reduced valley depth) parameter from the ISO 25178 material ratio curve. It represents the depth of the valley population within a measured region of interest.

Chapter 6 *Areal Surface Features* discusses the third and final question of this work to obtain a more accurate, holistic and functionality-based description of metal PBF surfaces. Feature-based characterisation does not solely focus on height variations on the surface, but enables the evaluation of various geometric properties (e.g. height, enclosed volume, projected area, surface area) of topography elements (e.g. hills, dales, particles). This characterisation method requires

areal data, and is hence connected to the findings of Chapter 4. To determine the relevant feature size, an approach using height pruning based on the particle size distribution of the used powder has been developed. It was demonstrated that resulting mean values for both, ISO 25178 feature parameters as well as process-specific feature characteristics, can be linked with the powder particle size distribution.

7.2. Contributions to the State of the Art

Chapter 4 provides the foundation of this thesis. It demonstrates the validity of optical measurements in the context of current industrial practice. Furthermore, potential pitfalls during measurement and processing of areal data from optical instruments are highlighted. A recently published milestone in metal PBF surface texture measurement is the ASTM "Standard Guide for Additive Manufacturing of Metals – Powder Bed Fusion – Measurement and Characterisation of Surface Texture"[80, 118], which provides guidance on measurement and filtering of profile and areal data, aligned with ISO 21920 and ISO 25178, respectively. Chapter 4 contributes a practice-oriented complement – a practical guide. It also stresses the importance of adapting characterisation processes when advancing manufacturing techniques, applying state-of-the-art measurement technology. The demonstrated comparability of 2D surface texture parameters from contact and non-contact measurements paves the way for the implementation of areal characterisation in industrial QA processes. It encourages and assists the development of part qualification processes using optical methods and areal surface texture parameters.

The outcomes of Chapter 4 are directly relevant to the users of surface texture measurement instruments (contact and non-contact) in academia and industry. The use of areal surface data is especially applicable for highly specialised/high-performance components manufactured by advanced manufacturing techniques. Even though standards on areal characterisation and optical methods are being developed and improved (e.g. ISO 25178, ASTM F3637), the transition from profile to areal characterisation in qualification processes requires the connection to existing practice. The ability to produce reproducible results from different measurement methods will not only enable the definition of part qualification processes in industry, but also the comparability of results from academic research, where not all users of optical instruments are aware of the associated challenges. The comparability will speed up the general advancement of AM and other advanced manufacturing technologies by allowing for meta-analysing results from different research groups in relevant fields around the world. While particularly the statistical limitation of 2D profiles was evident prior to the conceptualisation of Chapter 4, the systematic and application-based demonstration of the comparability of results from optical methods to stylus profiles, as well as major points of attention when processing optical data, will aid the advancement of their use and provides a basis for the development of practical guidelines.

The main advancement in the field of functionality-based characterisation for fatigue by Chapter 5 is the proposition of the reduced valley depth Svk, as it is representative of the commonly observed LPBF crack initiation from multiple surface defects. Regarding the optimisation of contour scan parameters, not only smooth surfaces as compared to other studies using AlSi7Mg0.6

material were produced, but also did they achieve competitive fatigue performance. This suggests that LPBF process optimisation can reduce the overall processing steps by making surface post-processing unnecessary. This is, however, still depending on materials, specific applications and qualification processes. In order to establish the application of AM parts with as-built surface condition, qualification processes have to be developed accordingly.

The Chapter 5 contributions have relevance for academic research and industrial research and applications. While it was expected to find a better representation of the observed surface quality by using the standardised parameter Svk, finding that it also provides an improved representation of the observed failure mechanism suggests a new direction for LPBF fatigue prediction. It requires the adaption of failure prediction models to effectively utilise the improved representation.

Regarding the improvement of surface quality by process adaptation, this topic has not yet been studied for many LPBF alloys. Currently, surface post-processing of metal AM parts and the related improvement of mechanical properties is a popular research topic. The opportunity to circumvent this step by process optimisation may cause a shift in research focus. While the improvement of fatigue performance with optimised as-built surfaces was to be expected, the competitive properties compared to post-processed and conventionally manufactured parts is a particularly promising finding.

Chapter 6 directly builds on the results from Chapters 4 and 5: Using the opportunities opened up by areal characterisation and the need for a more accurate, functionality-oriented description of AM surfaces led to the exploration of feature-based methods. The use of process-related inputs for this feature-based characterisation in order to define meaningful parameters by means of tailored pruning threshold selection is explored. The aim is to obtain characterisation parameters which reflect reality as closely as possible. In the presented case, using the powder particle size distribution as input for height pruning was found to produce good results regarding the detection of surface-attached particles. This marks a first milestone toward a more generalised recommendation of pruning threshold definitions for metal PBF surfaces. These findings provide a sound starting point for the investigation of metal PBF surfaces made from other materials or analysing different process-related inputs.

Chapter 6 presents an innovative concept, that will ultimately impact the industrial applications of AM and other advanced manufacturing processes with specialised surface quality and purposes. For the time being, it is mostly relevant to academic research, as further investigations on process-related definition of pruning thresholds is needed. Publications on the application of feature parameters to AM surfaces are still scarce, though a few studies with focus on segmentation algorithms exist. To the knowledge of the author, the connection between processing conditions and the definition of pruning thresholds in feature-based characterisation has not yet been addressed in published work. The concept is an original development of this doctoral research project. For highly specialised applications of AM and other advanced manufacturing components, tailored surface texture characterisation based on the proposed concept will become increasingly relevant to describe surface quality in a functionality-based context.

Continuous advancement of tailored surface texture characterisation plays a major role in understanding process-structure-property correlations of AM components. The presented approaches to the measurement and description of LPBF surfaces in regard to part functionality will ultimately enable an expanded and more sophisticated application of metal AM across various industrial branches.

7.3. Implementation in Industrial Practice

The structure of this thesis also provides a road map to implementation of improved surface characterisation methods in industrial part qualification processes. A very suitable quote in this regard is by Mark Twain: *"Continuous improvement is better than delayed perfection."* A first step toward improvement is the utilisation of optical methods, to achieve data more statistically representative of a surface. In the same category is the transition from 2D to 3D parameters. Even a shift from Ra to its areal equivalent Sa represents progress. The following step can be the implementation of standardised areal parameters to assess suitability for the required functionality. The example presented in this work is the use of Svk to account for the observed LPBF crack initiation from multiple surface defects. The adoption of Svk might not be the ultimate solution, though it is more exact than the use of individual extremes such as Sv and Sz. Other applications, e.g. coating or adhesion, might require different approaches. Much closer to a comprehensive description is feature-based characterisation. However, methods need to be developed and inputs need to be defined more clearly to gain acceptance and establishment in common practice.

7.4. Limitations and Future Work

While many important findings and opportunities were summarised previously, it is important to give a brief overview of this work's limitations and suggest directions for future work.

Practical limitations of this research project include the limited number of samples that were investigated and the availability of optical measurement instruments and mechanical testing systems. Time and budget constraints required a selection of analysis methods (e.g. the impact of contour scan variations on the near-surface microstructure is to be investigated in a future student project). The restrictions on lab work and international travel during the Covid-19 pandemic also influenced the project schedule and test matrix.

Beyond those practical limitations, there are also conceptual and technological constraints which are addressed in the following.

Even though optical measurements allow for areal characterisation, those measurements are limited to line-of-sight. Hence, AM-typical undercuts are not detected. Furthermore, optical methods are restricted with regard to access to internal surfaces. xCT can provide means to overcome those limitations. However, xCT machines and measurements are expensive, time-consuming and require a high level of expertise. Addressing the issue from a process-stability

point of view, meaning, that certain manufacturing conditions reliably and reproducibly lead to a specified part quality, will enable a design freedom to further improve load bearing and other functionally critical parts. Reproducible part and surface quality will eliminate the need for exhaustive inspection of inner surfaces (i.e. inspection of random samples will suffice) and optimisation of process parameters will aid reducing re-entrant features caused by particle attachments.

Another direction to assess undercuts can be the analysis of optical surface data considering shadowing effects on the surface, as suggested in Chapter 6. However, this will strongly depend on the chosen method and/or specific instrument type.

Considering functionality description (in this work the surface-fatigue relationship), the exploration of alternatives to current practice is ongoing. In Chapter 5, it was demonstrated that the direct correlation with the reduced valley depth Svk from the material ratio curve produced a good (exponential) fit. However, this conclusion is limited to the assessed material, powder type, AM machine, parameter combination and many more specific conditions. The adaption and development of generic prediction models is crucial to advance AM and the implementation of AM parts into (safety) critical systems. Also the functionality-based description in relation to other applications, i.e. adhesion, corrosion, coatability, bioactivity and many more, requires work to find and/or define appropriate surface quality and corresponding characterisation parameters.

As mentioned before, especially interesting regarding novel approaches to surface description is feature-based characterisation, as discussed in Chapter 6. While in literature, often individual samples are investigated to introduce and demonstrate concepts, this work features multiple samples of the same surface condition, analysed using a defined methodology. However, only one surface condition with manufacturing optimised for contour was examined. The initiation and continuous extension of a universally accessible AM surface data base for all users to benefit from is desirable. This will provide a good basis for the development of good practice and standardisation in the future to facilitate introduction to industrial practice. In an ongoing publicly funded project in the aerospace sector, work on the exploration of process-based inputs to feature-based characterisation for two high-strength aluminium alloys is included. In close collaboration with manufacturing experts, relevant defining factors within the processing chain are investigated and applied to assess surface features. Also the impact of contour scan strategy on microstructure is being investigated.

Even though standards exist and are being expanded and improved, a gap between academic knowledge and industrial practice remains. A planned project (currently at the proposal stage) on knowledge transfer will include the conceptualisation of an application-based training on surface measurement and characterisation practice, including the information provided by the new ASTM F3637 “Standard Guide for Additive Manufacturing of Metals – Powder Bed Fusion – Measurement and Characterisation of Surface Texture” [80, 118] in conjunction with the findings of this doctoral research project. In addition, the project will cover the development of methods to easily determine whether existing measurement systems are suitable for measurements on specific AM surfaces, depending on users’ requirements.

7.5. Future Prospects – The Big Picture

A more exact, functionality-based description of AM surfaces impacts the entire AM value chain. Enhancements in surface characterisation enable a more accurate prediction of functional performance, e.g. fatigue or adhesion. It also provides valuable feedback for the improvement of manufacturing parameters, especially with respect to contour scan adjustment to obtain predefined surface characteristics (e.g. smooth surfaces). The definition of functionality-based surface quality requirements is useful for designers to determine tolerances, directional dependencies and part placement in the build chamber. In consequence, safety factors on AM parts can be reduced and more lightweight parts can be designed.

When optimising contour scans, surface-enhancing post-processing steps can be reduced or omitted entirely, resulting in a shorter processing chain, cutting overall processing time, cost and greenhouse emissions. The geometrical freedom is extended as no accessibility by processing tools has to be taken into account.

Considering transportation or other powered operations, due to the weight savings on the final part, fuel consumption is reduced, lowering the total greenhouse emission during an AM part's operational lifetime [3, 119]. Users across industries will benefit from those advancements of AM technologies. Not only will aerospace and automotive industries be affected, but also medical applications (e.g. tailored prosthetics will become more affordable).

Thus, improving surface texture characterisation will lead to making manufacturing and operation of components across all relevant sectors more accessible and sustainable. This will expand the prospects for application of AM in various fields.

A. Full-length Publications

A.1. Publication 1 – Surface Texture Characterisation for Industrial Applications[1]

Abstract: Additive manufacturing technologies enable lightweight, functionally integrated designs and development of biomimetic structures. They contribute to the reduction of material waste and decrease in overall process duration. A major challenge for the qualification for aerospace applications is the surface quality. Considering Ti-64 laser powder bed fusion (LPBF) parts, particle agglomerations and resulting re-entrant features are characteristic of the upper surface layer. Wet-chemical post-processing of the components ensures reproducible surface quality for improved fatigue behaviour and application of functional coatings. The 3D SurFin® and chemical milling treatments result in smoother surface finishes with characteristic properties. In order to characterise these surfaces, three methods for surface texture measurement (contact and non-contact) were applied, namely confocal microscopy, fringe projection and stylus profilometry. The aim of this work was to show their suitability for measurement of laser powder bed fusion as-built and post-processed surfaces and compare results across the evaluated surface conditions. A user-oriented rating of the methods, summarising advantages and disadvantages of the used instruments specifically and the methods in general, is provided. Confocal microscopy reaches the highest resolution amongst the methods, but measurements take a long time. The raw data exhibit large measurement artefacts for as-built and chemically milled conditions, requiring proper data post-processing. The stylus method can only capture 2D profiles and the measurement was restricted by particle agglomerations and craters. However, the method (process and instrument) is entirely standardised and handheld devices are inexpensive, making it accessible for a large group of users. The fringe projection method was the quickest and easiest regarding measurement and data post-processing. Due to large areal coverage, reproduction of location when performing repeat measurements is possible. The spatial resolution is lower than for confocal microscopy but is still considered sufficiently high to characterise the investigated surface conditions.

1. Introduction

The maturation of metal additive manufacturing (AM) technologies offers new opportunities for the aerospace industry. The dimensional freedom enables lightweight designs and development of biomimetic structures, contributes to the reduction of material waste and decrease in manufacturing process duration [2, 5, 120].

The titanium–aluminium–vanadium alloy Ti-6Al-4V (Ti-64) is a popular aerospace alloy and has various load bearing applications in airplane and satellite structures [121–124]. Therefore, it is also a common research material in metal additive manufacturing [2, 7, 15, 20, 49, 51, 125].

One of the most common metal AM processes is laser powder bed fusion. Typical features that may be observed on as-built surfaces include powder particle agglomerations, re-entrant features or weld tracks. The near surface region may exhibit open and closed pores. This characteristic quality imposes new challenges on surface topography measurements, part qualification and quality assurance (QA) processes.

[1] *Published as:* Buchenau, Theresa; Mertens, Tobias; Lohner, Hubertus; Brüning, Hauke; Amkreutz, Marc (2023): Comparison of Optical and Stylus Methods for Surface Texture Characterisation in Industrial Quality Assurance of Post-processed Laser Metal Additive Ti-6Al-4V. In: Materials 16 (13), S. 4815. DOI: 10.3390/ma16134815

Metal AM parts are particularly interesting for load bearing applications, where surface finish might be critical for part qualification, and manufacturing of complex geometries. Therefore, wet-chemical surface treatment methods, such as electropolishing and chemical milling, seem appropriate [14, 15, 112]. These methods also accommodate material removal to eliminate near surface defects.

In order to properly characterise as-built and post-treated parts, different methods for surface topography measurement can be applied. The most widely known and applied method is contact stylus profilometry, which captures 2D linear height profiles. In recent years, optical measurement systems are increasingly gaining acceptance and are attractive regarding areal characterisation to obtain a statistically more representative depiction of the surfaces considered [6, 81, 82]. In this work, the comparability of results from selected optical methods to those from the well-known stylus method is investigated and the applicability of the chosen measurement methods to as-built and post-treated AM surfaces is tested.

Previous studies found in the literature on comparison of measurement methods for application to AM parts focussed on multiple non-contact areal methods [58–60, 126].

Thompson et al. and Senin et al. compared coherence scanning interferometry (CSI), confocal microscopy (CM), focus variation (FV) and X-ray computed tomography (xCT). They looked into surface topography using data sets from the different measurement techniques for one as-built Ti-64 sample. That way they studied aligned profiles extracted from areal measurements, areal texture parameters and reconstruction of typical metal powder bed fusion areal features such as powder particle agglomerations, weld tracks and others, by those methods [59, 60]. De Pastre et al. applied the same measurement methods to characterise an as-built polymer powder bed fusion sample and additionally included stylus profiles. They found that computed profile texture parameters from stylus were lower than from non-contact methods [126].

Tato et al. used a combined CSI, CM and FV instrument and compared evaluated areal parameters for co-located data sets on one vertical and one horizontal as-built 316L surface. They found that the CSI measurement was the most time consuming. The variations for most computed areal texture parameters were below 8% [58].

Whip et al. used fringe projection and (destructive) cross section analysis to characterise multiple as-built Inconel 718 surface conditions and found that texture parameters from fringe projection did not accurately represent maximum valley depth. They attributed this matter to residual loose powder and shadowing effects from powder particle agglomerations [62].

This work aims to assess the applicability and comparability of the chosen surface texture characterisation methods when applied for quality assurance (QA). It is explicitly not intended to compare the data of identical locations to show the difference in profile measured by the selected methods, but to address challenges during a realistic QA process.

In addition to the as-built surface condition, post-processed Ti-64 AM samples are examined, namely chemically milled (ChM), electropolished by 3D SurFin (3DS) and a combined treatment (3DS+).

In 2017, Todhunter et al. published a survey on the use of profile and areal surface texture parameters in research and industry. They found that *Ra* (arithmetic mean height) and *Rt* (total maximum height) were still among the most frequently used parameters, especially in automotive, aerospace and product manufacturing [81]. The parameters are also applied in recent publications on metal AM surface texture, sometimes in combination with their areal equivalents, and are generally well known in research and industry [6, 38, 83–86].

Therefore, the arithmetic mean height *Ra* and maximum total height *Rt* are adopted in this paper to make the results accessible and comprehensible for a broad range of readers. Another

reason for choosing profile characterisation was to be able to include the widely familiar stylus profilometry method in the comparison.

2. Materials and Methods

This section includes a description of the evaluated samples with manufacturing and surface treatment steps (see Figure 24), information on the utilised surface topography measurement systems, measurement settings, data processing and evaluation steps.

2.1. Samples

Figure 24 summarises the steps of manufacturing, surface treatment and characterisation methods for the used samples, whilst the focus of this work is on surface texture characterisation. The characterisation methods are applied to four different surface conditions of Ti-64 samples from LPBF. Conditions under investigation are as-built (AsB), after chemical milling (ChM), after 3D SurFin® (3DS) and after combined 3D SurFin® and chemical milling (3DS+). Figures 25 and 26 show sample photographs and microscopic images, respectively, and sample sizes and surface conditions are given in Table A.1.

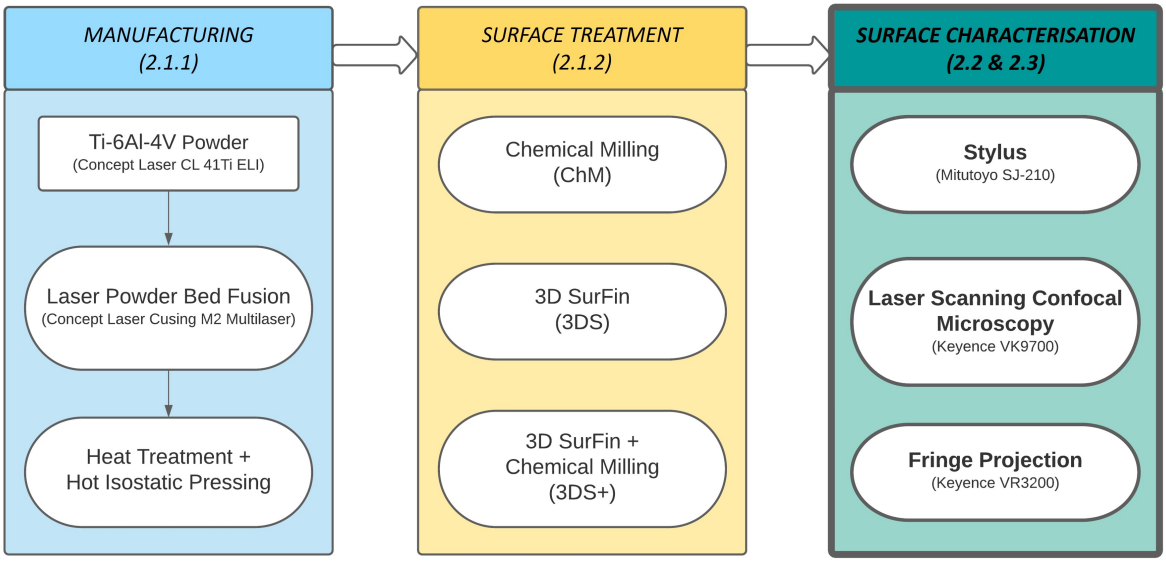

Figure 24.: Overview: manufacturing, surface treatment and surface characterisation of the evaluated samples. Surface characterisation (left box) is this work's focus; numbers indicate the corresponding sections

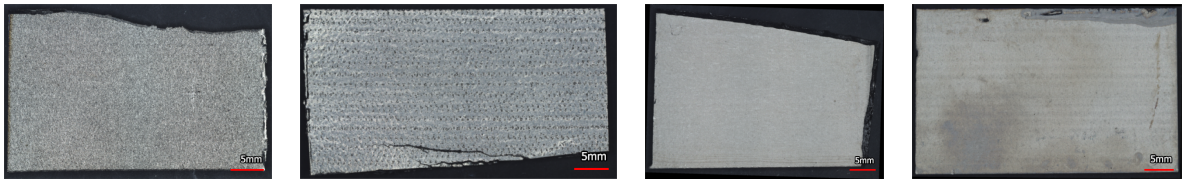

(a) (b) (c) (d)

Figure 25.: Sample photographs: (**a**) AsB—As-built surface condition; (**b**) ChM—after chemical milling treatment; (**c**) 3DS—after 3D SurFin® treatment; (**d**) 3DS+—after combined 3D SurFin® and chemical milling treatment

2.1.2. Manufacturing

The evaluated samples originate from a study on combined wet-chemical surface post-processing and were manufactured in an LPBF process on a Concept Laser Cusing M2 Multilaser using identical manufacturing parameters and Ti-6Al-4V powder (Concept Laser CL 41Ti ELI). After additive manufacturing, all samples were heat-treated for stress relief and hot isostatically pressed for bulk quality improvement.

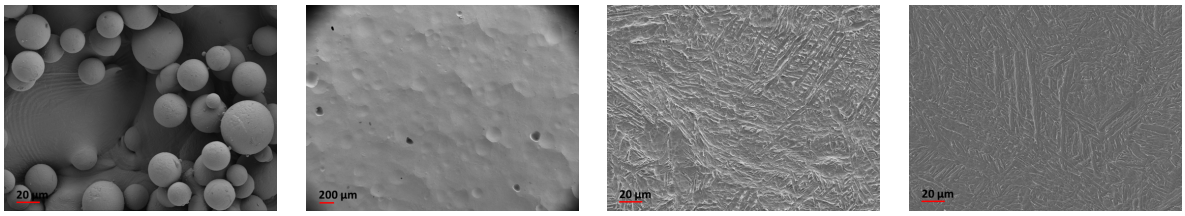

(a) (b) (c) (d)

Figure 26.: Images from scanning electron microscopy (SEM). (**a**) AsB—typical powder particle agglomerations; (**b**) ChM—characteristic craters from particle removal; (**c**) 3DS—etching marks after peak reduction; (**d**) 3DS+—etching marks, similar to 3DS

Table A.1.: Samples with corresponding surface conditions.

Sample	**Size (Approx.)**	**Surface Treatment**	**Duration**
AsB	42 mm × 25 mm	n/a	n/a
ChM	25 mm × 40 mm	Chemical milling	20 min
3DS	30 mm × 40 mm	3D SurFin®	15 min
3DS+	30 mm × 45 mm	3D SurFin® + Chemical milling	15 min + 20 min

2.1.3. Surface Treatment

Surface treatments applied to each of the evaluated samples are specified in Table A.1. The chemical composition of the bath and other specifics for both processes are summarised in Table A.2 [15]. Brief descriptions of 3D SurFin® and chemical milling processes are given subsequently. For detailed treatment process information, refer to [15].

3D SurFin®: The enhanced electropolishing process 3D SurFin® is a process specifically designed to remove peaks from a surface. It uses an electrolyte based on deionised water combined with ammonium fluoride, methylglycinediacetic acid and sulfuric acid and is operated at 80 °C [15, 127]. The water-based electrolyte enables the application of higher voltages (200–400 V), leading to a shorter process duration for the same material removal rate [128, 129].

Chemical Milling: Acidic etching baths for Ti-64 commonly consist of a mixture of distilled water, hydrofluoric acid HF and nitric acid HNO_3, which is the recommended standard according to ASTM B600 [130]. The actual material removal is caused by the hydrofluoric acid, reacting with the titanium oxide on the surface and forming titanium fluoride and hydrogen. The nitric acid HNO_3 acts as an oxidant and is responsible for bonding the atomic hydrogen [130, 131].

2.1.4. Macroscopic and Microscopic Visual Inspection

From visual and microscopic inspection, the as-built (AsB) surface shows characteristic powder particle agglomerations that are typical for LPBF surfaces (Figures 25 and 26), causing a high initial surface roughness [15, 132]. Figures 26 and 27 show these agglomerations of different sizes as well as resulting re-entrant features. The sample has a curvature (see Figure 28), which probably originates from residual stresses introduced during the manufacturing process.

Table A.2.: Applied surface treatments [15].

Treatment Process	**3D SurFin**	**Chemical Milling**
Temperature (range)/°C	80	55
Removal rate (range)/μm/min	8	12
Bath size/L	100	17
Bath components	NH_4F, H_2SO_4, $C_7H_8NNa_3O_6$ water based	HF, HNO_3 water based

After chemical milling (ChM) the surface exhibits craters and pits of various sizes and slopes (Figure 26). The linear pattern visible in the photo (Figure 25) corresponds to sequences of pits, similar to the one presented in Figure 29, supposedly originating from powder particles (as those present on the AsB surface) that were detached from the surface during the post-treatment process.

The 3DS sample was subjected to a 15 min 3D SurFin® treatment. The 3DS+ sample received an additional 20 min chemical milling treatment, resulting in higher material removal. Therefore it is likely, that more subsurface flaws were removed [15, 127]. With the bare eye, the 3DS and 3DS+ surfaces appear to be smooth (Figure 25); however, on a microscopic scale they show etching marks resulting from the different phases in the $\alpha - \beta-$ alloy Ti-64, appearing as random groove pattern (Figure 26).

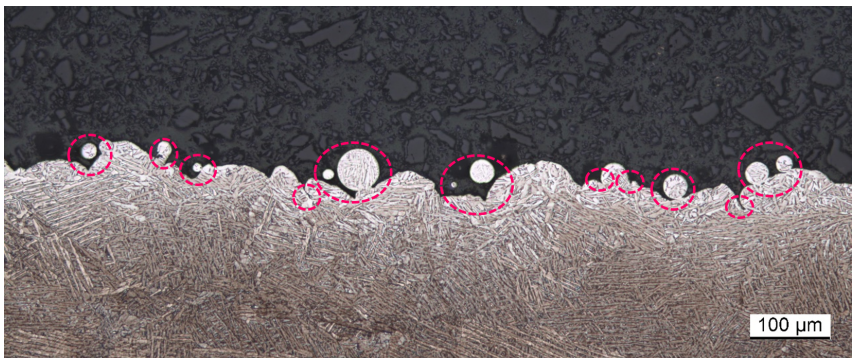

Figure 27.: AsB—cross section micrograph; markers highlight re-entrant features which cannot be detected by contact and line-of-sight methods

2.2. Surface Texture Characterisation – Theory

The surface characterisation methods chosen for this study are stylus measurements, laser scanning confocal microscopy (LSCM) and fringe projection (FP). Physical working principles

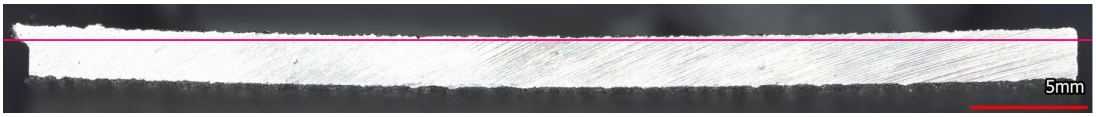

Figure 28.: AsB—cross section curvature, caused by residual stresses

and previous applications to metal AM surfaces of the methods as well as selected surface texture parameters are described subsequently.

2.2.1. Methods for Surface Texture Characterisation

Laser Scanning Confocal Microscopy (LSCM): In LSCM (Keyence VK9700), a laser scans the surface in different focal planes while only exposing the area portion in focus. Vertical scanning of the entire surface depth and layering of the resulting images leads to a 3D surface representation. A lateral resolution in the range of several hundred nanometres can be achieved [57, 69, 70].

The LSCM can be used for areal surface characterisation according to ISO 25178 and is listed as one of the optical methods suitable for surface characterisation in that same standard [16, 133]. Drawbacks of laser confocal microscopy are the long acquisition time in relation to the size of the measured area and the line-of-sight restriction, prohibiting the detection of re-entrant features (marked in Figure 27).

In the literature on AM surface characterisation, the method is mainly used for areal characterisation [57, 60, 125, 134, 135], but extracting and evaluating line profiles is possible.

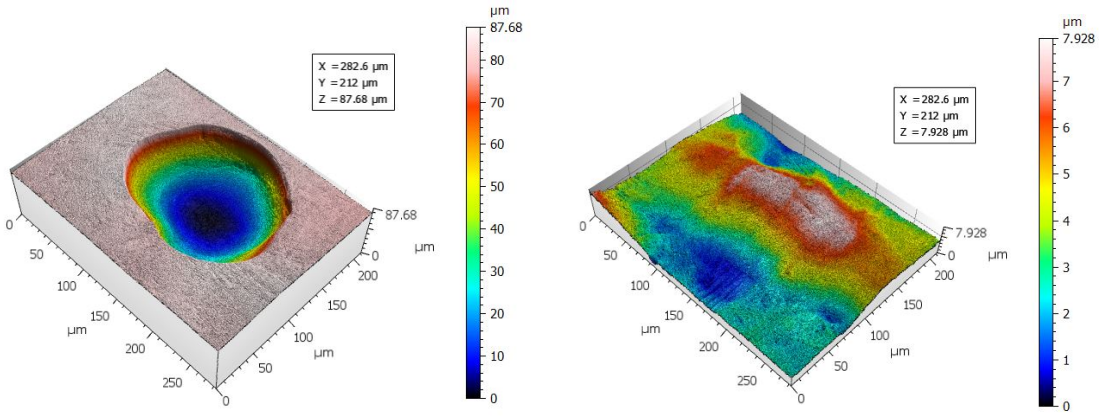

Figure 29.: ChM—3D surface plots from LSCM: two measured positions show fundamentally different surface characteristics on the same sample

Fringe Projection (FP): The fringe projection method is based on the projection of fringe patterns of different sizes onto a surface as visualised in Figure 30. The deviation between the projected pattern and its appearance on the surface is measured and, by means of triangulation of object, camera and projector, the 3D surface is reconstructed [63, 71]. The system (Keyence VR3200) measures 3D surface data of a representative surface portion within an acceptable period of time (i.e., 1 cm^2 in five minutes or less, depending on the resolution) and can return standardised surface parameters according to ISO 25178 [16] from these data. In ISO 25178, fringe projection is listed as suitable method for areal surface texture measurement [70, 133]. The extraction of line profile data and subsequent calculation of line roughness parameters

according to ISO 21920-2 [136] is possible. The method is line-of-sight and therefore unable to detect re-entrant features (as those shown in Figure 27).

In the literature, the method is mostly used for geometrical shape measurements on different scales (down to the size of microfibres) [71–74] or in-process monitoring for LPBF [75–78]. Fringe projection was used for metal AM surface topography measurement by Whip et al. [62] and Zheng et al. in comparison with focus variation microscopy [63]. We previously applied the method for areal characterisation in relation with fatigue data [137, 138].

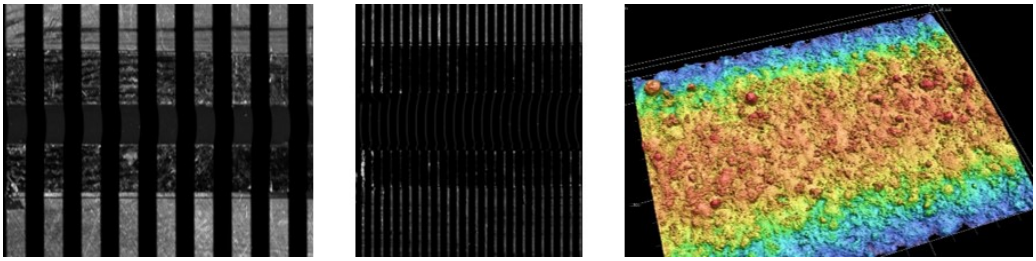

Figure 30.: Fringe projection process—projected patterns (*left,middle*); screenshots during measurement) and resulting 3D surface plot (*right*)

Stylus Profilometry: The stylus method (Mitutoyo SJ-210 instrument) is a contact measurement method using a conical diamond tip that is moved across the surface, following its contour, leading to a 2D profile. Parameters, tip, data filtering and measurement procedure are standardised in ISO 21920-2, ISO 21920-3 and ISO 3274 [136, 139, 140].

The achievable resolution of the method is mainly dependent on the size of the tip and the density of data points, as illustrated in Figure 31. If the tip is too large, valleys cannot be penetrated and the surface appears to be smoother. Furthermore, the circular tip shape may result in rounded peaks, while peak height remains unaffected. If the data point density is too low, some peaks and valleys remain undetected, leading to data smoothing as well. Another contributing factor is the cone angle, which also has an influence on the penetration depth of narrow valleys. Moreover, the detection of re-entrant features is not possible [141, 142].

Using too small a tip may result in its damage, as it will be subjected to a large force in horizontal direction when getting stuck in higher surface features [141]. ISO 3274, however, only specifies a minimum tip size required for a certain expected surface roughness [140].

Stylus measurements and the corresponding line parameters *Ra* and *Rt* are still industry standard and widely used across literature on surface characterisation in general [6, 81]. The same is true for metal AM surface characterisation in particular. A few examples are cited subsequently [6, 8, 15, 91, 127, 132, 135, 143–148].

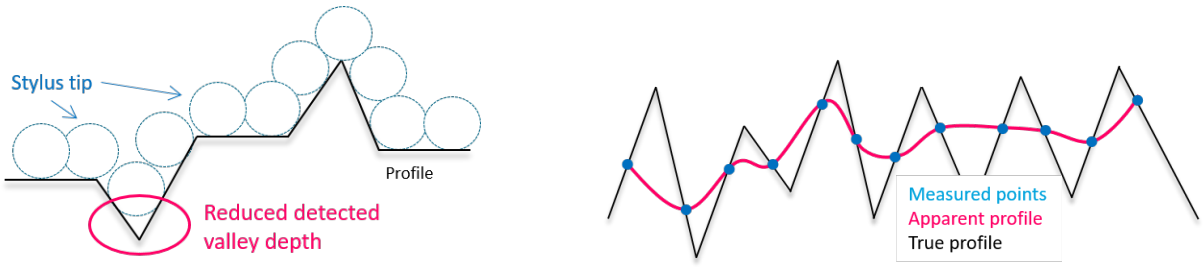

Figure 31.: Reduced valley penetration depth due to stylus tip size (*left*); surface smoothing due to low data point density (*right*) [Based on [141, 149]]

2.2.2. Parameters for Surface Texture Characterisation

The surface characterisation parameters selected for the method comparison are the arithmetic mean height of the roughness profile Ra and the maximum total height of the profile Rt. They were chosen because they are the established parameters for different industrial applications and are widely used throughout the literature to characterise metal AM surfaces [6, 8, 127, 132, 135].

2.3. Surface Texture Characterisation – Experimental Approach

In order to examine the applicability of the selected profile and areal surface characterisation methods, four samples of different surface condition have been selected for examination:

- Initial surface condition (AsB);
- Chemically milled surface condition (ChM);
- Surface condition after 3D SurFin® (3DS);
- Surface condition after combined 3D SurFin® and subsequent chemical milling (3DS+).

On each sample, measurements were taken within a marked area. Due to instrument restrictions, area portions of varying size were covered. Specific values are indicated in Table A.3. An illustration of different sizes of covered areas due to method-specific restrictions is given in Figure 32. Furthermore, the same low and high pass filters as specified in ISO 3274 [140] were applied to the data retrieved from all methods (see Table A.4).

2.3.1. Measurement Setup

The measured area length for the optical measurements of each sample was selected according to the expected surface roughness as specified in ISO 21920 [136, 139] (includes, a.o., updates of the withdrawn profile surface texture standards ISO 4287 and ISO 4288 [150, 151]) and instrument restrictions.

The used handheld stylus instrument was unable to capture an entire 40 mm profile in one go. Therefore, multiple line profiles were combined to obtain the required evaluation length. Similarly, due to the sample curvature, multiple shorter areas were captured using the confocal microscopy system and up to five parallel profiles were extracted and combined. This was to enable a smaller measurement z-range to minimise artefacts, as discussed in [152]. Furthermore, from the fringe projection data, parallel lines were combined for the as-built condition. This enabled higher resolution, as data points are reduced when stitching, and even faster measurement speed. The width resulted from the respective instrument field of view (FOV) and is given in Table A.3.

Even though the line roughness measurements were not matched exactly as the alignment of profile measurements is difficult, taking an average value for multiple lines within the same marked area and filtering the same bandwidth is assumed to produce comparable results. This procedure is meant to reproduce realistic QA process conditions.
The resolution for stylus measurements depends on multiple factors, therefore, both point cloud density (1.5 μm) and tip size (2.0 μm) are specified in Table A.3. The resolution of the confocal microscopy measurements from stitched data was 1.38 μm. Fringe projection achieved an xy-resolution of 3.70 μm Table A.3.

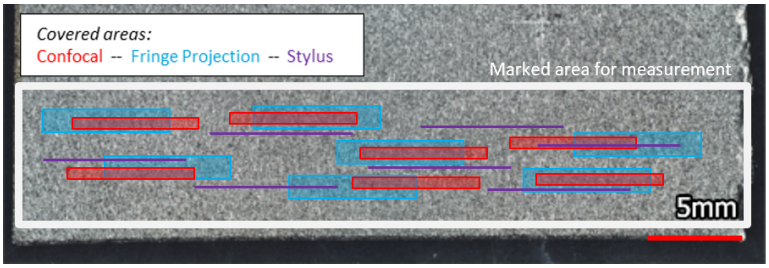

Figure 32.: Data Acquisition—within a marked region on each sample, multiple measurements by every method were performed, distributed across the entire region

Table A.3.: Measurement details for each method and sample

Method		Evaluation Length/mm	Measured Area Length/mm	Measured Area Width/mm (Approx.)	Magnification	Lateral Resolution/μm *for Stylus: Point Distance / Tip Diameter*	Approx. Acquisition Time/min
Confocal Keyence VK9700	AsB	40.00	7 × 9.36	0.50	20x	1.38	380
	ChM	12.50	7 × 8.12	0.50	20x	1.38	80
	3DS	12.50	7 × 15.54	0.50	20x	1.38	60
	3DS+	12.50	7 × 17.39	0.50	20x	1.38	40
Fringe projection Keyence VR3200	AsB	40.00	7 × 10.22	5.17	80x	3.70	12
	ChM	12.50	7 × 3.61	2.84	80x	3.70	4
	3DS	12.50	7 × 3.61	2.84	80x	3.70	4
	3DS+	12.50	7 × 3.61	2.84	80x	3.70	4
Stylus Mitutoyo SJ-210	AsB	40.00	21 × 17.50	n/a	n/a	1.50 | 2.00	70
	ChM	12.50	7 × 15.00	n/a	n/a	1.50 | 2.00	25
	3DS	12.50	7 × 15.00	n/a	n/a	1.50 | 2.00	15
	3DS+	12.50	7 × 15.00	n/a	n/a	1.50 | 2.00	15

2.3.2. Preparation of Measurement Data

Data preparation and evaluation were performed using the MountainsMap® V9 software by DigitalSurf.

The measured areas from random locations (as indicated in Figure 32) were processed as follows. Outliers were removed applying the 'soft' setting and non-measured points were interpolated. As previously mentioned, parallel profiles extracted from the same areal measurement were stitched to obtain the required evaluation length. This was performed for 7 measured locations per surface condition and measurement method.

2.3.3. Evaluation of Surface Texture Parameters

Data filtering, including form removal, high pass (λ_c/μm) and low pass (λ_s/μm) filtering, was performed as described in ISO 21920-3 [139]. Applied filtering values per sample are summarised in Table A.4. In order to ensure comparability, the same bandwidth was extracted from the data obtained from each method. Rt, the maximum total height, and Ra, the arithmetic mean deviation from the roughness profile, were evaluated on evaluation lengths of 12.5 mm for ChM, 3DS and 3DS+, and 40 mm for the AsB condition.

3. Results and Discussion

This section starts out with the comparison and correlation of the results obtained from stylus measurement, fringe projection and confocal microscopy. Subsequently, method-specific challenges

Table A.4.: Filters applied to measurement data of all methods for each sample [139]: high pass filter λ_c/mm and low pass filter λ_s/μm

Sample	$\boldsymbol{\lambda_c}$**/mm**	$\boldsymbol{\lambda_s/\mu}$**m**
AsB	8.0	25.0
ChM	2.5	8.0
3DS	2.5	8.0
3DS+	2.5	8.0

are discussed and summarised.

3.1. Comparison of Ra and Rt from Confocal, Fringe Projection and Stylus Data

Figures 33 and 34 show plots of the data obtained from the three evaluated surface characterisation methods for as-built (AsB)—the 'roughest'—and combined post-processing (3DS+)—the 'smoothest'—surface conditions. Seven data points per sample and method are displayed. In each plot, the blue line indicates the data mean, dashed blue lines mark two standard deviation from the mean (2SD), the dashed box encloses data between the first and third quartile of the data set and the whiskers extending from the box denote highest and lowest values. Outliers are determined with regard to the inter-quartile range (IQR), where near outliers (orange +'s) are defined between 1.5 and 3 IQR and far outliers (red x's) outside of 3 IQR.

Looking at the data presented in Tables A.5 and A.6, especially for Ra, good correspondence across the measurement methods is observed, suggesting that all three methods detect comparable surface quality for each of the three surface conditions (as-built and post-processed).

For the AsB condition, the Ra values from fringe projection are slightly lower. This may be due to apparent profile smoothing (Figure 31) from lower data point density. Additionally, the area covered by fringe projection is the largest, so the variation could also simply be caused by a variation in physical surface properties. Looking at the stylus results, the majority of values shows no variation, indicated by the very narrow box plot. This is caused by measurability issues. Many locations could not be measured due to the tip movement being restricted by surface features. Obtaining seven full profiles on the AsB surface (consisting of 21 individual measurements in total) required more than 30 individual measurements (i.e., almost 1/3 of measurement attempts were unsuccessful). Hence, this very small variation in results is not related to a homogeneous surface quality, but to a pre-selection of measurable locations. A similar effect was observed for the ChM sample, due to the typical crater features (Figure 29). The 3DS and 3DS+ stylus measurements were undisturbed as restricting features were successfully removed during surface treatment.

Considering the Rt results, individual Rt values range from 150 μm to 220 μm for AsB, Figure 33. The highest mean value of 193 μm is obtained from the confocal measurements. The parameter itself is designed to give one extreme value, making it highly dependent on the measured location. One possible explanation for the increased values may be that data post-processing did not remove the occurring spike artefacts (see Figure 35) entirely, which has an enormous impact on the extreme value Rt. This matter is addressed in more detail in Section A.1. Another option is the influence of location and measured area width. The parallel profiles combined to obtain the necessary evaluation length was quite narrow (approx. 500 μm, see Table A.3).

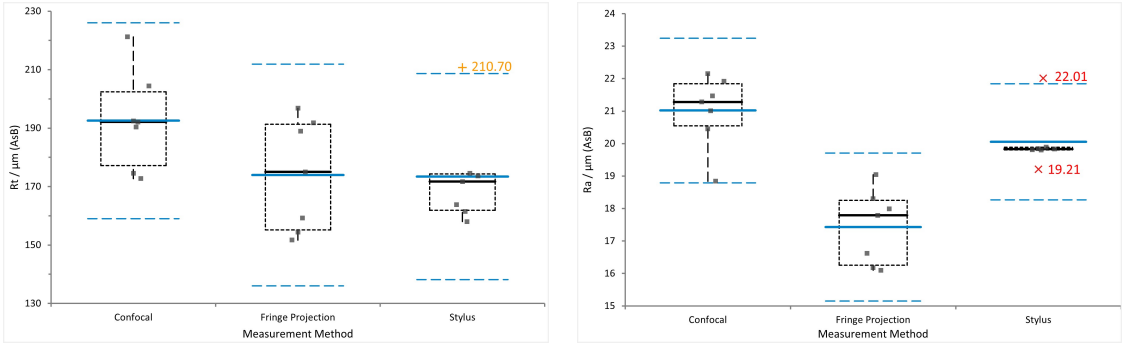

Figure 33.: AsB—*Rt* (*left*) and *Ra* (*right*) data from confocal, fringe projection and stylus measurements

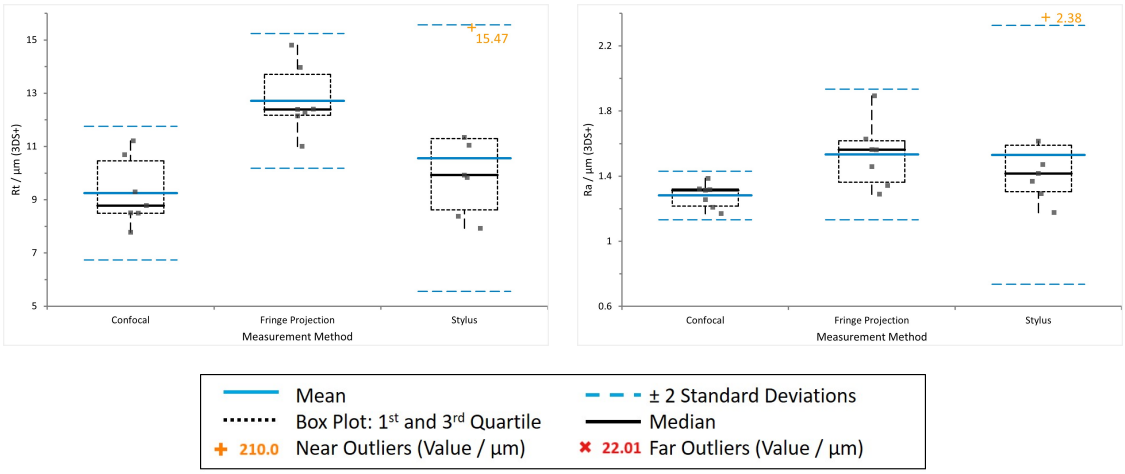

Figure 34.: 3DS+—*Rt* (*left*) and *Ra* (*right*) data from confocal, fringe projection and stylus measurements

A similar observation is made on the ChM surface, where confocal results have a 44% higher *Rt* than the fringe projection data. Their 2SD regions still overlap, meaning they are not statistically distinctive applying a 95% confidence interval. Furthermore, the typical crater-like features, as shown in Figure 29, have sharp edges, causing spike artefacts similar to those on the AsB data. These may, again, not be fully removed by data post-processing (see Figure 36). Apparent profile smoothing in fringe projection and stylus measurements as well as reduced valley penetration depth may also play a role in this consideration. For the stylus results, profile flattening by the tip during measurement may contribute to the result, as the contact measurement can have an influence on its result [149].

The variations within one method and from one method to the other illustrate one of the major drawbacks of profile characterisation altogether, namely the lack of reproducibility and surface representation. If areal measurements and characterisation parameters [16] are used instead, a more representative surface portion can be covered and the chance to capture the largest height variation on the examined surface increases. In general, areal surface characterisation is more powerful with respect to the extraction of 3D topography information [57, 82], even though limited to line-of-sight data, when using optical measurement methods [6, 70, 153].

3.2. Correlation of Results from Evaluated Methods

Taking a look at the correlation of the data from the evaluated methods across the different

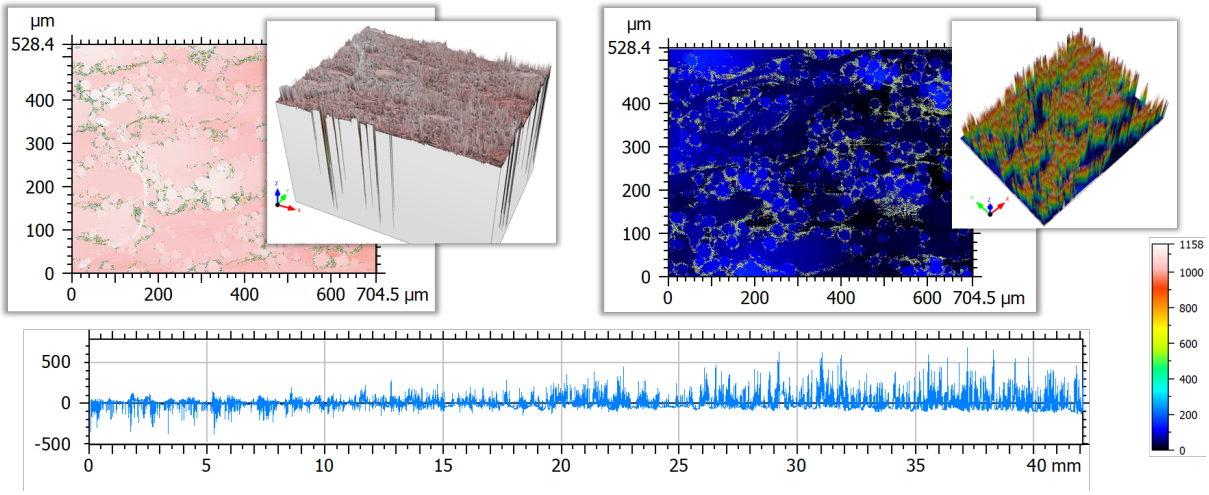

Figure 35.: AsB —height distributions of outer left and right images from LSCM measurement showing spike artefacts along particle boundaries (*top*), LSCM profile data after form removal showing spike size variations along the measured profile (*bottom*)

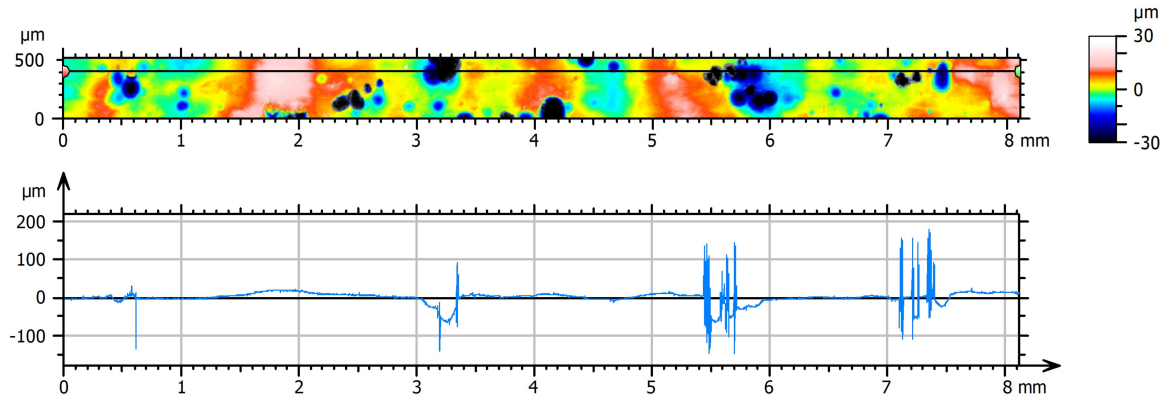

Figure 36.: ChM —spike artefacts in ChM raw data (after form removal) from LSCM associated with crater features; location of extracted profile: black line, bordered by red and green markers

surface conditions, good correspondence can be observed, as shown in Table A.7. Correlation coefficients of at least 0.984 between the data sets and R^2-values of more than 0.967 for a linear regression model show that—when filtering the same bandwidth and restricting the measurement area—fringe projection, confocal microscopy and stylus profilometry achieve comparable results despite the scattering of profile parameters. A similar observation was made by Piska et al. [154] in their comparison of stylus and focus variation results for machined surfaces. Independent from the individual method-specific challenges discussed subsequently, this leads to the conclusion that all methods give valid results for the assessed surface conditions and selected parameters. All correlation coefficients (CC) and R^2-values are given in Table A.7.

3.3. Discussion of Method-Specific Challenges

In the previous sections, the surface texture characterisation results of four different surface conditions using three measurement methods and various influences on the results were discussed. It was demonstrated that all of the applied measurement systems produced comparable results. In this section, hands-on experiences from measurement and data post-processing are discussed. The qualitative findings with regard to acquisition time, operator effort, surface

Table A.5.: Summary of results—*Rt*

Rt		**AsB**	**ChM**	**3DS**	**3DS+**
Confocal	Mean	192.53	71.27	29.52	9.25
N = 7	St.-dev.	15.52	10.47	6.87	1.16
	% St.-dev.	8.06%	14.69%	23.28%	12.57%
Fringe projection	Mean	173.97	48.66	34.23	12.71
N = 7	St.-dev.	17.57	13.69	5.08	1.17
	% St.-dev.	10.10%	28.12%	14.85%	9.20%
Stylus	Mean	173.40	41.75	27.22	10.56
N = 7	St.-dev.	16.33	9.42	2.28	2.32
	% St.-dev.	9.42%	22.57%	8.37%	21.94%

Table A.6.: Summary of results—*Ra*

Ra		**AsB**	**ChM**	**3DS**	**3DS+**
Confocal	Mean	21.02	5.78	4.11	1.28
N = 7	St.-dev.	1.03	0.85	0.66	0.00
	% St.-dev.	4.90%	14.68%	15.98%	0.00%
Fringe projection	Mean	17.43	5.10	5.04	1.53
N = 7	St.-dev.	1.05	1.09	0.73	0.19
	% St.-dev.	6.05%	21.30%	14.55%	12.11%
Stylus	Mean	20.06	4.65	3.91	1.53
N = 7	St.-dev.	0.83	0.48	0.38	0.37
	% St.-dev.	4.12%	10.29%	9.75%	24.03%

Table A.7.: Correlation coefficients (CC) and R^2 of stylus profilometry, confocal microscopy and fringe projection

		Confocal		**Fringe Projection**		**Stylus**	
		CC	***R²***	***CC***	***R²***	***CC***	***R²***
Confocal	*CC*			0.987		0.992	
	R^2				0.969		0.984
Fringe	*CC*	0.987				0.984	
Projection	R^2		0.969				0.967
Stylus	*CC*	0.992		0.984			
	R^2		0.984		0.967		

coverage, reproducibility, operator skill and other aspects are summarised in Table A.8 in Appendix A.1.

A common shortcoming of all of the evaluated methods is the lack of re-entrant feature detection capability. Recognition of re-entrant features can be provided by X-ray computed tomography measurements, which are, in addition, able to acquire information on a parts' bulk quality. Drawbacks are the long acquisition time, limitation of object size and high cost of the system, as well as the requirement of highly specialised operators. However, its potential for a holistic description and understanding of metal AM part quality is undeniable [6, 67, 89].

This being said, areal measurements do offer a better statistical representation of a surface than 2D profile data and are increasingly applied in academic and industrial contexts. The application of these methods, however, currently requires a higher level of skill than the established stylus method, as not all aspects of the measurements and data post-processing are standardised (yet). Though, the areal surface characterisation standard is continuously being updated and its current version does contain a list of optical methods considered suitable for this purpose.

3.3.1. Laser Scanning Confocal Microscopy (LSCM)

Amongst the assessed methods, confocal microscopy offers the highest resolution (Table A.3). A major disadvantage of the method is the measured area in relation to acquisition time. Though this may vary from one confocal instrument to the other, higher resolution measurements generally take longer.

Initially it was intended to capture the entire evaluation length required for a surface condition based on expected roughness in one single measurement. However, looking at the AsB condition, the required evaluation length of 40 mm required a acquisition time of more than 12 h. Additionally, due to the sample's curvature (Figure 28), a fairly high z-range setting was necessary to capture the height variation across the entire length (the VK9700 system used in this study only allows for one z-range setting for the entire measurement, other instruments may offer the options to apply a variable z-range). In combination with shadowing effects from visible agglomerated powder particles and surface inclination, this resulted in large spike artefacts of up to 0.7 mm in size, as is shown in Figure 35. Cross-section micrographs clearly confirm the spikes being measurement artefacts (Figure 27). Figure 36 visualises that spike artefacts also occurred in the ChM data, caused by the crater features present on the surface.

It is observed from the raw data after form removal that the full-length profile exhibits valley spikes to the left and peak spikes to the right of the measured area (Figure 35). This illustrates that the artefacts depend on the angle of the surface with regard to the light source, meaning, that the distribution of artefacts would likely be different when changing the positioning due to changed surface inclination. The size of the spikes appears to be restricted by the pre-defined z-range specified before the measurement, illustrated by Figure 37, were the same location was measured twice with adjusted z-range setting (part of the figure is reproduced from [152]). The effect of measurement z-range and selected data post-processing setting are discussed in [152].

Attempts to remove those spike artefacts during the data post-processing step resulted in a large number of non-measured points, which is why it was decided to measure shorter areas and combine parallel profiles.

Due to the long duration of measurements it is tempting to capture smaller areas, especially when the aim is to gain a qualitative understanding of the surface texture to be investigated. The issue when capturing smaller areas, however, is shown in Figure 29. Two positions on the ChM samples were measured, showing very different surface features due to its inhomogeneous surface finish. These measurements could be obtained within a relatively short time (15 to 20 min, dependent on measurement z-range). However, they do not succeed to capture a representative portion of the surface to evaluate its quality. When performing areal surface texture measurements, it is essential to select a sufficiently large representative area portion. For profile roughness evaluation, the required length is clearly indicated in the ISO 21920 standard [136, 139]. Considering areal characterisation, the ISO 25178 indicates to use at least five times the size of the largest feature of interest [155].

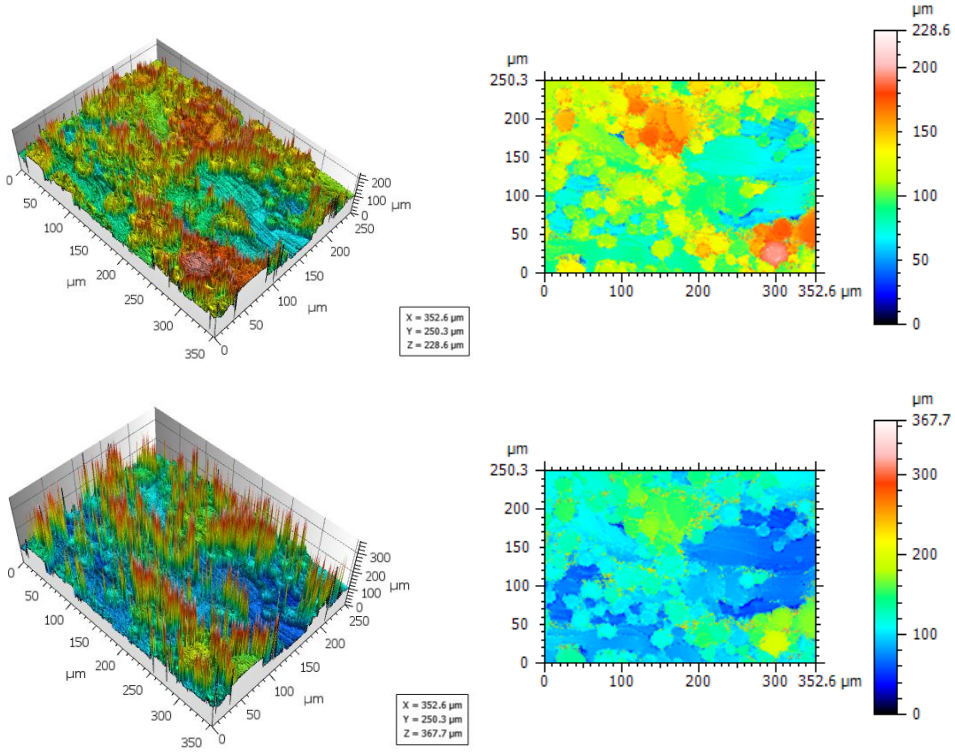

Figure 37.: AsB—spike size with variation in pre-selected measurement z-range from LSCM: $\Delta z = 229$ μm (*top*), $\Delta z = 368$ μm (*bottom*). Spike size is increased with larger pre-selected z-range [152].

3.3.2. Fringe Projection

Fringe projection is the quickest of the assessed measurement methods (approx. 10 mm × 5 mm in 4 min), but also has a considerably lower resolution than confocal microscopy (refer to Table A.3). The achieved lateral resolution of 3.7 µm was also used by Whip et al., when they measured as-built metal AM surface texture [62]. It is comparable to or higher than some resolution values found in the literature for AM surface texture characterisation with focus variation instruments [6, 64, 91]. Triantaphyllou et al. [91], for example, worked with a lateral resolution of 8 μm on their focus variation instrument. When applying standard profile roughness filter values (Table A.4), the resolution reached by the fringe projection instrument is considered sufficiently high for this application.

As for other optical surface topography measurement methods, a drawback of fringe projection is the line-of-sight measurement, meaning re-entrant features (see Figure 27) cannot be detected[70].

Considerable advantages of the method are the quick measurement speed and large area coverage as well as little required data post-processing for this specific application. However, fringe projection instruments do have troubles accurately depicting reflective surfaces, especially when inclined, as found in [156] for machined fatigue specimens. When covering larger areas with the VR3200 system by stitching, the resolution is reduced to decrease the data size. This has to be paid attention to as it can lead to an apparent surface smoothing effect, illustrated in Figure 31.

3.3.3. Stylus Profilometry

When taking stylus measurements, a strong dependence on measured location was observed. Additionally, not every location could be measured due to the tip movement being hindered by particle agglomerations, other surface appearances or due to sample curvature. Measurability is improved when decreasing the movement speed of the tip, as abrupt impact forces when hitting vertical features are decreased. These impact forces may cause damage to the tip itself. Additionally, the measured surfaces may be scratched from the contact measurement [149], possibly compromising mechanical performance or corrosion resistance.

The stylus method is incapable of detecting re-entrant features [6, 141, 157] and application to complex geometries is restricted by instrument and measurement requirements. The accurate alignment of measurements (direction of individual measurements, parallelity of multiple profiles in same direction) for the applied handheld Mituyoto SJ210 is hardly possible. Due to the maximum available length of 17.5 mm for measurement, rougher surfaces may require manual stitching and data processing with software tools, such as the MountainsMap® software applied in this work. Issues regarding alignment and measurement length may not arise when using fixed frame instruments.

Generally, a stylus profiler captures 2D line profiles, which cannot be considered representative, especially in case of coarse and irregular as-built LPBF surfaces. Furthermore, measurements are hardly reproducible as it is unlikely to match exact locations when performing repeat measurements.

Advantages of this method are, however, that its physical working principle is fully understood and it is entirely standardised (method, instrument and data filtering in ISO 21920-2, ISO 21920-3 and ISO 3274 [136, 139, 140]). The equipment is affordable and the measurement execution is straight forward, making the method accessible to a broad range of users.

4. Conclusions

This work aimed at demonstrating the suitability of three different methods to measure surface topography of as-built and post-processed Ti-64 surfaces from LPBF, and at comparing these methods. The applied methods, confocal microscopy, fringe projection and stylus profilometry, showed good correspondence of results for the characterisation of as-built and wet-chemically post-processed LPBF surfaces, rated by linear correlation coefficients (>0.984) and corresponding R^2-values (>0.967). For quick reference, a qualitative summary of the method comparison is included in Table A.8.

Confocal microscopy offered the highest resolution but was also time consuming. In the AsB and ChM raw data, spike artefacts from feature interaction with the light source (sharp edges, shadowing) occurred, requiring appropriate post-processing.

Fringe projection was the quickest and easiest of the investigated methods regarding measurement and data post-processing. When covering large area portions, reproduction of location when performing repeat measurements is possible. The spatial resolution is lower than for confocal microscopy but is still considered sufficiently high to characterise the investigated surface conditions. The computed Ra values for the AsB condition are lower than for confocal (approx. 20% on mean) and stylus (approx. 15%) methods, which may be attributed to a combination of lower point spacing and physical variations on the sample.

The main disadvantages of the observed stylus method were the data pre-selection due to feature-caused restriction of tip movement and limitation to 2D profile measurement. For the AsB and

ChM surface conditions, the measurability was strongly restricted by characteristic features (powder particle agglomerations, craters). For the AsB surface, only two out of three measurement attempts were successful, leading to a significant increase in effort and acquisition time. However, being entirely standardised and handheld instruments being inexpensive, the method is accessible to a large group of users.

To accommodate the use of optical measurement instruments for qualification and QA processes, tolerance values will have to be defined accounting for differences in data acquisition and representation. Exploiting the full scope of advantages of optical systems will ultimately enable a more accurate, precise and reproducible description of surface quality.

Concerning parameters for metal AM surface characterisation, Ra and Rt were used in this study as they are commonly known and accepted in order to demonstrate the methods' applicability and comparability. Areal parameters, however, do offer information on a larger, more representative surface portion and a statistically more meaningful depiction [82]. The areal equivalents to Ra and Rt according to ISO 28175-2 are Sa and Sz [16]. Within this standard, many other parameters are available. In recent years, areal parameters are increasingly evaluated. However, Todhunter et al. found, that this is especially the case for research institutions and metrology and calibration industry [81].

In order to facilitate industry's transition from profile to areal characterisation and from stylus to optical instruments, user oriented education and guidance is needed. Therefore, a broader investigation, including methods based on different physical working principles, instruments by different manufacturers and surface conditions from different manufacturing processes, is required for the development of guidelines and standards.

Table A.8.: Summary —comparison of confocal microscopy, fringe projection and stylus profilometry for metal AM surface texture characterisation.

	Confocal Microscopy	**Fringe Projection**	**Stylus Profilometry**
Acquisition time	very long–large z-range required to capture entire evaluation length in one meas.	short–larger FOV, stitching of few images for full evaluation length	long (multiple individual line measurements necessary, restricted tip movement due to surface features)
Lateral/spatial resolution	high	sufficient	sufficient
Representative surface coverage	yes	yes	no
Linear/areal parameters	both	both	linear
Standardization	listed as suitable method	listed as suitable method	fully standardized (instrument, data processing, parameters)
Physical principle	optical/non-contact; layering of in-focus z-data	optical/non-contact; pattern projection, triangulation	contact measurement
Surface damage	no	no	possible
Detection of re-entrant features	no	no	no
Reproducibility	medium/high— localisation of small area portions is possible but challenging using macroscopic markers	high—large area portions can been measured and located by means of macroscopic markers	low—individual lines unlikely to be located when repeating measurement, surface may be influenced by first (contact) measurement
Measurability	good	good	restriction of tip movement (powder particle agglomerations, craters), limited z-range (handheld devices)
Operator skill	high level of proficiency required to select measurement settings appropriately and perform data processing	medium high level of proficiency required to select measurement settings appropriately and perform data processing	handheld devices are easy to use, process is fully standardised, alignment of multiple (parallel) measurements is highly difficult
Operator effort	medium/low – complex initial setup, automated measurement	low – fairly straightforward initial setup, automated measurement	labour-intensive – every location has to be selected and measured individually (for handheld devices)

A.2. Publication 2 – Post-processing of Areal Surface Topography Data[2]

Abstract: Surfaces of additively manufactured metal parts from powder-based processes typically show powder particle agglomerations and other features, resulting in high surface roughness. Proper characterisation of those surfaces is necessary in order to assess part quality with respect to coatability, mechanical performance or corrosion resistance for use in aerospace, automotive, medical and more industrial applications. Optical surface texture measurement allows for collection of areal surface data, while the established contact stylus method only captures line profile data. When applying optical methods for surface topography measurements, proper data acquisition and post-processing in order to assess surface texture may be complex. A number of variables can be adjusted, such as measurement settings, approaches to outlier removal, evaluated area size or form removal. This work shows the influence of selected z-range prior to measurement and the influence of choosing pre-defined outlier removal settings in MountainsMap 9.2 on selected ISO 25178-2:2022 parameters calculated from data obtained from confocal microscopy for as-built Ti6Al4V from laser powder bed fusion. The aim is to show the impact of variation in measurement and post-processing on calculated surface texture parameters and stress the importance of proper documentation in order to achieve reproducibility of data for quality management.

1. Introduction

The application of metal additive manufacturing in various fields requires new approaches to quality assurance. With regard to fatigue performance, measurement of the surfaces and characterisation of surface texture are of interest. Surfaces from laser powder bed fusion (LPBF) typically exhibit agglomerations of attached powder particles (Figure 38) of different size and shape are typical for these surfaces and this special nature imposes new challenges on measurement systems and their application.

The stylus method is still most commonly applied in industry and has the advantages of easy application and full standardisation. It is, however, a contact method, meaning, that damage to the surface is possible. Looking at LPBF, the stylus tip movement may be restricted by particle agglomerations during measurement due to resulting undercuts and high slopes (see Figure 38).

In recent years, optical measurement systems are gaining acceptance. They offer non-contact measurements with representative areal coverage and enable application of areal surface texture characterisation. Optical measurements and post-processing of data are not yet standardised. However, a number of methods are listed in ISO 25178-6 [133] as suitable methods for characterisation of areal surface texture and the standard is continuously updated.

When specifically considering laser scanning confocal microscopy (LSCM), large spikes can occur (see Figure 40) in the data having a significant influence on typically used areal parameters such as Sa (arithmetic mean height), Sq (root mean square height) or Sz (maximum height), as these depend exclusively on height values and are hence very sensitive to local extremes.

Information on data acquisition and processing, such as outlier removal, reduction of measurement noise or levelling is often missing in studies on AM surface texture characterisation [6, 158].

[2] *Published as:* Buchenau, Theresa; Brüning, Hauke; Amkreutz, Marc (2022): Post-processing of Surface Topography Data for As-built Metal Additive Surface Texture Characterisation. In: Journal of Additive Manufacturing Technologies 2 (2), S. 697. DOI: 10.18416/JAMTECH.2212697

However, where areal methods are applied, this information is crucial for reproducibility since those processing steps can heavily influence the result.

This work aims at showing the impact of selected measurement and post-processing settings on surface texture parameters and stressing the importance of proper documentation of data acquisition and post-processing steps. The effects of changing the z-range for the measurement, the outlier removal setting and interpolating non-measured points (NMP) on Sq (root mean square height), Sz (maximum height), Sk (core height) and Svk (reduced valley depth) are discussed.

2. Material and Methods

2.1. Laser Scanning Confocal Microscopy

In laser scanning confocal microscopy (LSCM), the surface is scanned by a laser in different focal planes, only exposing the area portion in focus. The 3D surface representation is created by layering data across the focal planes [70]. The method is line-of-sight, meaning that re-entrant features, shown in Figure 38, cannot be detected.

The used instrument in this study is the Keyence VK 9700 with the 20x magnification lens, achieving a spatial resolution of 0.69 µm. Measurement uncertainty is not included in the presented results. An overview of data acquisition and processing steps is given in Figure 39.

In ISO 25178-6 [133], the method is listed as suitable method for areal surface texture characterisation. Details on measurement and post-processing are not yet included in the standard. Taking a look at literature, the method is mainly used for areal surface texture characterisation and high-resolution imaging [57, 68, 125, 135].

2.2. Data Sets

The evaluated data sets originate from a Ti6Al4V sample in as-built condition from LPBF (Figure 38). Typical powder particle agglomerations of different sizes are visible in scanning electron microscopy (SEM) images. Both data sets show an identical, randomly chosen location on the sample and the only difference in measurement settings is the predefined z-range the confocal microscope. One measurement was taken with a z-range of 229 µm, the second with 368 µm. The first value was selected based on the surface topography; the second value resulted from increasing the z-range in positive direction to study its effect.

When only looking at an individual image, it may be unclear why the effect of increasing z-range is interesting. However, when measuring larger surface portions requiring stitching of multiple images, the z-range for the used instrument (Keyence VK 9700, lens with 20x magnification) has to be set according to the highest height variation to be detected.

2.3. Surface Data Evaluation

The data evaluation was performed using MountainsMap® version 9.2. The raw data from confocal microscopy was imported and outlier removal ‘soft’, ‘normal’ and ‘strong’ was applied for the two evaluated data sets. The MountainsMap® outlier removal algorithm uses median filters (of variable size according to setting) to smooth isolated outliers and removes outliers

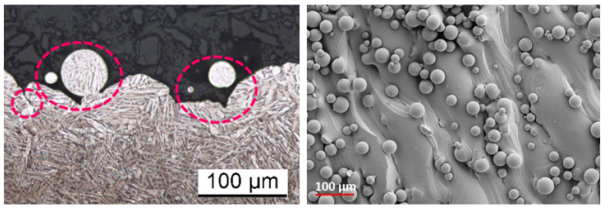

Figure 38.: Powder particle agglomerations on as-built Ti6Al4V surfaces from LPBF: Cross section micrograph, illustration of undercuts *(left)*, SEM showing agglomerations of different sizes and underlying waviness *(right)*

around edges and converts them into non-measured points (for increased strength, more points are removed).

In order to quantify the influence of the chosen variations, the ISO 25178-2 parameters Sq (root mean square height), Sz (maximum total height), Sk (core height) and Svk (reduced valley depth) are compared amongst the post-processed data set versions. Sq and Sz are frequently applied in industrial environments while Sk and Svk are less common. The latter are calculated from the material ratio curve and were found to have potential for metal AM surface texture characterisation in previous studies by the authors [137, 159].

Prior to the parameter calculation a Gaussian S-filter of 2.5 µm and a Gaussian L-filter of 0.5 mm was applied to the processed surface data. The steps taken are summarised in Figure 39.

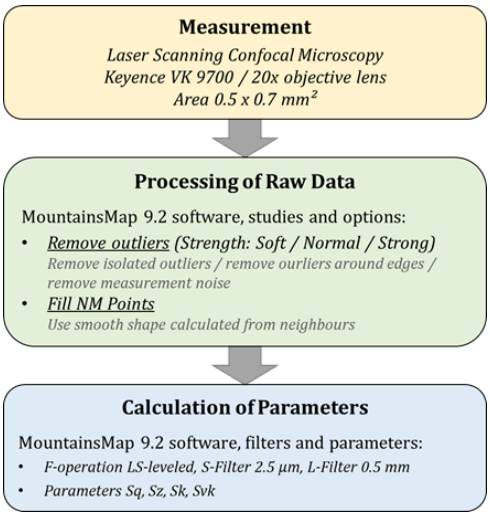

Figure 39.: Measurement, data processing and evaluation steps; Studies, options, filters and parameters selected in MountainsMap® 9.2

3. Results and Discussion

Typical confocal microscopy raw data of LPBF surfaces show large spikes (see Figure 40, also refer to [158]), that occur around the edges of powder particles. Comparing the raw data to the microscopic images (i.e. Figure 38) clearly shows these spikes are not physically present on the measured surfaces. The spikes are artefacts arising during data acquisition with the LSCM.

A likely origin of the spikes are particle agglomerations, which are LPBF specific surface features. Confocal microscopy is a line-of-sight method and as-built LPBF surfaces show undercuts (see

Figure 38), which cannot be detected. On the boundaries of attached particles, the instrument detects two signals, one from the boundary and one from the surface below, leading to the display of a spike artefact.

Furthermore, it is observed, that the spherical shapes of the powder particles are not accurately depicted, which is a known phenomenon in confocal microscopy [68, 160, 161].

From previous measurement results it was observed that the spikes have the size of the measured z-range. Figure 40 shows measurements at identical location with variation of the pre-set z-range. The raw data illustration confirms the assumption that the size of the artefact does not depend on the size of surface features but is mostly defined by the measurement setting. The following main aspects were considered in the data evaluation:

- Effect of increasing the measured Δz
- Effect of outlier removal and fitting non-measured points

3.1. Raw Data with Different Δz

Looking at the chosen parameters, there is a significant difference between the $\Delta z = 229$ µm and $\Delta z = 368$ µm data sets. As expected, the largest deviation is observed for the extreme value Sz (maximum total height), namely 40%. Note that due to filtering the data to separate roughness from waviness components (L-filter 0.5 mm), the value is smaller than the maximum measured z-range of the respective data sets.

Smaller but still significant is the difference of the root mean square height Sq, which amounts to 39%. This shows that Sq, being a parameter that is supposed to characterise the overall surface quality [137], is very sensitive local extreme values, which are in this case caused by the measurement setting.

Considering the selected parameters from the material ratio curve, the difference is relatively low, namely 12% for the core height Sk and 4% for the reduced valley depth Svk and hence react less sensitively to the size of the spike artefacts.

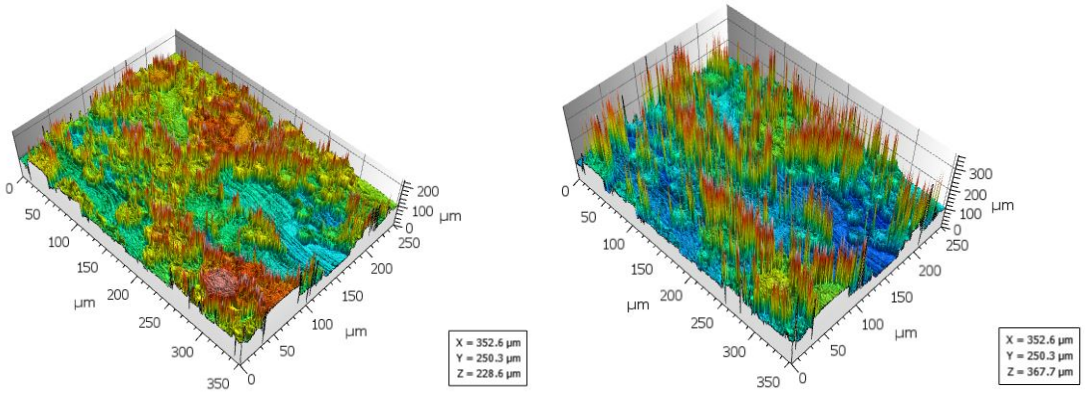

Figure 40.: Spikes in confocal raw data of as-built Ti6Al4V. Top and bottom images show identical locations on the surface with different Δz setting

Table A.9 summarises the above-mentioned numerical values. When comparing the surface texture parameters for both data sets it is also notable, that while all other values increase with increasing Δz, Svk decreases slightly. This is possibly due to the spikes creating an increased number of data points, not only in the peak, but also in core portion of the profile, resulting in a slightly flatter main slope. Since the z-range in this case was only extended in positive

Table A.9.: ISO 25178 parameters for Δz = 229 µm and Δz = 368 µm (S-filter 2.5 µm, L-filter 0.5 mm)

Parameter	Δz = 229 µm	Δz = 368 µm	Deviation
Sq / µm	24.38	39.83	39%
Sz / µm	191.40	320.80	40%
Sk / µm	59.54	67.44	12%
Svk / µm	14.31	13.78	-4%

direction ("peak portion"), the effect on the valley parameter is small. For detailed information on the material ratio curve parameter calculation, please refer to [82, 137]. These results clearly show the necessity of properly post-processing data from confocal microscopy (and other optical methods) in order to mitigate the effect of measurement artefacts.

Previous round-robin testing on best-practice measurement and characterisation of surface texture with different labs has shown that some users are unfamiliar with how to choose post-processing settings for raw data from optical measurement, which supports the previous statement.

3.2. Outlier Removal and Non-measured Points

Depending on the chosen strength of the applied outlier removal, the non-measured points (NMP) amount to roughly 15% for the setting 'soft', 20% for 'normal' and 30% for 'strong' for both data sets.

In general, a trend of lower parameter values for stronger outlier removal was observed (Table A.11). The strongest effect is on Sz, since with removing more spikes, more extreme values are eliminated.

When removing a spike, it is usually eliminated starting from its root, which is why there are data points missing within the core part of the profile, as visible in Figure 41 and Figure 42, causing differences in Sk, Svk and Sq.

Table A.10.: Non-measured points, dependence on outlier removal strength and Δz

Data Set / Outlier Removal	Δz = 229 µm	Δz = 368 µm
Soft	15.55%	14.52%
Normal	20.15%	19.20%
Strong	31.75%	30.08%

3.3. Interpolation of Non-measured Points

Filling the NMP with interpolated values causes a variation of parameter values of up to 11% for Δz = 229 µm and 12% (Table A.11) for Δz = 368 µm. The parameter Sz is not affected by the interpolation.

This issue is illustrated by an extracted profile with nearly 18% NMP and interpolated points in Figure 41. After the outlier removal step, data is mainly missing in the core portion (close to the centre line) of the profile. The material ratio curve is hence gaining core material when interpolating NMP, resulting in flattening the curve (more data points per height level), which causes a slight decrease of Sk and a slight increase of Svk. Figure 41 and Figure 42 clearly show

Table A.11.: Resulting ISO 25178 parameters for variation of outlier removal strength and fitting non-measured points for $\Delta z = 229$ µm

	Soft	Normal	Strong
Sq (NMP) / µm	22.85	22.81	22.54
Sq (NMP filled) / µm	22.63	22.44	21.88
Deviation	1%	2%	3%
Sz (NMP) / µm	186.40	184.00	170.80
Sz (NMP filled) / µm	186.40	184.00	170.80
Deviation	0%	0%	0%
Sk (NMP) / µm	55.26	55.15	54.36
Sk (NMP filled) / µm	54.58	54.03	52.60
Deviation	1%	2%	3%
Svk (NMP) / µm	13.42	13.05	11.86
Svk (NMP filled) / µm	14.18	13.98	13.16
Deviation	-6%	-7%	-11%

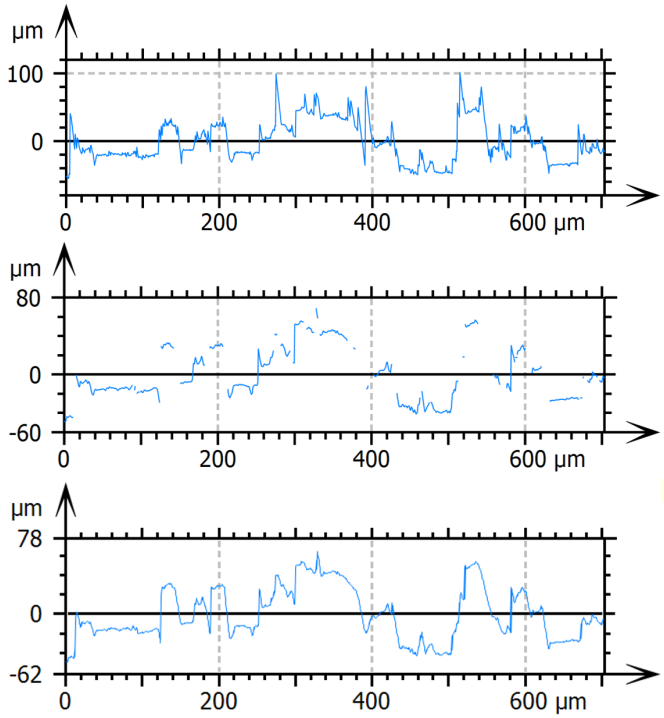

Figure 41.: Profiles extracted from $\Delta z = 229$ µm data set: Original *(top)*, after outlier removal with NMP 17.8% *(middle)* and with interpolated NMP *(bottom)*

the difference between 'normal' and 'strong' outlier removal. The interpolated curve in Figure 41 still shows some sharp edges while Figure 42 is relatively smooth.

4. Conclusions

The presented data show that changing measurement settings and use of different post-processing options can cause a large variation on surface texture parameters (up to 40%). Many publications do not state the applied steps. In addition, round-robin testing, where metal additive surface measurement and characterisation were compared, showed that there are users who are unfamiliar with post-processing of raw data from optical measurements. In order to ensure reproducibility

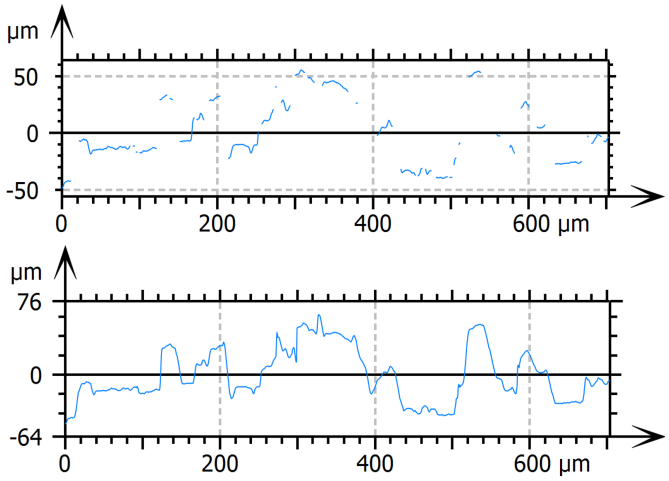

Figure 42.: Profiles extracted from $\Delta z = 229$ µm data set: After outlier removal with NMP 29.5% *(top)* and with interpolated NMP *(bottom)*

of results, specification, documentation and standardisation are essential. Outlier removal and interpolation of non-measured points may have a significant effect on the resulting parameters. Outlier removal settings have the strongest impact on the extreme value Sz. Filling in NMP does not alter Sz but does have an influence on the material ratio curve parameters Sk and Svk and the root mean square Sq due to the addition of data points in the core portion. When choosing the appropriate setting for outlier removal for one's confocal microscopy data, it is recommended to take a look at the 3D view to check the spikes' size and quantity. The authors will mostly use the 'soft' or 'normal' setting in MountainsMap® 9.2, to keep as much of the measured data as possible while getting rid of the artefacts. The NMP interpolation, although adding points that were not measured may distort the results, is considered a valid approximation, since the measured surface is continuous. Due to the large number of settings to be varied, the strong impact of their modification and lack of standardisation, the application of optical measurement systems requires a high level of expertise. A major advantage of confocal measurements and other optical systems is the areal coverage, allowing for three-dimensional data acquisition (with the limitation to line-of-sight) rather than just a single profile as attained from the stylus method. This does not only accommodate a better representation of the surface from a statistical point of view, but also enables the characterisation of process-specific surface features, such as powder particle agglomerations in LPBF.

A.3. Publication 3 – Influence of Contour Scan Variation[3]

Abstract: Metal additive manufacturing technologies have great potential for future use in load-bearing aerospace applications, requiring a deeper understanding of mechanical performance and influencing factors. The objective of this study was to investigate the influence of contour scan variation on surface quality, tensile and fatigue strength for laser powder bed fusion samples made of AlSi7Mg0.6 material and to create high-quality as-built surfaces. The samples were produced with identical bulk and different contour scan parameters to accommodate the investigation of the impact of as-built surface texture on mechanical properties. The bulk quality was evaluated by density measurements according to Archimedes' principle and tensile testing. The surfaces were investigated using the optical fringe projection method, and surface quality was assessed by the areal surface texture parameters Sa (arithmetic mean height) and Sk (core height, derived from material ratio curve). Fatigue life was tested at different load levels, and the endurance limit was estimated based on a logarithmic-linear relation between number of cycles and stress. All samples were found to have a relative density of more than 99%. Surface conditions distinctive in Sa and Sk were successfully created. The resulting mean values of the ultimate tensile strength σ_{ult} are between 375 and 405 MPa for 7 different surface conditions. It was confirmed that the influence of contour scan variation on bulk quality is insignificant for the assessed samples. Regarding fatigue, one as-built condition was found to perform as well as surface post-processed parts and better than the as-cast material (compared to literature values). The fatigue strength at the endurance limit for 10^6 cycles is between 45 and 84 MPa for the three considered surface conditions.

1. Introduction

Additive manufacturing (AM) technologies, in particular laser powder bed fusion (LPBF), are of extraordinary interest to the aerospace industry. Advantages of these technologies include a large increase in geometrical freedom and potential savings of material and overall production cost [1, 2, 120, 162].

It is also desirable to use AM technology in load-bearing applications, but standards for part certification and quality assurance are not yet established. Hence, there is currently still a restriction to non-critical parts in aerospace systems [7, 13]. Part of the work done to gain an understanding of the process–material–property relations needed as a foundation for part qualification is summarised in Section A.3. Section A.3 explains the contribution of this work to that same understanding.

1.1. Mechanical Properties of LPBF-Processed AlSi Alloys

Different review papers have suggested that there is an extensive number of studies on LPBF processing of materials like Ti-64 [8, 39–41, 163], Inconel 718 [22, 42, 43, 163] or 316L steel [44–47, 164]. LPBF-processing of aluminium alloys, however, has only gained importance in recent years [9, 20, 49–52]. Aboulkhair et al. found that this is related to the particularly challenging properties of aluminium alloys and aluminium alloy powders for laser processing. The powders are generally characterised by low flowability, which impacts powder layer recoating, and are prone to oxidation, causing porosities. Moreover, the high reflectivity of the common LPBF process wavelength range, low laser absorption and high thermal conductivity result in a need for high laser power [20].

[3] *Published as:* Buchenau, Theresa; Amkreutz, Marc; Brüning, Hauke; Mayer, Bernd (2023): Influence of Contour Scan Variation on Surface, Bulk and Mechanical Properties of LPBF-Processed AlSi7Mg0.6. In: Materials 16 (8), S. 3169. DOI: 10.3390/ma16083169

Nonetheless, LPBF processing of aluminium alloys is interesting, especially for lightweight construction applications, as they are lightweight, strong, corrosion-resistant and highly weldable. Combined with the geometrical freedom enabled by LPBF processing, they are suitable for tailoring parts for numerous purposes within automotive, aerospace and other industries [20].

The best LPBF-processable alloys are aluminium–silicon-based, and the most commonly-investigated one is AlSi10Mg. The silicon phase in the solidified LPBF material contributes to limit crack initiation and propagation due to the LPBF-typical fine microstructure and improves its tensile strength as compared to the cast material [1, 51, 53].

In particular, the alloys AlSi10Mg, AlSi12 and AlSi7Mg are considered 'highly printable' [51]. For these materials, ultimate tensile strength (UTS) values between 300 and 450 MPa in as-built condition are reported [1, 26, 29, 31, 32, 51, 105–110].

Many publications assess the effect of heat treatment [24, 26–32, 37], and there is some work addressing the effect of surface post-processing [33–36] or positioning on the build platform [37, 38] on mechanical properties.

In this section, an overview of recent work on mechanical properties is given. The focus is on investigations on tensile and fatigue behaviour of LPBF-processed aluminium alloys, particularly the AlSi7Mg0.6 alloy.

Tensile Properties: Yang et al. investigated the effect of heat treatments on microstructure and mechanical behaviour anisotropy for the AlSi7Mg0.6 alloy. They observed the typical LPBF fine microstructure in as-built condition due to the material's fast cooling rate and a resulting higher strength than the as-cast alloy. Of the heat-treated samples, directly aged (T5) samples showed the highest strength and stress-relieved samples showed the largest elongation at fracture [29].

Similarly, Rao et al. found better tensile strength in as-built LPBF compared to the as-cast condition and observed that stress relaxation had a negative effect on yield strength (YS) and UTS while causing a slight improvement in ductility. A short solution heat treatment improved ductile behaviour, and a longer treatment led to a decrease in YS and ductility [26].

Pereira et al. compared microstructure and mechanical properties of AlSi7Mg0.6 from LPBF and investment casting. They found that mechanical properties of LPBF can exceed aerospace qualification requirements for heat treated (T6) investment casting parts. They used direct ageing heat treatment to improve ductility and hardness of LPBF-processed samples while maintaining a similar tensile strength as compared to as-built samples (e.g., mean UTS (as-built, vertical) of 435 MPa, after heat treatment 431 MPa) [31].

Zhang et al. looked into the effect of heat treatment for Er-containing AlSi7Mg0.6 and found that tensile properties are superior to the non-Er-containing alloy. The applied heat treatments improved ductility from 8% up to 19% for stress-relieved samples (with reduced tensile strength). Direct ageing and T6 heat treatment both resulted in increased YS [32].

Advantages and disadvantages of different heat treatments compared to as-built ones were discussed by Mauduit et al. Amongst others, they found that the investigated heat treatments soft annealing and T6 resulted in isotropic mechanical properties. Soft annealing reduced tensile strength but removed residual stresses, artificial ageing created the best UTS, but samples exhibited anisotropic mechanical properties. As-built samples already reached good mechanical properties but showed anisotropy. However, not applying heat treatment led to shorter production time and was less expensive [30].

Menezes et al. evaluated the effect of orientation on the build plate for as-built and heat-treated samples. Both conditions showed anisotropic behaviour, where vertical specimens had lower YS and higher UTS. Comparing artificially aged and as-built samples, the latter showed lower YS [165].

Next to vertically (90°) and horizontally built (0°) samples, Denti included specimens built at a 45° angle in their investigation and observed a (slight) tendency for increasing tensile strength and decreasing elongation at fracture for steeper build angles [166].

In addition to heat treatment, Han et al. looked into the effect of laser surface remelting (LSR) for LPBF-processed AlSi10Mg and found that Ra (arithmetic mean of profile height variation) can be significantly improved by LSR. For as-built surfaces, they report an $Ra > 19$ μm that improved to values below 1 µm for LSR-processed samples. In addition, LSR led to increasing micro-hardness. The applied heat treatment led to reduced tensile strength and improved ductility from 6% to 22% [24].

Fatigue Properties: A full tension–tension loading Wöhler curve assessment with $R = 0$ of the AlSi7Mg0.6 alloy using an endurance limit of 2×10^6 cycles was performed by Bassoli et al. [115]. They obtained a result of 60 ± 5.3 MPa and found that the alloy's fatigue performance under the applied processing conditions was slightly lower but still comparable to reported literature values for the AlSi10Mg alloy [167]. Surface texture parameters were not specified, but they mentioned that the samples had not received any post-treatment.

Grande et al. [37] investigated the relationship of heat treatment and tensile strength as well as the effect of position on the build platform on fatigue life. They produced specimens with densities > 98.8% and as-built YS of 222 MPa and UTS of 417 MPa. They found that stress relief reduced tensile performance. Their fatigue results suggest that the position on the build platform does not have a significant influence on the endurance limit (at 10^7 cycles: 127 MPa internal vs. 137 MPa external regions) of the heat-treated specimens. Fatigue samples were sandblasted to improve surface texture prior to fatigue testing.

Denti and Sola [34] looked into the effect of different post-processing technologies (e.g., sand-blasting, plastic media blasting and laser shock processing) on axial fatigue. They found that the evaluated surface processing techniques improved the areal arithmetic mean surface height deviation Sa by up to 77%. The lowest Sa values were achieved by plastic media blasting. The peak stress level at the endurance limit of 2×10^6 was improved by up to 80% with respect to the as-built σ_{max} of 50 MPa. Fatigue performance was also improved by post-processing techniques not enhancing the surface quality, which led them to the conclusion that both the improvement of surface quality and the introduction of compressive residual stresses can play a role when looking at LPBF-processed aluminium alloy parts.

The impact of sample location on the build platform, orientation and variation between production batches was studied by Cacace et al. [38]. By analysing mechanical property data of three batches with randomly allocated sample positions, they found that part position did not have an influence on tensile strength but did affect low cycle fatigue performance.

Nasab et al. [168] investigated the combined effect of volumetric and surface defects. They looked into as-built surfaces with different contour scans, trying to promote typical defects to show their effect on rotating bending fatigue. The defect depths were analysed by optical line-of-sight measurement, as well as polished cross-sections. Material removal depths of up to 200 μm were suggested, depending on the surface condition. They state that contact and non-contact surface texture measurements cannot provide information on fatigue-critical surface features as comprehensively as investigations into polished cross-sections.

In previously published work, the authors of this paper evaluated crack initiation behaviour and surface fatigue relations for AlSi7Mg0.6 for three different groups of as-built samples. We assessed the applicability of valley depth Sv and reduced valley depth Svk and found that Svk is especially useful when considering coarser as-built surfaces, since they tend to exhibit crack initiation from multiple surface defects [137].

1.2. Motivation and Objective

Most of the studies summarised deal with the influence of heat treatment and build direction (horizontal/vertical) on tensile properties. While tensile properties are an important starting point in understanding a material's mechanical behaviour and are certainly relevant for various applications, for many aerospace, automotive, biomedical or other industrial purposes, resistance to periodic loading is of interest. In regard to fatigue life, surface texture plays an important role [1, 7].

The majority of studies including the effect of surface condition on fatigue performance of the LPBF-processed AlSi7Mg0.6 material, as well as other aluminium alloys and other typical LPBF powder materials (e.g., Ti-64, 316L steel or Inconel 718), evaluate the application of different surface post-processing strategies, e.g., [33, 36, 39, 41, 44, 112–114].

However, especially when considering complex geometries or parts with inner surfaces that are difficult to access with post-processing tools, it is desirable to produce as-built surfaces (including near-surface regions) good enough to perform reasonably well under cyclic loading. In addition to accessibility issues, using as-built parts saves time and cost due to reducing processing steps, since extensive post-processing becomes unnecessary.
In this paper, the effect of the as-built surface condition on mechanical properties is discussed. The ultimate aim is to create high-quality as-built surfaces.

The first step is to create distinctive as-built surface conditions by varying contour scan parameters (Section A.3). Afterwards, the effect of these variations on bulk quality, characterised by density (Section A.3) and UTS (Section A.3), is investigated. Finally, a first selection of fatigue results is presented, showing the influence of as-built surface condition on fatigue resistance at a load level of $0.5\sigma_{ult}$ and the endurance limit (Section A.3).

2. Materials and Methods

2.1. Manufacturing

The evaluated samples were manufactured in an LPBF process on a Trumpf TruePrint 1000 from AlSi7Mg0.6 aluminium alloy powder. The powder composition along with mass fractions of alloying elements are shown in Table A.12. Specifications of geometries and manufacturing settings are given subsequently.

Table A.12.: AlSi7Mg0.6 powder composition: mass fraction per alloying element

Al	**Si**	**Mg**	**Ti**	**Fe**
93.13	6.15	0.6	0.09	0.05

Sample Geometry: Two kinds of samples are used in this work: cuboids (height 10 mm, width 10 mm, thickness 5 mm) and fatigue specimens according to ASTM 466-15 [169] (height 80 mm, smallest cross-section 6 mm, thickness 3 mm). The latter type is shown in Figure 43.

Manufacturing Parameters: Detailed information on the manufacturing process is presented in Tables A.13 and A.14 as well as Figures 43 and 44.

Powder layers were exposed to the laser by a pattern of parallel lines in the bulk, changing direction by 66° after each layer, and a continuous scan of the geometric contour. Sky writing was applied to ensure the laser source was moving at the chosen speed prior to exposure.

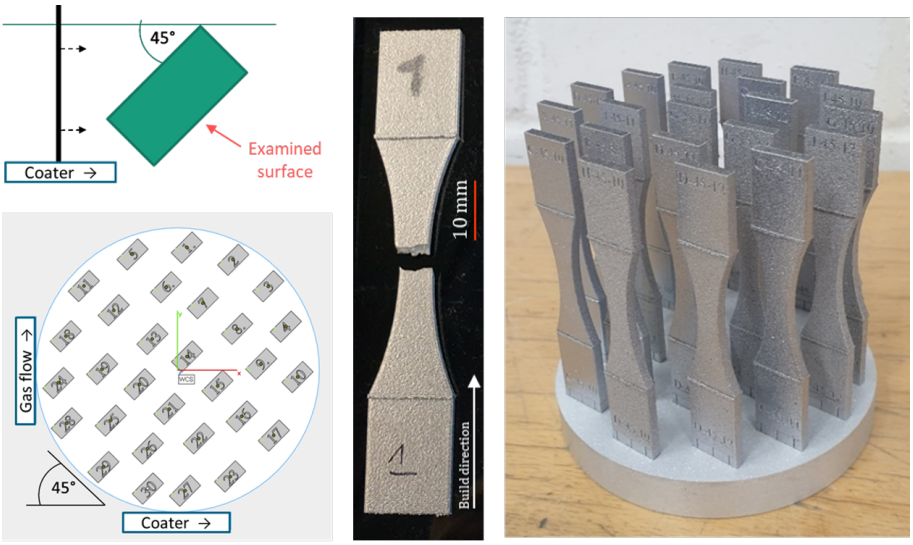

Figure 43.: Top view: sample orientation with respect to coater (top left); example of build job layout (bottom left); individual tested sample (middle); finished build job on platform (right)

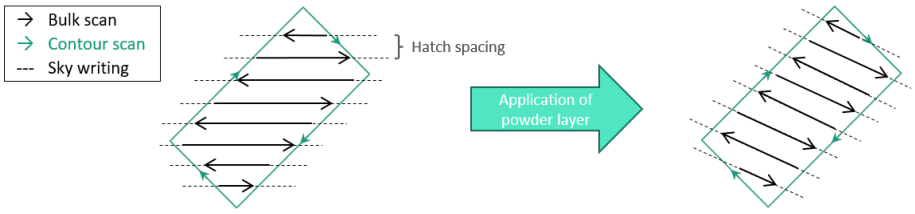

Figure 44.: Exposure strategy for bulk and contour scan: bulk scan direction is rotated by 66° (schematic representation, not true to scale) after each powder layer application

The samples were placed on the build platform at a 45° angle with respect to the coater and gas flow, as shown in Figure 43. This angle was found to be most suitable regarding surface texture. In preliminary studies, comparable surface texture parameter values were found for both sides of the sample, supposedly because the effects of coater and gas flow compensate each other.

Bulk scan parameters were identical for all samples, as specified in Table A.13, and originate from a previous density optimisation study.

The contour scan parameters were varied, intending to achieve a variation of surface properties. Maintaining layer thickness, hatch distance and laser power, the scan speed was modified between 300 mm/s and 1800 mm/s, paired with the settings with and without additional

pre-sinter at 50% laser power, resulting in a total of 10 manufacturing parameter combinations.

The samples with identical parameter combinations were named with a designated letter according to Table A.15, with consecutive numbering; e.g., A1 → Contour parameter set A (scan speed 300 mm/s, with pre-sinter), mechanical testing sample No. 1.

Table A.13.: Bulk scan parameters

Material	**Layer Thickness**	**Hatch Distance**	**Scan Speed**	**Laser Power**	**Pre-Sinter**
AlSi7Mg0.6	30 µm	0.12 mm	1000 mm/s	195 W	No

Table A.14.: Variation of contour scan parameters

Material	**Layer Thickness**	**Hatch Distance**	**Scan Speed**	**Laser Power**	**Pre-Sinter**
AlSi7Mg0.6	30 µm	0.12 mm	300 mm/s 600 mm/s 900 mm/s 1200 mm/s 1800 mm/s	195 W	Yes No

Table A.15.: Naming of sample groups based on contour scan variation

Scan Speed in mm/s	300	600	900	1200	1800
Pre-Sinter	A	C	E	G	I
No Pre-Sinter	B	D	F	H	J

2.2. Characterisation and Testing

Surface Texture: The surfaces were measured using a Keyence VR3200 fringe projection system. The micro camera setting at a magnification of 40× was applied, resulting in a lateral resolution of 7.4 µm. For the cuboid samples, selected ISO 25178 areal parameters were evaluated for a square area with an 8 mm length, measured perpendicular to the build direction on the side facing away from the coater, as indicated in Figure 43. A linear level operation, an S-filter of 20 µm and an L-filter of 0.25 mm were applied.

The chosen areal surface texture parameters to assess surface quality are Sa, the arithmetic mean height, and Sk, the core height from the material ratio curve. Sa was selected due to its common use in research and industry [6]. Sk is used because it gives more distinctive information on the surface texture (for details, refer to [17], p. 56).

The surface fatigue relation is shown using the material ratio curve parameter Svk, which is the reduced valley depth. The parameter was chosen because it describes the size of the valley population on the considered surface, rather than individual extreme values such as the maximum height Sz and the maximum valley depth Sv. More details can be found in [137]. Sa, Sk and Svk are defined in the ISO 25178-2 standard [16].

Density: The first step toward the assessment of bulk quality was the measurement of part density. For this purpose, the cuboid samples were weighed in air and ethanol using the Mettler Toledo Delta Range XS603S precision balance. The density was calculated according to Archimedes' principle as specified in ISO 3369 [170]. Each measurement was performed three times, and the final density result reported per sample is the respective mean value.

Tensile Testing: The tensile strength was tested using a ZWICK/Z050 in accordance with ASTM E8M [171]. A preloading of 35 N and a speed setting of 0.48 mm/min were selected.

The required cross-sectional areas of the tested specimens were obtained from digital caliper measurements.

Fatigue Testing: Fatigue life was tested on a DYNA-MESS 4S 20kN Z/D system at a frequency of 20 Hz and a stress ratio $R = 0.1$. The load levels were defined with respect to the mean value of the UTS for the tested surface conditions, $\sigma_{ult,mean} = 392$ MPa. Corresponding values are specified in Table A.16.

Table A.16.: Load levels and stress values for $\sigma_{ult} = 392$ MPa and $R = 0.1$ [137]

Load Level $\sigma_{max}/\sigma_{ult}$	**σ_{max}/MPa**	**σ_{min}/MPa**	**σ_{mean}/MPa**
0.4	156.8	15.7	86.2
0.5	196.0	19.6	107.8
0.6	235.2	23.5	129.4
0.7	274.4	27.4	150.9

2.3. Workflow Summary

Figure 45 gives an overview of this work's process steps.

At the first manufacturing stage, 30 cuboid samples were made. All of these were manufactured with identical bulk scan parameters, paired with 10 variations of contour scan parameters, resulting in 3 cuboid samples per parameter set combination.

Afterwards, the cuboids' densities and surfaces were measured in order to get a first assessment of bulk quality and a rating based on the surface quality. Based on these evaluations, parameter sets were selected to produce samples for mechanical testing.

For seven manufacturing parameter sets chosen based on the cuboid assessment, six samples each were made for tensile testing. Tensile testing according ASTM E8M [171] was performed.

Finally, fatigue life was tested for a first selection of contour parameter sets, and their relationship with surface texture is discussed.

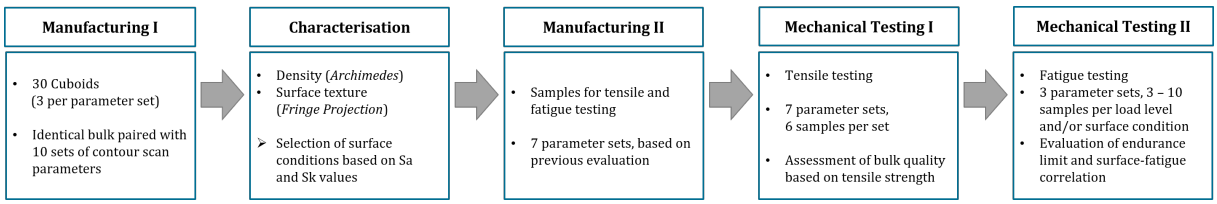

Figure 45.: Workflow summary.

3. Results and Discussion of Preliminary Findings

The results presented in this section comprise density and surface texture characterisation of the cuboid samples. The outcome is a selection of contour scan parameter sets for manufacturing the specimens for mechanical testing.

3.1. Surface Texture

Visual Perception of Surface Quality: From visual inspection of the microscopic images in Figure 46, it can be observed that, at first sight, a variety of as-built surface conditions was achieved.

The A and B conditions look mostly smooth with small dots and few linear defects (length below 1 mm, oriented parallel to the layers). Increasing the contour scan speed, surfaces appear to have more and bulkier linear defects (C and D). The D image also seems a little blurry, which is a sign of increasing height variation on the surface. This effect becomes more clear when increasing scan speed even further (E and F). On surface F, there are a few circular shadows present, which may be spatter or local accumulations of powder particles. Surfaces G to J are hardly distinguishable visually. All show circular shadows of different sizes, which are mostly particle agglomerations and accumulations, and an underlying irregular structure. Surface G shows some darker areas, which may be an issue of different lighting conditions or height differences on the surface itself.

With increasing scan speed, the energy absorbed by the powder in the scanned path decreases. Due to the low energy, powder particles are only partially molten and attached to the surface, causing coarse surface quality.

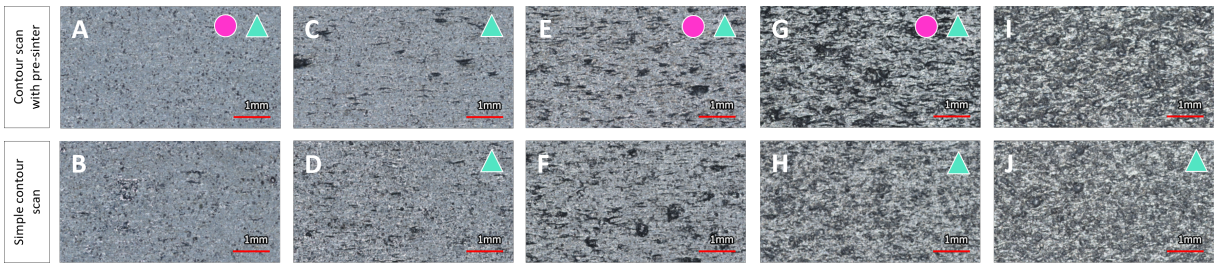

Figure 46.: Microscopic images of samples with variation of contour scan speed, from lowest *(left)* to highest *(right)*

Selection of Contour Variation for Mechanical Testing from Surface Texture: Figure 47 shows Sa (left) and Sk (right) values. The surface conditions are sorted by contour scan parameters. To the right, results for sample sets exposed to pre-sinter are presented, while to the left of each graph, results for simple contour scans are shown. The scan speed increases from the middle to the edge.

The graphs give the mean (blue line) ± two standard deviations (SD, dashed blue line). Colours mark the surface conditions that are distinctive per a 95% confidence interval (±2SD) applied to the parameter results for Sa and Sk. The first group (red) includes surface conditions A to D; conditions E and F form the second group (green); conditions G and H (purple) are the third group; and finally, the fourth group (orange) comprises conditions I and J.

A superficial look at the graphs presented in Figure 47 already confirms that the objective of creating surfaces with varying surface quality was met. This is also supported by the microscopic images in Figure 46. Numerical values are included in Table A.21.

Based on the graphs, parameter sets to produce specimens for mechanical testing were selected.

From the smooth (red) group including surface conditions A to D, A was chosen as the set with the lowest mean values for Sa and Sk. C and D were selected to compare the possible impact of pre-sinter with otherwise identical process settings (see Table A.15). G and H from the purple group are both considered for the same reason as conditions with higher parameter values.

Conditions E and F (green group) show comparable mean values for Sa and Sk, and it was decided to use set E, as it was the original starting parameter set of the contour variation study, and to discard condition F.

Parameter set J is chosen as the set with the highest mean value for Sa. Condition I, as the second coarse texture set (orange group), has a larger SD for both considered surface texture parameters and was discarded.

In summary, the following contour parameter sets are applied to produce the specimens for mechanical testing:

- Smooth surface parameter sets A, C and D (red group),
- Original parameter set E (green group),
- Coarse (purple group) and very coarse (orange group) parameter sets G, H and J.

3.2. Density

The data shown in Figure 48 confirm a density of over 99% for all of the measured samples, denoted by the grey squares in the graph, with a reference density of 2.68 g/cm^3 (theoretical maximum).

When taking a 95% confidence interval (2SD), denoted by the dashed blue whiskers, into account, data sets A and B are below that 99% value. Data set A has a lower boundary value at 98.84%, which is also the lowest overall value.

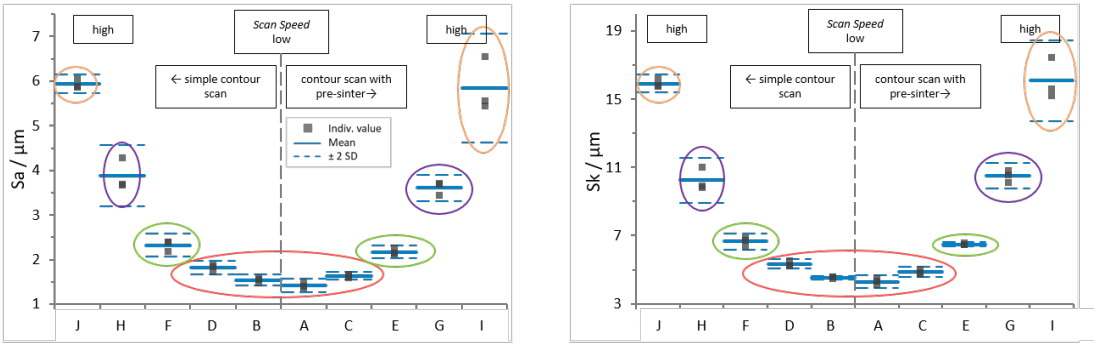

Figure 47.: Sa and Sk for samples with different contour scan; L-filter 0.25 mm, S-filter 20 µm, Mean ± 2SD

From all data sets, the only statistically distinctive sets considering the depicted 95% confidence interval (2SD) are B and G. However, they cannot be distinguished from the remaining data sets by that requirement.

In Figure 48, an increasing tendency of density for higher scan speed (A—lowest scan speed to J—highest scan speed) is observed. Supposedly, this is caused by the occurrence of closed porosities that can not be filled with ethanol during weighing. Possibly, the close proximity of the cuboids on the build platform during production plays a role as well, as the trend cannot be observed in the density data of the mechanical testing samples included in Table A.22.

However, the overall mean and %SD including all 90 measured values (3 samples each for 10 contour parameter sets, 3 measurements each) are 99.5% and 0.3%, respectively. The mean and %SD taking individual groups A to J into account amount to 99.5% and 0.17%, respectively.

In conclusion, the evaluated sample sets are considered comparable. It is found from the presented results that the bulk scan parameters predominantly define the part density. Thus, varying contour scan parameters has no statistically significant influence on the density.

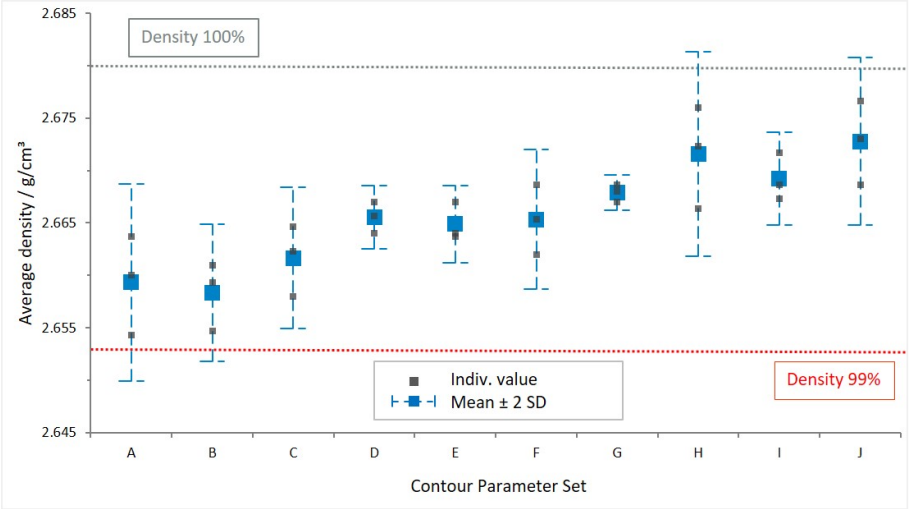

Figure 48.: Density per manufacturing parameter set, mean ± 2SD; reference density: 100% = 2.68 g/cm^3

4. Results and Discussion of Mechanical Characterisation

4.1. Tensile Properties

Figure 49 shows the tensile testing results for longitudinal specimens manufactured using the contour parameter sets A, C, D, E, G, H and J. Density values for the mechanical testing samples, along with all numerical data presented in Figure 49, are included in Appendix A.

Similar to the results from density determination, there is no statistically significant difference in UTS. The mean values of the individual surface conditions are between 374 and 406 MPa. For context, values reported in the literature for as-built of the same material and build direction vary from 300 MPa [115] to over 400 MPa [26, 30, 37]. For the cast alloy with T6 heat treatment, typically values of UTS between 320 and 360 MPa are reported [26]. Hence, the tested samples perform equally well or better than other as-built LPBF AlSi7Mg0.6 specimens and mostly exceed the strength of the cast material.

From the graph, it can be observed that the standard deviation increases for rougher surface textures. A possible influencing factor is the caliper cross-section measurement, since the UTS depends on the cross-sectional area. The caliper may be locked by protruding features, leading to variation in measured cross-section.

Moreover, the combination of line energy and powder application is a potential explanation. Poor flowability properties affect the homogeneity of powder dispersion within a layer. At higher contour scan speeds, the high reflectivity and fast heat dissipation may lead to irregular density of molten material, causing coarser surface texture and different microstructural properties. The latter will have to be confirmed by a microstructural analysis.

The overall SD of UTS values, including all 40 test results, is low—3.8% (14.94 MPa). The SD within each group (1.3% to 4.4%) is of the same order of magnitude as the SD between the groups (2.5% between mean values). Hence, the sample groups produced with different contour scan parameters are considered comparable with regard to tensile strength.

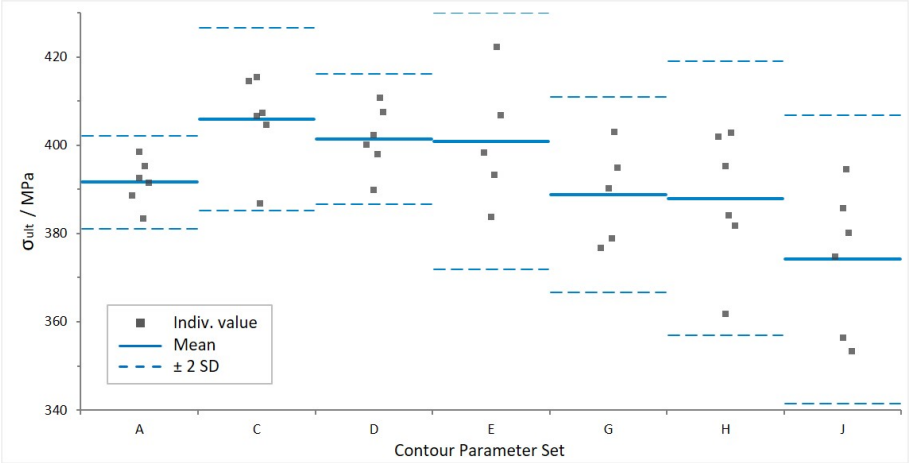

Figure 49.: Ultimate tensile strength for seven different surface conditions, mean ± 2SD

4.2. Fatigue Properties

The fatigue testing results for surface conditions A, E and G for load levels $\sigma_{max}/\sigma_{ult}$ 0.4, 0.5, 0.6 and 0.7 are presented in Figure 50. The smoothest surface condition, A, has the best fatigue performance for all load levels and low scatter, as expected. Even for the highest tested load level, cycle numbers above 10^4 are reached. Surface condition E exhibits some scattering for higher load levels, while condition G already shows scatter for load level $0.5\sigma_{ult}$. A clear tendency towards higher fatigue resistance for smoother surfaces is visible. The same is reported in surface fatigue studies that include post-processing [34, 36, 39, 41, 44, 113]. A possible explanation for the scatter on E and G is that, for these sample groups, the non-linear low cycle regime is reached. On a Wöhler curve, the logarithmic-linear relationship between stress and number of cycles is only valid in the high cycle fatigue regime [116]. Another reason may be the coarser surface texture caused by lower line energy and the possibly uneven powder distribution, as previously mentioned in Sections A.3 and A.3.

The data in Figure 50 were previously published in [137], where the following sample naming was used: A—AsB-smooth, E—AsB-medium and G—AsB-rough. In [137], more detailed evaluations of surface texture and crack initiation are shown.

Comparison with As-built Surface Data from Literature: To allow for comparison with surface quality data from the literature [37, 38, 168], Table A.17 contains surface texture parameters generated with the respective cut-off values for one sample per surface condition.

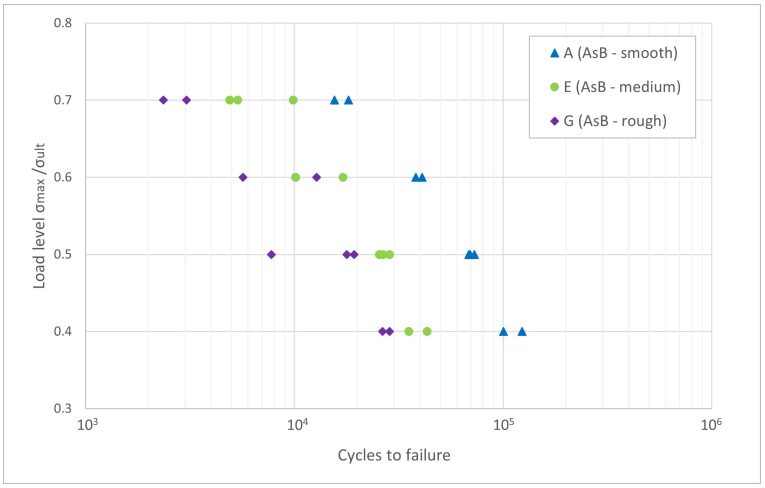

Figure 50.: $\sigma - N$-curve for surface conditions A (AsB-smooth), E (AsB-medium) and G (AsB-rough), reference stress $\sigma_{ult} =$ 392 MPa. Reproduced from [137]

Ra was determined from a 12 mm line profile, as indicated by Cacace et al. [38]. Sa and Sv were calculated from a 3 mm $\times$ 20 mm measured area. For measurement details, refer to [137]. A cut-off L-Filter of 0.8 mm was applied, as applied by Nasab et al. [168]. Please note that, deviating from Nasab et al., a least squares plane F-operation was used. The difference in F-operation is due to the sample geometries. This study assessed a flat sample geometry, while Nasab et al. evaluated cylindrical specimens.

Table A.17.: Surface texture parameters for comparison with the literature, cut-off 0.8 mm; Evaluated for one specimen per surface condition

Surface Condition	$\boldsymbol{Ra/\mu m}$	$\boldsymbol{Sa/\mu m}$	$\boldsymbol{Sv/\mu m}$
A (AsB-smooth)	3.153	3.478	20.09
E (AsB-medium)	5.649	6.987	93.78
G (AsB-rough)	7.362	9.316	96.57

Similarly to this paper, Nasab et al. [168] also used different as-built surfaces. However, taking a closer look at their considered surface conditions denoted S01, S05 and S07, they report larger Sv-values. Their best surface condition is S01 with $Sv = 112$ µm, having the order of magnitude of the roughest surface considered in this study, G (AsB-rough). S05 with $Sv = 190$ µm and S07 with $Sv = 205$ µm largely exceed the values presented in Table A.17. In their work, they induced defects to demonstrate their influence on rotating bending fatigue. They suggested a minimum material removal based on surface texture parameter results to improve surface quality. In contrast, this work was aimed at producing high-quality surfaces (described by Sa and Sk) in as-built condition with no intention of surface post-processing.

Additionally, the samples investigated in this work have a smoother surface finish (see Table A.17) in comparison with Cacace et al., who state an as-built $Ra > 10$ µm. They sandblasted the samples to achieve an $Ra < 10$ µm, as required for standard fatigue testing. The same holds for Grande et al., who reported an as-built Ra µm with $10 < Ra < 15$ µm [37, 38].

Estimation of Stress at the Endurance Limit: The stress at the endurance limit was estimated based on the horizon method, using the logarithmic-linear equation

$$lg(N) = m \cdot lg(\sigma) + c \tag{A.1}$$

as described by Einbock [116]. For the sample groups A, E and G, the mean values for each load level were used to obtain their respective logarithmic-linear relations. The coefficients per surface condition are given in Table A.18. For condition G, data points for load level 0.7 were in the LCF range with $N_{mean} = 2.7 \times 10^3$. They are most likely not on the linear part of the S–N curve and were therefore excluded from this calculation.

Table A.18.: Coefficients of logarithmic-linear equation $lg(N) = m \cdot lg(\sigma) + c$ for three surface conditions

Coefficient	**A (AsB-Smooth)**	**E (AsB-Medium)**	**G (AsB-Rough)**
m	−3.292	−3.244	−2.892
c	3.794	3.364	3.283

From this equation, the stress at endurance limit σ_L was calculated for $N_{L1} = 10^6$, $N_{L2} = 2\times10^6$ and $N_{L3} = 10^7$ and is presented in Table A.19 and Figure 51. N_{L1} to N_{L3} were chosen to allow for comparison with literature values [34, 36–38, 115, 117].

$\sigma_{L2} = 49$ MPa for surface condition E corresponds well with the experimental findings of Denti and Sola [34] and Gatto et al. [36], who report mean values of 50 MPa for as-built specimens. Bassoli et al. [115] found a slightly higher σ_{L2} of 60 MPa, which is in between groups A and E. However, as they did not evaluate surface quality, no direct comparison is possible.

Cacace et al. and Grande et al. [37, 38] found experimental endurance limit stress values at $N_{L3} = 10^7$ between 122 and 137 MPa for different positions on the build platform, being three times as high as found for A, the best performing condition studied here. As previously mentioned, they applied a sandblasting finish to meet the requirement for fatigue testing. Not only did this improve the surface finish, it also introduced compressive residual stresses, which prevent crack propagation [34, 167].

Compared to the post-processed surface conditions presented by Denti and Sola [34] and Gatto et al. [36], the A condition's endurance stress matches the performance of laser shot processed and metal shot peened (S70) specimens.

Considering conventionally manufactured parts, Dezecot and Brochu estimated a fatigue strength of 73 MPa for as-cast AlSi7Mg0.6 material from investment casting [117] at $N_L = 10^6$. Surface condition A exceeds this value by 15%. This increased strength is supposedly related to the fine microstructure due to faster solidification of the material in the LPBF process.

Table A.19.: Estimated stress for different endurance limit values N_L

Surface Condition	**A (AsB-Smooth)**	**E (AsB-Medium)**	**G (AsB-Rough)**
σ_{L1} at $N_{L1} = 10^6$/MPa	84	60	45
σ_{L2} at $N_{L2} = 2 \times 10^6$/MPa	68	49	35
σ_{L3} at $N_{L3} = 10^7$/MPa	42	30	20

Relationship of Surface Quality and Fatigue: In addition to the surface fatigue relationship shown in [137] for experimental values, this section presents data factorised to a load level of $0.5\sigma_{ult}$.

The factorisation was done based on a linear regression across all data from the tested load levels. The exponential fit of Svk vs. the number of cycles to failure data in Figure 52 is described by

$$N = 159843e^{-0.273 \cdot Svk} \tag{A.2}$$

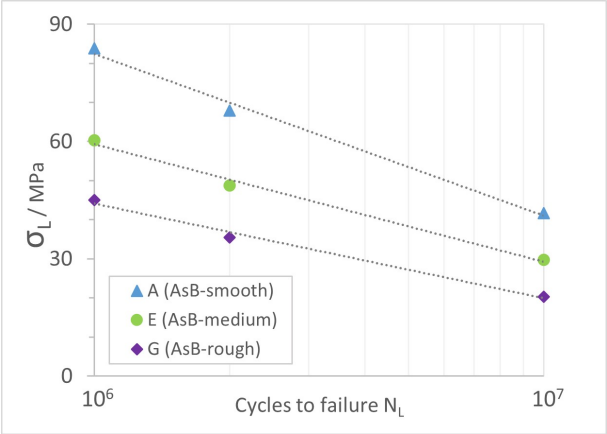

Figure 51.: Estimated stress for different endurance limit values N_L

with $R^2 = 0.8721$. Numerical values for Svk are given in Table A.20. Apart from the previously presented data for the A, E and G groups, there were also a few test results available from surface condition C samples, which were included in this fit.

The reduced valley depth Svk, derived from the material ratio curve, was chosen because it represents the valley population of a sample (within the measured area), as opposed to the common parameters for surface fatigue correlations Sz and Sv, which are individual extreme values and may not be representative of the considered surface.

This parameter choice is confirmed by the data shown in Tables A.17 and A.19. Surface conditions E and G have comparable Sv but different Ra and Sa. As previously discussed, the fatigue life for both groups clearly differs as well.

Furthermore, especially when looking at rougher surface conditions, cracks tend to start from multiple locations at the surface. Among the tested samples, this was observed for all group G specimens and half of group E specimens (for details, refer to [137]). Hence, considering the specific nature of typical LPBF-processed surfaces, it makes sense to consider more than just one extreme value per surface.

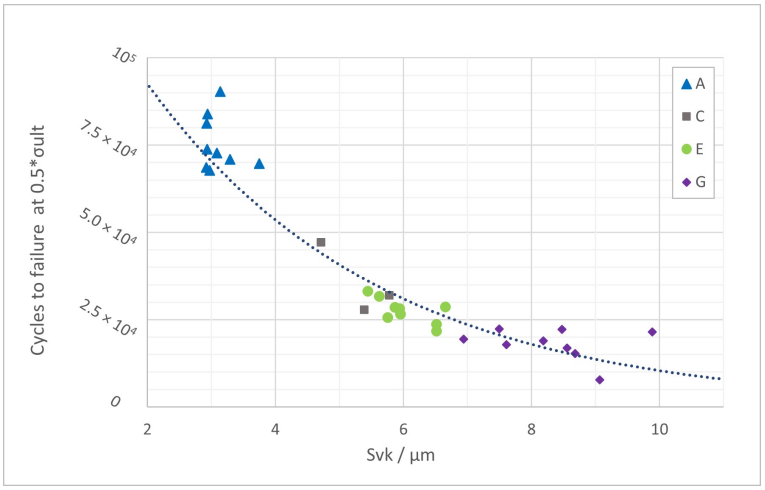

Figure 52.: Exponential fit Svk vs. cycles to failure at $0.5\sigma_{ult}$

Table A.20.: Svk for fatigue-tested samples

Surface Condition	**Mean Svk/µm**	**SD Svk/µm**
A	3.105	0.271
C	5.296	0.539
E	6.028	0.431
G	8.321	0.890

5. Conclusions

This work aimed to produce samples with identical bulk and different surface quality, including high quality, to assess the impact of as-built surface texture on mechanical properties.

The evaluation of as-built surfaces was motivated by the desire to apply LPBF for complex geometries and inner surfaces, which may be complicated or infeasible to post-process. In addition, achieving the same surface finish and fatigue performance without post-processing saves time and resources.

The variation in surface texture was achieved by varying contour scan speed. The comparability of bulk quality for the different sample groups was confirmed by means of Archimedes' density and tensile testing. The endurance limit was estimated based on four tested fatigue load levels. The relationship between the reduced valley depth Svk for the different surface quality groups was shown using data factorised to load level $0.5\sigma_{ult}$.

The following main conclusions are derived from the presented work:

- Distinctive surface conditions with Sk (L-filter 0.25 mm) between 4 µm and 16 µm were produced.
- All tested specimens have a density $> 99\%$; thus, the influence of contour scan parameters is considered insignificant regarding density.
- The ultimate tensile strength of 393 ± 9.98 MPa was found to be independent of contour scan variation.
- Optimised contour scan parameters result in as-built quality superior to some post-processed surfaces, enabling the reduction of processing steps and time.
- Condition A reaches a fatigue resistance of 84 MPa at 10^6 cycles, exceeding values for as-cast and some surface post-processed literature results.
- The reduced valley depth Svk results in a good fit across the groups for the factorised surface fatigue relation. Therefore, Svk was found to be a suitable parameter to describe surface quality.

Appendix A

Table A.21.: Sa and Sk for cuboid samples, 10 surface conditions L-filter 0.25 mm, S-filter 20 µm. With pre-sinter *(right)*, without pre-sinter *(left)*

Parameter Set	**J**	**H**	**F**	**D**	**B**	**A**	**C**	**E**	**G**	**I**
Scan Speed/mm/s	**1800**	**1200**	**900**	**600**	**300**	**300**	**600**	**900**	**1200**	**1800**
Sa/µm, Mean (N = 3)	5.94	3.88	2.33	1.82	1.54	1.42	1.63	2.17	3.61	5.85
Sa/µm, SD	0.10	0.34	0.13	0.08	0.06	0.08	0.04	0.07	0.15	0.61
Sk/µm, Mean (N = 3)	15.93	10.25	6.66	5.35	4.53	4.30	4.88	6.49	10.50	16.09
Sk/µm, SD	0.26	0.67	0.24	0.15	0.05	0.18	0.15	0.06	0.37	1.18

Table A.22.: Ultimate tensile strength and relative density of tensile samples. Reference density 2.68 g/cm^3. Seven surface conditions.

Parameter Set	**A**	**C**	**D**	**E**	**G**	**H**	**J**
N	**6**	**6**	**6**	**6**	**6**	**5**	**5**
σ_{ult}/MPa, Mean	391.63	405.90	401.42	400.87	388.79	387.96	374.21
σ_{ult}/MPa, SD	5.26	10.33	7.37	14.54	11.04	15.55	16.33
Relative Density/%, Mean	99.85	99.68	99.52	99.61	99.69	99.58	99.74
Relative Density/%, SD	0.17	0.15	0.18	0.11	0.17	0.28	0.20

A.4. Publication 4 – Surface Texture and High Cycle Fatigue[4]

Abstract: The aluminium silicon alloy AlSi7Mg0.6 is gaining importance in additive manufacturing. This work is showing a correlation of surface quality and fatigue properties of three different AlSi7Mg0.6 as-built surfaces manufactured by laser powder bed fusion. All specimens were built in z-direction and the difference in surface quality was achieved by variation of the contour scanning parameters in the manufacturing process. Focus of the evaluation is on the reduced valley depth Svk rather than the commonly applied Ra (arithmetic mean of the line roughness profile) and Rt (maximum total height of the line roughness profile) and their areal equivalents Sa and Sz. Svk is derived from the material ratio curve and is a measure of the size of the valley population across the sample. It was found to show a better correlation with number of cycles to failure than parameters based on local extreme values such as Sz and Sv (depth of deepest detected valley).

1. Introduction

Additive manufacturing (AM) technologies enable geometrical freedom, material savings and functional integration unimaginable with conventional subtractive methods. Laser powder bed fusion (LPBF) is one of the most commonly used additive manufacturing technologies. Typical surface features of as-built LPBF surfaces are powder particle agglomerations and re-entrant features, leading to a high initial surface roughness, which is associated with poor fatigue performance [2].

In recent years, aluminium alloys are increasingly used in AM due to their applications in the automotive and aerospace industries. The interest in AlSi7Mg0.6 specifically has been growing as it has good corrosion resistance, weldability and mechanical properties [30].

1.1. Surface Characterisation for Metal AM

Surface texture is often described by means of the ISO 4287 parameters Ra (arithmetic mean of the line roughness profile) and Rt (maximum total height of the line roughness profile), determined by use of contact stylus measurements [151]. Both, parameters and metrology, are established and still widely used in industry and literature and likewise for metal AM surface texture characterisation [6, 8, 14, 85, 91, 129, 135, 145, 147].

While the areal equivalents to those commonly used parameters, Sa and Sz, at least offer a more statistically significant representation of the evaluated surface as compared to line roughness, Sa and Sz are still sensitive to local extreme values and are certainly not the best fit when a description of overall surface quality is required. Literature shows investigations on various ISO 25178 parameters, such as Sa, Sz, Sv (deepest valley depth) or Ssk (shift of height distribution below or above mean plane, equal to zero for symmetrical distribution) [87, 172] and feature based approaches [100].

In this work, parameters derived from the material ratio curve [16, 82], particularly the core height Sk, reduced valley depth Svk and lower profile portion $Smr2$, are applied as they offer a more robust description of the as-built LPBF surface condition [159].

[4] *Published as:* Buchenau, Theresa; Amkreutz, Marc; Brüning, Hauke (2021): Surface Texture and High Cycle Fatigue of As-built Metal Additive AlSi7Mg0.6. In: Journal of Additive Manufacturing Technologies 1 (2), S. 531. DOI: 10.18416/JAMTECH.2111531

1.2. Mechanical Properties of AlSi7Mg0.6 from Laser Powder Bed Fusion

Ultimate tensile strength values for AlSi7Mg0.6 specimens manufactured in an LPBF process in vertical direction (layer-by-layer built-up perpendicular to the applied force in mechanical testing), vary between approximately 300 MPa [115] and over 400 MPa [26, 30, 37]. This means most of the values for as-built LPBF samples exceed the ultimate strength of the cast alloy with T6 heat treatment, which is between 320 and 360 MPa [26].

There are only a few studies on fatigue behaviour of the AlSi7Mg0.6 alloy. Some work on rotating bending fatigue with variation of LPBF contour scan parameters was done by Nasab et al. [168]. Bassoli et al. [115] performed a full Wöhler curve characterisation of one set of as-built specimens.

1.3. Objective

Numerous studies look into the correlation of surface texture and fatigue properties for metal AM parts, mostly utilising common parameters such as Ra, Rz, Rt, Sa, Sz or Sv [8, 14, 85, 129]. Literature mainly shows studies on different surface states obtained from post-processing [129] or from variation of build orientation [8]. However, the latter also affects the bulk properties of a tested sample, resulting in the assessment of a combined bulk and surface effect.

The fatigue specimens used in this work were manufactured with identical bulk parameters and build orientation, only varying the contour scan parameters to obtain differences in surface quality while maintaining bulk properties. By varying the contour scan speed, three different as-built surface conditions could be achieved and analysed.

This work aims at showing the difference in mechanical performance under axial cyclic loading for three as-built LPBF surface conditions of AlSi7Mg0.6 specimens and correlation of fatigue life with alternative standardised parameters.

2. Material and Methods

2.1. Evaluated Samples

Three sets of samples of as-built surface condition exhibiting different surface quality and features were created, namely AsB–smooth, AsB–medium and AsB–rough. The manufacturing conditions on the Trumpf TruePrint 1000 LPBF system are given in Table A.23. The manufacturing parameters only differ in the contour scan speed, the bulk parameters were identical. All samples had a density higher than 99%.

Table A.23.: AlSi7Mg0.6 manufacturing parameters on Trumpf TruePrint 1000

	Bulk	Contour (smooth/ medium/ rough)
Layer thickness / µm	30	30
Hatch distance / mm	0.12	0.12
Laser power / W	166	195
Pre-sinter / [-]	No	Yes
Scan speed / mm/s	1000	300 / 900 / 1200

The fatigue specimen geometry was developed in line with ASTM 466–15 with the following theoretical geometrical specifications: Total height 80 mm, smallest cross section width 6 mm,

and thickness 3 mm. Figure 53 shows a fatigue specimen after mechanical testing with indication of build direction.

Macroscopic and microscopic visual inspection of the samples confirm that they indeed show differences in surface quality. Differences in size and quantity of particle agglomerations can be seen in Figure 54.

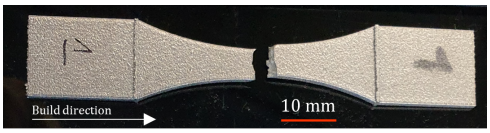

Figure 53.: Fatigue specimen after mechanical testing

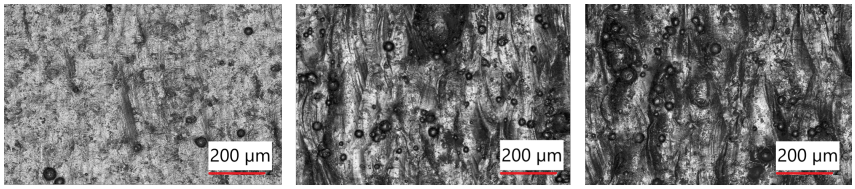

Figure 54.: Microscopic images of evaluated surface conditions, showing particle agglomerations of different size and quantity: AsB–smooth *(left)*, AsB–medium *(middle)* and AsB–rough *(right)*

2.2. Surface Characterisation

For the surface texture characterisation, the Keyence VR3200 fringe projection system was used at a lateral resolution of 3.7 µm. In the style of the ISO 4287 line parameters, ISO 25178 areal parameters were evaluated by averaging results from 5 individual areas, illustrated in Figure 55.

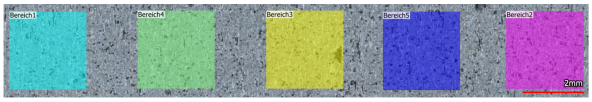

Figure 55.: ISO 25178 parameter evaluation: Mean values of 5 individual square areas of 2.5 x 2.5 mm^2, similar to the ISO 4287 line roughness calculation

The selected surface texture parameters are the commonly used areal parameters Sa (absolute mean height), Sq (root mean square height), Sz (maximum total height) and Sv (maximum valley depth), as well as the material ratio curve parameters Sk (core height), Svk (reduced valley depth) and $Smr2$ (valley profile portion). Sk, Svk and $Smr2$ are illustrated in Figure 56. Sk (spacing between horizontal green dashed lines) is determined from the intersection of the curve's main slope (red dashed line) with vertical lines at 0% and 100%. Svk is the height of a right-angled triangle (purple) enclosing an area equal to the valley portion area. $Smr2$ marks the percentage above which the valley portion of the profile is depicted on the curve. For more detailed information on the parameters briefly explained above, please refer to [16, 82, 159].

2.3. Mechanical Testing

Fatigue testing was performed on a DYNA-MESS 4S 20kN Z/D system at a frequency of 20 Hz and a stress ratio R = 0.1. The load levels were defined w.r.t. the ultimate strength acquired from tensile testing, $\sigma_{ult} = 392 \pm 5$ MPa, corresponding values are specified in Table A.24.

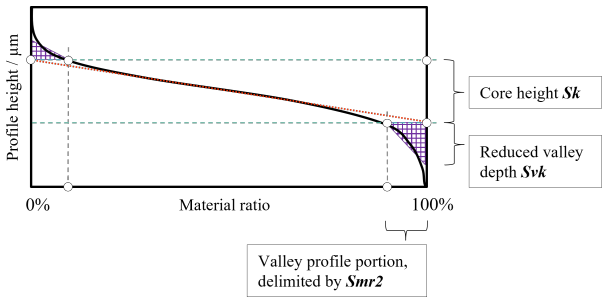

Figure 56.: Material ratio curve, determination of Sk, Svk and $Smr2$

Table A.24.: Load levels and stress values for σ_{ult} = 392 MPa and R = 0.1

Load level $\sigma_{max}/\sigma_{ult}$	σ_{max} / MPa	σ_{min} / MPa	σ_{mean} / MPa
0.4	156.8	15.7	86.2
0.5	196.0	19.6	107.8
0.6	235.2	23.5	129.4
0.7	274.4	27.4	150.9

3. Results and Discussion

3.1. Surface Characterisation

Table A.25 shows results of the commonly used parameters Sa, Sq, Sz and Sv and the material ratio curve parameters Sk, Svk and $Smr2$. For each set of samples, at least 9 specimens were included in the evaluation of mean and standard deviation values presented. When grouping the parameters w.r.t. their contained information, Sa, Sq and Sk can be categorised as indicators for the overall surface quality as they are related to the mean profile height. Sz, Sv and Svk on the other hand, are measures for extreme values, while Sz and Sv are absolute maxima and Svk represents an average value of valley depths. $Smr2$ is the profile percentage marking the portion of the profile associated with valleys below the core material. It is believed that this parameter has the potential to give an indication of the profile share critical for crack initiation. In this work, Svk is interpreted as a measure for the average size of potential crack initiation points present on the surface and is compared to Sv, the maximum valley depth, in particular concerning the correlation with fatigue properties.

Looking at the results presented in Table A.25, the three considered as-built surface conditions can be clearly distinguished by all of the chosen surface texture parameters. The standard deviation is in the same order of magnitude for all mean/core height related parameters (Sa, Sq, Sk) between 3% and 7%. For Svk, the standard deviation is slightly higher (up to 10%), while it reaches between 8% and 28% for Sz and Sv. The large standard deviations for parameters representing extreme values across the profile make sense as they are strongly dependent on the measured location. This circumstance also results in the possibility of not detecting the deepest valleys. $Smr2$ values of around 90% for all of the as-built surface conditions suggest that 10% of the areal profile belong to the reduced valley portion. Svk values of 3.1, 6.0 and 8.3 μm for the smooth, medium and rough set, respectively, indicate the average depth of the corresponding valleys.

Table A.25.: Surface texture parameters for AsB–smooth, AsB–medium and AsB–rough, L-filter = 0.25 mm, S-filter = 8 μm, R^2_{adj} for Sz, Sv and Svk for exponential fit at 0.5*σ_{ult}

		Sa / µm	**Sq / µm**	**Sk / µm**	**Sz / µm**	**Sv / µm**	**Svk / µm**	**Smr2 / %**
R²adj for 0.5*σult		n/a	n/a	n/a	0.849	0.895	0.971	n/a
AsB–smooth	*Mean*	2.58	3.36	7.89	49.90	16.55	3.10	90.31
	St.-dev.	0.161	0.221	0.490	5.768	1.355	0.256	0.158
	% St.-dev.	6	7	6	12	8	8	0.2
AsB–medium	*Mean*	4.74	6.05	14.96	79.94	36.69	6.00	90.05
	St.-dev.	0.173	0.259	0.527	13.811	7.109	0.396	0.161
	% St.-dev.	4	4	4	17	19	7	0.2
AsB–rough	*Mean*	5.99	8.14	17.37	124.59	63.76	8.32	89.61
	St.-dev.	0.222	0.314	0.558	23.561	17.918	0.839	0.446
	% St.-dev.	4	4	3	19	28	10	0.5

3.2. Fatigue

The fatigue results for the three as-built surface conditions are presented in Figure 57. The AsB–smooth samples clearly endure the highest number of cycles, AsB–medium and AsB–smooth results overlap at load level 0.6*σ_{ult}. The number of cycles to failure for the AsB–rough set of samples at load level 0.4*σ_{ult} and 0.5*σ_{ult} correspond with values determined by Bassoli et al., 2018. However, their study did not include surface quality of the tested specimens and was performed at R=0 [115].

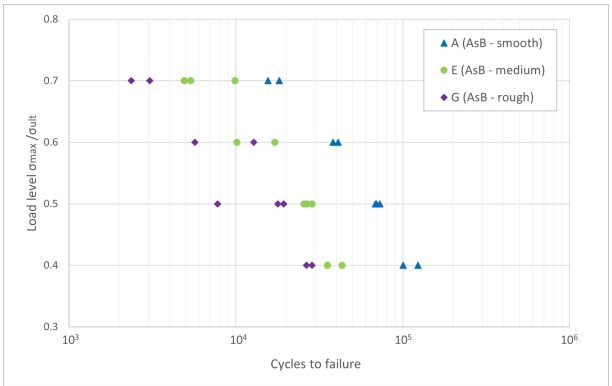

Figure 57.: Fatigue results for three surface conditions at four load levels each. Load levels are specified i.t.o. σ_{ult}

Looking at the fracture areas, it can be confirmed, that for the AsB–medium and AsB–rough specimens, all cracks started from the surface, in many cases even multiple crack initiation was observed, which is a common phenomenon for as-built AM surfaces [85]. 5 out of 10 AsB–medium specimens and 9 out of 9 AsB–rough specimens exhibited multiple crack initiation from the surface. Among the AsB–smooth specimens, only one case of multiple crack initiation from the surface was observed. 5 out of 9 fatigue failures started from individual surface cracks, 3 out of 9 started from bulk defects. Table A.26 gives a summary of failure initiation for all evaluated specimens, Figure 58 shows examples of the different observed types of crack initiation.

The collected data confirms that AM surfaces with a higher roughness (i.e., higher density of particle agglomerations) are more likely to experience multiple crack initiation during cyclic loading, resulting in failure after a fewer number of cycles. Smoother as-built surfaces, such as AsB–smooth, appear to be less likely to experience multiple crack initiation.

Table A.26.: Crack initiation for specimens of the three evaluated surface conditions

Surface condition	Total no. of samples	Crack initiation type / No. of samples	No. multiple crack initiation
AsB–smooth	9	Surface / 6 Bulk / 3	1
AsB–medium	10	Surface / 10	5
AsB–rough	9	Surface / 9	9

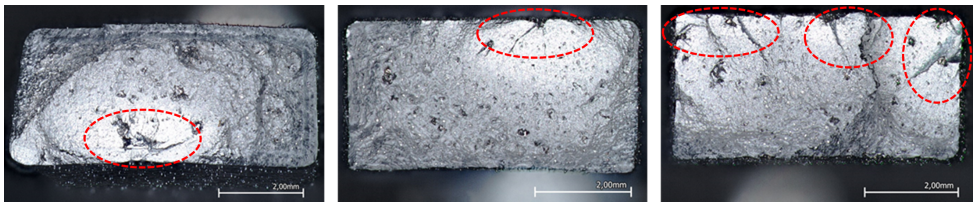

Figure 58.: A / AsB-smooth *(left)*: Crack propagation from bulk defect, E / AsB-medium *(middle)*: Crack propagation from surface defect, G / AsB-rough *(right)*: Crack propagation from multiple surface defects.

3.3. Fitting fatigue and surface quality data

When plotting data of all three surface conditions for individual load levels, an exponential function results in a good fit for the data. Figures 59 and 60 show the number of cycles vs. Svk and Sv, respectively. Comparing both curves, it can be observed that the Svk fit (red line) is closer to the actual data points (grey squares) than for Sv, quantifiable by the respective R^2_{adj}-values of 0.971 (Svk) and 0.895 (Sv). Additionally, Table A.25 contains the R^2_{adj}-value of Sz, equal to 0.849.

The curve for the number of cycles to failure (no. cycles) as a function of Svk at a load level of $0.5{*}\sigma_{ult}$ is described by

$$No.\ cycles\ (Svk) \ = \ 2.207 \ \cdot \ 10^5 \ \cdot \ 0.7016^{Svk} \tag{A.3}$$

The presented results suggest that the Svk parameter gives a better correlation of the surface condition and fatigue behaviour than Sv and Sz. Rather than only comprising information on individual extreme values, it provides information on the valley population across a sample. Especially when taking into account that multiple crack initiation from surface defects is a typical cause of failure for as-built AM parts, it seems reasonable to use Svk when correlating surface and fatigue properties. Also, the combination with $Smr2$ might be worthwhile looking into.

4. Conclusions

At the current state of this research, the following conclusions can be drawn:

- The reduced valley depth Svk (derived from the material ratio curve) is more robust and reproducible than maximum valley depth Sv and maximum total profile height Sz.
- The fatigue behaviour of as-built AlSi7Mg0.6 LPBF parts is strongly related to the surface quality. AsB–smooth specimens hardly experience multiple crack initiation while it is common for AsB–rough specimens.

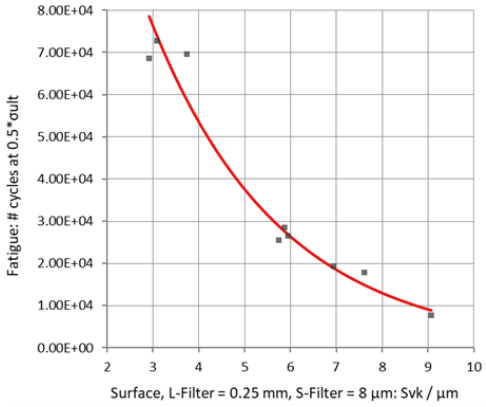

Figure 59.: Number of cycles vs. Svk for all surface conditions, exponential fit with $R^2_{adj} = 0.971$

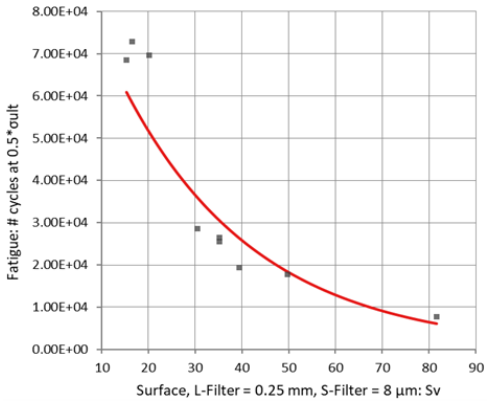

Figure 60.: Number of cycles vs. Sv for all surface conditions, exponential fit with $R^2_{adj} = 0.895$

- Rougher AM surfaces are associated with higher individual profile extreme values Sz and Sv, which are frequently applied when correlating surface quality and fatigue behaviour. However, these surfaces are also likely to exhibit multiple crack initiation, justifying the shift toward using Svk, which characterises the valley population present on the surface.
- Svk shows a better correlation than the more frequently used Sv with number of cycles to failure for the evaluated load levels and surface conditions.

In order to fully characterise the fatigue behaviour of as-built LPBF AlSi7Mg0.6 parts, full Wöhler curve assessment, residual stress measurement and fatigue limit determination for all created surface conditions is ongoing. This will enable the application of existing models for the correlation of fatigue and defects to less commonly used surface texture parameters like Svk.

A.5. Publication 5 – Surface Feature Parameters[5]

Kurzfassung: Additive Fertigungstechnologien (AM) bieten Potenzial für die Entwicklung funktional integrierter Leichtbaukonstruktionen, biomimetischer Strukturen und Materialeinsparungen. Typischer-weise sind die Oberflächen im Ur-Zustand (d.h., ohne Nachbearbeitung) durch Pulverpartikelagglomera-tionen und andere typische Merkmale gekennzeichnet, was zu einer hohen initialen Oberflächenrauheit führt, die einen negativen Einfluss auf die Dauerfestigkeit von Bauteilen hat. Um alle Vorteile der Technologie nutzen zu können, müssen die kritischen Oberflächenmerkmale für die Rissentstehung bei Ermüdungsbeanspruchung identifiziert werden, insbesondere für Anwendungen in der Luft- und Raumfahrt. Ein erster Schritt zur Verwirklichung dieses Ziels ist die Charakterisierung der Oberflächentextur auf Grundlage der Quantifizierung von Oberflächenmerkmalen mittels Elementparametern. Ausgewählte Elementparameter werden für drei verschiedene Oberflächenzustände von Aluminiumlegierungsproben aus dem Selektiven Laserstrahlschmelzverfahren (LPBF) ausgewertet und verglichen.

Abstract: Additive manufacturing (AM) technologies show potential for the development of functionally integrated lightweight designs, biomimetic structures and material savings. Typically, as-built surfaces are characterised by powder particle agglomerations and re-entrant features, leading to a high initial surface roughness, which is associated with poor fatigue performance. In order to make use of the full range of advantages with special focus on aerospace applications, critical features for crack initiation when subjected to fatigue loading need to be identified and mitigated. A first step toward achieving this goal is the surface texture characterisation based on the quantification of surface features by means of surface feature parameters. Selected areal feature parameters are evaluated and compared for three different as-built surface conditions of aluminium alloy samples from laser powder bed fusion (LPBF).

1. Einleitung

Die Oberflächen additiv gefertigter (AM) Metallteile aus pulverbasierten Verfahren weisen in der Regel Pulverpartikelagglomerationen und andere typische Merkmale auf, die zu einer hohen Oberflächenrauheit führen und sie deutlich von Oberflächen aus subtraktiven Fertigungsverfahren unterscheiden. Eine angepasste Charakterisierung ist notwendig, um die Qualität der AM-Teile hinsichtlich Beschichtbarkeit, mechanischer Eigenschaften oder Korrosionsbe-ständigkeit für den Einsatz in der Luft- und Raumfahrt, im Automobilbau, in der Medizin und in anderen industriellen Anwendungen zu beurteilen.

Die Charakterisierung von Oberflächen für AM Bauteile stellt nach wie vor eine Herausforderung dar. In industriellen Qualitätssicherungsprozessen sind noch immer Profilparameter wie Ra (mittlere Rautiefe), Rz (mittlere Maximalhöhe über 5 Einzelmesstrecken) und Rt (maximale Profilhöhe) etabliert, inzwischen gewinnen dort aber auch die entsprechenden flächenhaft ausgewerteten Äquivalente Sa (flächenhafte mittlere Rautiefe, äquivalent zu Ra) und Sz (maximale Profilhöhe innerhalb der ausgewerteten Fläche, äquivalent zu Rt) zur Bewertung der Oberflächengüte an Bedeutung. Da bei der Ermittlung dieser Parameter aber ausschließlich Höhendifferenzen betrachtet werden, können sehr unterschiedliche Oberflächentexturen identische Kennzahlen aufweisen [17]. Elementparameter bieten hier Potenzial um individuelle Texturformen zu beschreiben und so zum Beispiel mögliche Rissstellen zu identifizieren oder Kontaktflächen zu bestimmen. So kann u.a. auch untersucht werden, inwiefern sich die Form einer Senke (oder anderer Oberflächenelemente) z.B. auf die Rissentstehung und –ausbreitung auswirkt.

[5] *Published as:* Buchenau, Theresa; Brüning, Hauke; Amkreutz, Marc (2022): Elementparameter zur Oberflächencharakterisierung additiv gefertigter Metallkomponenten. Feature parameters for Metal Additive Surface Texture Characterisation. In: Martina Zimmermann (Hg.): Werkstoffe und Bauteile auf dem Prüfstand. Prüftechnik – Kennwertermittlung – Schadensvermeidung. Sankt Augustin: Deutsche Gesellschaft für Materialkunde e.V, S. 117–123. ISBN: 978-3-88355-430-3; DGM 40. Vortrags- und Diskussionstagung Werkstoffprüfung. Dresden (Germany) & Online, October 2022.

In dieser Arbeit werden am Beispiel von drei AlSi7Mg0.6 Oberflächen aus dem Selektiven Laserstrahlschmelzverfahren (laser powder bed fusion = LPBF) einige Möglichkeiten und Herausforderungen der neuartigen Charakterisierung mit Elementparametern herausgearbeitet.

2. Experimentelle Details

2.1. Untersuchte Proben

Es wurden drei im LPBF-Verfahren hergestellte Proben aus der Legierung AlSi7Mg0.6 mit unterschiedlichen Oberflächenqualitäten und -merkmalen ausgewählt, nämlich AsB - smooth, AsB - medium und AsB - rough. Die Herstellungsbedingungen auf dem Trumpf TruePrint 1000 LPBF-System sind in Table A.27 aufgeführt. Die Herstellungsparameter unterscheiden sich nur in der Kontur-Scangeschwindigkeit, die Druckparameter der Probenkerne sind identisch. Alle untersuchten Proben weisen eine Dichte von mehr als 99% auf.

Table A.27.: Prozessparameter auf der Trumpf TruePrint 1000 Anlage / Manufacturing parameters on Trumpf TruePrint 1000

	Bulk-Scan	Contour-Scan (smooth/ medium/ rough)
Layer thickness / µm	30	30
Hatch distance / mm	0.12	0.12
Laser power / W	166	195
Pre-sinter / [-]	No	Yes
Scan speed / mm/s	1000	300 / 900 / 1200

Die Geometrie der Ermüdungsproben wurde in Anlehnung an ASTM 466-15 mit den folgenden theoretischen geometrischen Spezifikationen entwickelt: Flachprobe mit Gesamthöhe 80 mm, kleinste Querschnittsbreite 6 mm und Dicke 3 mm. Figure 61 zeigt eine Ermüdungsprobe nach der mechanischen Prüfung mit Angabe der Baurichtung.

Die makroskopische und mikroskopische Sichtprüfung der Proben bestätigt, dass diese tatsächlich Unterschiede in der Oberflächenqualität aufweisen. Unterschiede in Größe und Menge der Partikelagglomerationen sowie Welligkeit sind qualitativ in Figure 62 zu erkennen.

Für Proben der hier vorgestellten Oberflächenzustände wurden bereits Zugversuche und Dauerschwingversuche (axiale Belastung mit R = 0.1) zur mechanischen Charakterisierung durchgeführt. Ein Teil dieser Ergebnisse wurde in [137] veröffentlicht.

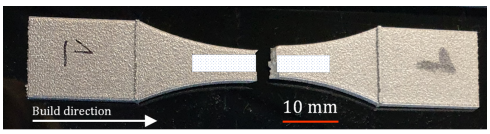

Figure 61.: Ermüdungsprobe nach mechanischer Prüfung mit Markierung der gemessenen Fläche / Fatigue specimen after mechanical testing with measured area marking

2.2. Oberflächenmessung

Für die Messung der Oberflächen wurde das Streifenlichtprojektionssystem Keyence VR3200 mit einer lateralen Auflösung von 3,7 µm verwendet. Die Messunsicherheit wird vom Herstel¬ler mit 1 µm auf die Höhenmessung angegeben. Der Messbereich (s. Figure 61) ist etwa 3 mm x 20 mm groß und wurde auf den Proben durch vier aufgedruckte Punkte markiert.

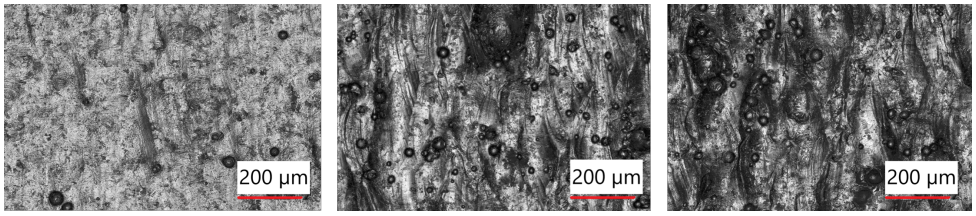

Figure 62.: Mikroskopische Aufnahme der untersuchten Oberflächenzustände mit Partikelagglomerationen unterschiedlicher Große und Dichte, *v.l.n.r:* AsB – smooth, AsB – medium, AsB – rough / Microscopic images of evaluated surface conditions, showing particle agglomerations of different size and quantity: AsB – smooth *(left)*, AsB – medium *(middle)* and AsB – rough *(right)*

2.3. Ausgewählte Parameter zur Oberflächencharakterisierung

Zur Bestimmung von Elementparametern ist zunächst die Segmentierung der betrachteten Oberfläche und anschließendes Zusammenführen kleinerer Elemente durch Wolfbeschneidung notwendig. Dabei werden Täler und Hügel voneinander getrennt und Elemente, die den Prunenschwellwert (i.d.R. angegeben in %Sz) unterschreiten, mit dem nächstgelegenen größeren Element kombiniert, wie veranschaulicht in Figure 63. In der ISO 25178 [16] ist für einige Elementparameter der Standard-Schwellwert mit 5% angegeben. Für detaillierte Informationen wird auf [16, 18, 82, 103] verwiesen.

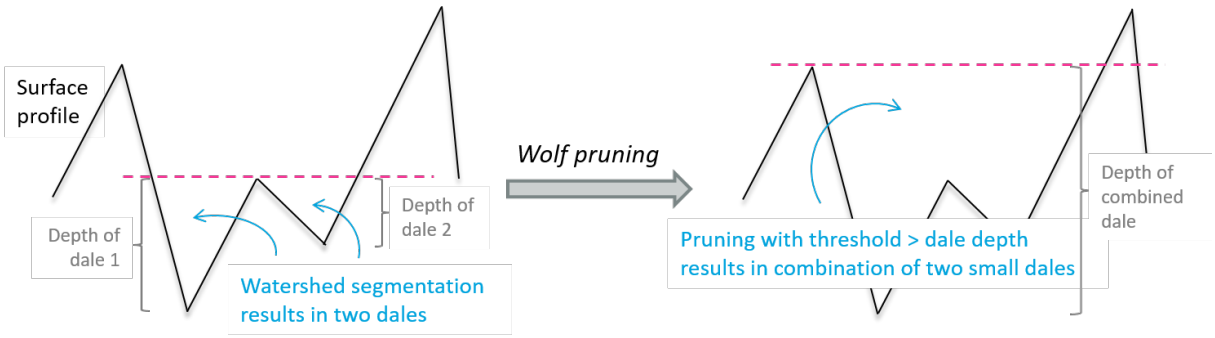

Figure 63.: Kombination kleiner Täler durch Wolfbeschneidung / Combination of small dales by Wolf pruning

Es werden in dieser Arbeit Charakteristika von Senken betrachtet, da in Folgearbeiten vor allem der Zusammenhang mit der Dauerfestigkeit thematisiert wird. Die folgenden Elementparameter wurden ausgewählt:

- $Svd \rightarrow$ Senkendichte in $1/mm^2$
- $Sdd \rightarrow$ Mittlere Senkentiefe in µm
- $Sded \rightarrow$ Mittlerer Senkendurchmesser in mm

2.4. Auswertung der Oberflächendaten

Zur Datenauswertung wurde die Software MountainsMap V9.2 genutzt. Folgende Filter wurden angewandt: S-Filter = 8 µm, L-Filter = 0.25 mm. Weitere Details zur Datenauswertung werden auf Anfrage gerne von den Autoren zur Verfügung gestellt.

Zusätzlich zu den beschriebenen Elementparametern wurden als weithin bekannte Referenzwerte Sa (arithmetischer Höhenmittelwert) und Sz (maximale Profilhöhe) ausgewertet.

Die Elementparameter wurden jeweils mit den Schwellwerten 5%Sz und 10%Sz ausgewertet.

3. Ergebnisse

Table A.28 und Figure 64 zeigen Auswertungsergebnisse gewählter Elementparameter für die drei Proben AsB-smooth, AsB-medium und AsB-rough. Es werden jeweils Werte für die Prunenschwellwerte 5%Sz und 10%Sz gegenübergestellt. Der Fokus liegt hierbei auf Parametern, die Senkeneigenschaften beschreiben, da in zukünftigen Arbeiten die Dauerfestigkeit thematisiert wird, die in Zusammenhang mit Oberflächensenken steht.

Table A.28 gibt einen Überblick über die ausgewählten Elementparameter *Svd* (Senkendichte), *Sdd* (mittlere Senkentiefe) und *Sded* (mittlerer Senkendurchmesser). Als Referenzwerte werden auch die häufig verwendeten Parameter *Sa* (mittlere Rauhtiefe) und *Sz* (Maximale Profilhöhendifferenz) angegeben. Rauere Oberflächen weisen i.d.R. höhere *Sa*- und *Sz*-Werte auf. Die Sortierung der Proben in Figure 64 und Table A.28 startet von der am wenigstens rauen Oberfläche AsB-smooth.

Die numerischen Werte der einzelnen Prunenschwellwerte für alle betrachteten Oberflächen sind in Figure 64 (oben links) veranschaulicht, um deren Variabilität zu verdeutlichen, die durch die Unterschiede in den Sz-Werten zustande kommt. Die Werte werden jeweils größer für rauere Oberflächen.

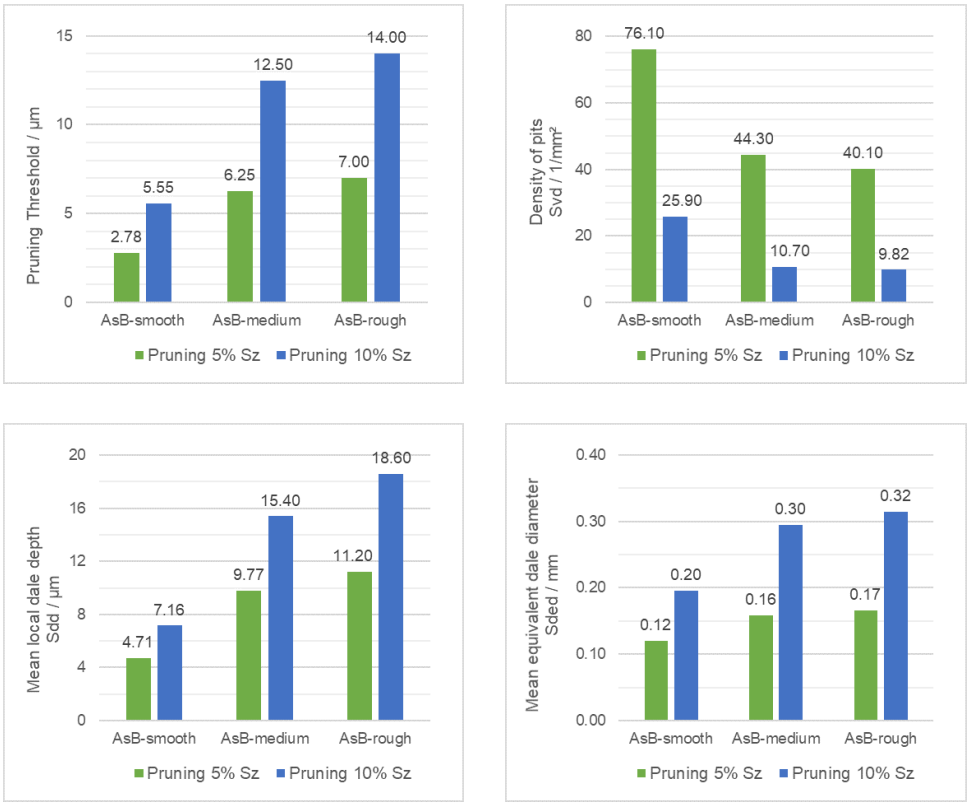

Figure 64.: Variation des Prunenschwellwertes *(oben links)*, der Senkendichte *Svd (oben rechts)*, der Senkentiefe *Sdd (unten links)* und des Senkendurchmessers *Sded (unten rechts)* für drei Oberflächenzustände / Variation of pruning threshold *(top left)*, pit density *Svd (top right)*, dale depth *Sdd (bottom left)* and dale diameter *Sded (bottom right)* for three surface conditions

Die Senkendichte (Svd, Figure 64 oben rechts) sinkt unter den betrachteten Bedingungen für rauere Oberflächen für beide Prunenschwellwerte (5% und 10%Sz), wobei der größere Schwellwert zu kleineren Zahlenwerten führt. Die mittlere Senkentiefe (Sdd, unten links) hingegen wird größer für rauere Oberflächen und ist jeweils größer für den größeren Schwellwert. Der mittlere Senkendurchmesser ($Sded$, unten rechts) unterscheidet sich für AsB-medium und AsB-rough bei gleichem Schwellwertprozentsatz kaum und fällt im Vergleich etwas geringer aus für AsB-smooth.

Table A.28.: Ausgewählte Elementparameter für drei Oberflächenzustände / Selected feature parameters for three surface conditions

Parameter	AsB-smooth		AsB-medium		AsB-rough	
Sz / µm	55.50		125.00		140.00	
Sa / µm	2.74		4.54		5.49	
Pruning	5% Sz	10% Sz	5% Sz	10% Sz	5% Sz	10% Sz
Pruning / µm	2.78	5.55	6.25	12.50	7.00	14.00
Svd / 1/mm²	76.10	25.90	44.30	10.70	40.10	9.82
Sdd / µm	4.71	7.16	9.77	15.40	11.20	18.60
$Sded$ / mm	0.12	0.20	0.16	0.30	0.17	0.32

4. Diskussion

Die Datenauswertung zeigt, dass vor allem die Oberfläche mit der geringsten Rauheit, sich in den betrachteten Elementparametern deutlich von den anderen beiden unterscheidet. Die vergleichsweise große Senkendichte Svd der AsB-smooth - Oberfläche kann auf den ersten Blick überraschen, weshalb hier eine genauere Betrachtung nötig ist. Denn werden auch Sdd und $Sded$, die mittleren Dimensionen der Senken, mitberücksichtigt, wird ersichtlich, dass diese große Anzahl im Vergleich deutlich kleinere Elemente beziffert als bei den raueren Oberflächen.

Bei Letzteren werden solche Elemente, die im Vergleich zur Gesamthöhe Sz klein sind, durch die Anwendung des Schwellwertes zusammengefasst, wodurch sich insgesamt die Senkenanzahl verringert (siehe auch [82], S. 183f.). Bei der Betrachtung von Figure 62 sind auf der AsB-smooth – Oberfläche beispielsweise deutlich weniger anhaftende Pulverpartikel zu sehen, als bei AsB-medium und AsB-rough.

Außerdem zeigt sich im Vergleich der Ergebnisse mit 5%Sz und 10%Sz Schwellwert sehr eindeutig dessen großer Einfluss: Die Senkendichte ist um mehr als 2/3 reduziert. Die Maximalhöhe Sz ist ein Extremwert (der Abstand zwischen tiefstem und höchstem Punkt auf der Oberfläche), der bereits durch einen Ausreißer (z.B. Messartefakt, oder für AM: große Pulveranhaftung) stark variiert. Es ist fraglich, wie sinnvoll die Abhängigkeit des Prunenschwellwerts von diesem Wert ist, da der Prozess dazu dienen soll, charakteristische Elemente herauszustellen und eine Über- und Untersegmentierung zu vermeiden. Die Angabe des Schwellwertes ist bei der Verwendung von Elementparametern immer notwendig. Weiterführende Informationen sind in [82] und [103] zu finden.

Der Unterschied zwischen AsB-medium und AsB-rough fällt eher gering aus, mit etwa 10% für Svd bei 5%Sz Prunenschwellwert. Für weitere Auswertungen wäre es zum einen interessant, mehrere Proben dieser Oberflächenzustände zu betrachten, um die Eignung der Prunenschwellwerte zu überprüfen. In [137] wurden beispielweise Durchschnittswerte von 7 AsB-medium Proben gebildet und der Sz fiel mit knapp 80 µm deutlich geringer aus (Achtung: Hier wurde die ausgewertete Fläche in 5 Einzelbereiche unterteilt, sodass der Effekt von Aus-reißern reduziert wurde). Zum anderen sollten weitere ISO 25178 Elementparameter, die Form und Größe

beschreiben, einbezogen werden. Auch die Entwicklung AM-spezifischer Elementparameter würde hier interessante Möglichkeiten bieten.

Insbesondere bei der Ermittlung von Senkeneigenschaften sollte beachtet werden, dass optische Messsysteme, die die Probe ausschließlich in der Draufsicht erfassen, u.U. durch Abschattungen oder Hinterschneidungen keine vollständigen Informationen liefern. µCT-Aufnahmen können eine Alternative sein, allerdings ist die Methode deutlich zeitintensiver und komplexer als beispielsweise Streifenlichtprojektion oder Konfokalmikroskopie [68].

5. Schlussfolgerungen und Ausblick

Elementparameter bieten die Möglichkeit einer Oberflächencharakterisierung unabhängig von Profilmittellinien oder Materialanteilen. Senken und Hügel werden durch Segmentierung und Wolfbeschneidung (Setzen des Prunenschwellwerts) voneinander getrennt, sodass ihre di-versen Eigenschaften als Elementparameter bestimmt werden können, und nicht mehr der Abstand von Punkten zur Mittellinie. Außerdem ergibt sich die Möglichkeit, den Einfluss der Form einer Senke (oder anderer Oberflächenelemente) z.B. auf die Rissentstehung und -ausbreitung zu untersuchen.

Die Auswahl eines passenden Schwellwertes kann eine Herausforderung darstellen und des-sen Angabe ist zwingend erforderlich um Vergleichbarkeit und Reproduzierbarkeit der Ergeb-nisse zu gewährleisten. Außerdem ist es sinnvoll, mehrere Elementeigenschaften bzw. -parameter im Zusammenhang zu betrachten, um z.B. eine große Senkendichte (Svd) entsprechend einzuordnen.

In Zukunft kann insbesondere für die Bewertung von AM-Oberflächen die Definition und Auswertung von prozessspezifischen Topographieelementen, wie z.B. Größe und Dichte anhaftender Pulverpartikel, partikelfreier Oberflächenanteil, Breite von Laserspuren usw., interessant werden. Hier können Elemente in Zusammenhang mit der Oberflächenfunktion gebracht und beispielweise mit mechanischer Performance, Korrosion oder Adhäsionseigenschaften korreliert werden.

Die elementbasierte Auswertung von Hügeln, Senken und zukünftig definierten Elementen, bringt auch neue Anforderungen an die genutzten Messsysteme bezüglich der Darstellung dieser charakteristischen Elemente mit sich [82]. Beispiele hierfür sind die Abbildung von Kugel(-segmenten) bei der Laserkonfokal-Messung [68] oder der Erkennung einzelner Senken bei der Fokusvariationsmessung [60]. Auch Abschattungseffekte und Hinterschneidungen spielen hier eine Rolle.

Zu den in dieser Arbeit betrachteten Proben wurden bereits Dauerschwingversuche durchgeführt [137] und Auswertungen in Zusammenhang mit Elementparametern sind in Vorbereitung.

A.6. Publication 6 – Process-specific Surface Features[6]

Abstract: Additive manufacturing (AM) technologies show potential for the development of functionally integrated lightweight designs, biomimetic structures and material savings. Typically, as-built surfaces show powder particle agglomerations and re-entrant features, leading to rough surfaces, which are associated with poor fatigue performance. To benefit from the full range of advantages with special focus on aerospace applications, critical features for crack initiation when subjected to fatigue loading need to be identified and mitigated. A first step toward achieving this goal is the surface texture characterisation based on the quantification of surface features. In this paper, selected areal height, functional and feature parameters from ISO 25178-2:2022 are generated and process-specific features are examined for as-built AlSi7Mg0.6 from laser powder bed fusion (PBF-LB). A connection with the particle size distribution of the used powder is demonstrated. It is shown that surface feature analysis opens up opportunities to use physically meaningful surface characteristics in future quality assurance and part qualification processes.

1. Introduction

Over the last two decades, additive manufacturing (AM) technologies evolved from rapid prototyping of porous structures to production of high-quality parts. AM enables design freedom, as well as reduction of material waste and cost [2, 120]. However, when qualifying an AM part for load-bearing aerospace applications, surface texture is of particular interest with respect to fatigue performance [2] and requires new approaches to quality assessment (QA). In industrial QA, the generation of profile parameters such as Ra (arithmetic mean deviation of the assessed profile) or Rt (total height of profile), for data acquired using a contact stylus measurement system, is the status quo [6]. Due to the low statistical relevance of individual profile measurements for the assessment of surface quality [82] and the increasing application of optical measurement systems, their areal equivalent parameters, Sa and Sz, have gained relative acceptance in recent years. However, Sa and Sz are still based on height variation with respect to a mean plane, rather than representing the actual size of a topography element. The restriction to height variation leads to the same value of Ra/Sa representing surfaces with different surface features, different material ratios [17] and different mechanical, adhesive and corrosive behaviours.

Areal measurements, as compared to profile measurements, offer a more representative depiction of surface topography and enable the extraction of characteristic surface features [6, 82, 97]. Several feature parameters describing various geometric properties of hills and dales are included in the latest version of ISO 25178 [16]. Beyond the consideration of hills and dales, process-related surface features can be evaluated. Frequently observed features in powder-based AM are particle agglomerations of different size. In recent years, extensive work has been done on developing methods for segmentation and feature detection and their application to AM surfaces [18, 19, 60, 65, 100, 103, 173].

In this work, we focus on the evaluation of surface properties related to powder particle agglomerations, such as size and quantity, as well as the area portion of the surface covered by attached particles and their relation to the particle size distribution of the powder used in the process. Furthermore, selected ISO 25178 [16] feature parameters derived from hill and dale properties after watershed segmentation are generated.

[6] *Published as:* Buchenau, Theresa; Thompson, Adam; Brüning, Hauke; Amkreutz, Marc; Mayer, Bernd; Piano, Samanta (2023): Surface Features of As-built Metal Additive AlSi7Mg0.6. In: Preprints 2023, 2023030174. DOI: 10.20944/preprints202303.0174.v2; 17th ECSSMET. Toulouse (France), March 2023.

The surface topography is measured by focus variation (FV) microscopy, which is an optical non-contact method based on stacking images from different focal planes of the same location in z-direction. An advantage of this technology is its robustness to variation of optical surface properties such as reflectivity [64, 174]. Surfaces of fatigue specimens in as-built condition from a laser-beam powder bed fusion (PBF-LB) process made of AlSi7Mg0.6 material are examined in this study.

2. Materials and Methods

2.1. Samples

The evaluated samples are fatigue specimens according to ASTM 466–15 (total height 80 mm, smallest cross section width 6 mm, and thickness 3 mm, shown in Figure 65) produced in a laser-based powder bed fusion (PBF-LB) process from AlSi7Mg0.6 material, manufactured on a Trumpf TruePrint 1000 system using the parameter settings specified in Table A.29. Bulk and contour parameter sets were previously optimised for density and surface texture, respectively [138]. The optimisation resulted in a layer thickness of 30 µm and a hatch spacing of 0.12 mm for both, bulk and contour. The specimen bulk was produced with a laser power of 166 W at a scan speed of 1000 mm/s. For the contour scan, these settings were adjusted to 195 W and 300 mm/s. The eight specimens examined in this work originate from a larger surface variation study and are part of the smoothest surface group produced (for details, see [137, 138, 175]).

Table A.29.: AlSi7Mg0.6 manufacturing parameters for bulk and contour.

	Bulk	Contour
Layer thickness / µm	30	30
Hatch distance / mm	0.12	0.12
Laser power / W	166	195
Pre-sinter / [-]	No	Yes
Scan speed / mm/s	1000	300

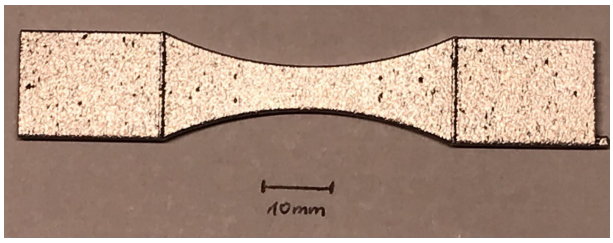

Figure 65.: Fatigue specimen geometry according to ASTM 466-15.

2.2. Surface Measurement

The surfaces were measured using an Alicona Infinite Focus G5 focus variation (FV) instrument with unpolarised coaxial lighting at 10× magnification with an individual image field of view (FOV) of 1.62 mm × 1.62 mm. To measure the entire marked area of about 3 mm × 20 mm on each sample, up to 3 × 14 images were stitched. All measurements were taken with a vertical resolution < 0.1 µm and a lateral resolution of 2.5 µm.

2.3. Surface Data Evaluation

The data evaluation was performed in MountainsMap® V9.2. To reduce calculation time, a 3 mm × 6 mm area portion centred within the measured area was extracted and a total number of eight data sets from different samples (I to VIII) was used to obtain the results presented in this work. For reference, height and functional parameters form ISO 25178 were generated. An overview of all parameters used is given in Table A.30. Feature parameter evaluation according to ISO 25178 and process-specific feature analysis were performed. Pruning threshold values were selected in accordance with powder characteristics, namely half the $d10$ diameter of the used AlSi7Mg0.6 powder [156], resulting in the applied height pruning value of 13.5 µm.

Table A.30.: Overview of Parameters generated.

Parameter / Unit	Description
Sz/µm	Maximum total height of profile
Sa/µm	Arithmetic mean height of profile
Sk/µm	Core height
Spk/µm	Reduced peak height
Svk/µm	Reduced valley depth
Spd/mm^{-2}	No. of peaks per unit area
Svd/mm^{-2}	No. of valleys per unit area
Shh/µm	Mean local hill height
d_{max}/µm	Average max. particle diameter
z_{max}/µm	Average max. particle z-height
Area covered/%	Particle coverage
Particle density/mm^{-2}	No. of particles per unit area

2.3.1. Surface Feature Parameters from ISO 25178

Selected surface feature parameters were calculated after applying a Gaussian convolution S-filter of 5.3 µm, a least-squares plane level operation and an L-filter of 0.25 mm. The feature parameters specified in ISO 25178 describe hill and dale properties and are obtained from surface data after watershed segmentation and height pruning. For more information, refer to [82, 103]. The considered parameters are the density of valleys, Svd, the density of peaks, Spd, and the mean local hill height Shh. For details on the individual calculation of these parameters, refer to [82].

2.3.2. Process-specific Areal Surface Features

Particle agglomerations are significant process-specific features observed on PBF-LB surfaces. The circle detection method implemented in the MountainsMap® particle analysis module was used to isolate the specific features on the surfaces. For this purpose, at first, a very small bandwidth was filtered to only maintain sharp edges (= particle boundaries), applying an L-filter of 0.0055 mm. Subsequently, the circle detection algorithm was applied, using limit values for detection diameters again, based on the particle size distribution values $d10$ = 27 µm and $d90$ = 67 µm. The minimum diameter for detection was set to 20 µm, somewhat lower than $d10$, while the maximum was chosen as 200 µm, roughly three times $d90$ to account for the possibility of clustered agglomerations. In order to find the original height of the detected particles, the previously obtained mask was applied to the initial (primary) surface (after application of S-filter

and F-operation). The evaluated characteristics are the average maximum particle diameter d_{max}, maximum particle z-height z_{max}, percentage area portion covered by detected particles and finally, the particle density.

3. Results

The 3D representation of one of the examined surfaces and the corresponding focus variation microscopic image in Figure 66 show powder particle agglomerations as the dominant process-specific feature at the considered scale for this surface type. This upcoming results section is split in three subsections, where ISO 25178 height and functional parameters, standardised feature parameters, and finally, characteristic values derived from process-specific areal surface features are presented.

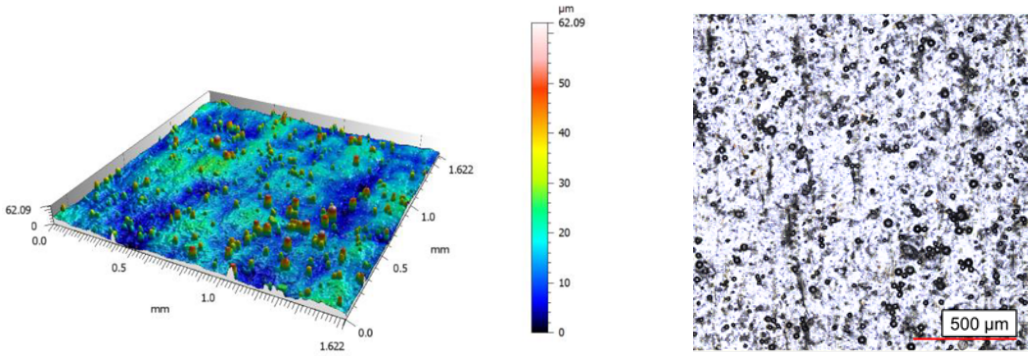

Figure 66.: 3D view *(left)*, Focus variation microscopy image *(right)*; As-built AlSi7Mg0.6 surface, 1 FoV (1.62 mm × 1.62 mm), showing PBF-LB- typical particle agglomeration features.

3.1. Height and Functional Surface Texture Parameters from ISO 25178

For reference, the areal surface texture parameters Sa (arithmetic mean height of profile) and Sz (maximum total height of profile) were calculated. Furthermore, the material ratio curve parameters Sk (core height), Spk (reduced peak height) and Svk (reduced valley depth) were generated. Numerical results including mean value and standard deviation (SD) for the listed parameters are given in Table A.31.

Table A.31.: Common parameters Sa and Sz, Material ratio curve parameters Sk, Spk and Svk; L-filter 0.25 mm, N = 8

$N = 8$	Sz/µm	Sa/µm	Sk/µm	Spk/µm	Svk/µm
Mean	61.74	1.76	4.87	5.21	2.12
SD	7.68	0.11	0.23	0.90	0.13

Figure 67 shows the exemplary material ratio curve of sample IV. From the curve, combined with the numerical values, a relatively flat core slope with steep decreases from the peak and toward the valley portion can be observed.

3.2. Surface Feature Parameters from ISO 25178

Figure 68 shows the watershed segmentation of the extracted 3 mm by 6 mm area of sample IV based on hill features; (+) denotes the location of the highest point of each segment. The

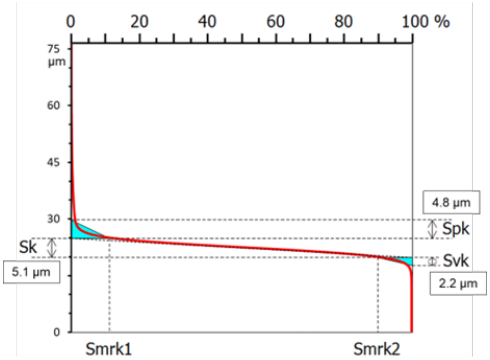

Figure 67.: Material ratio curve (sample IV), L-filter 0.25 mm.

colours are used to simplify the visual differentiation of adjacent particles. Due to the selected height pruning threshold of 13.5 µm, features smaller than half the $d10$ diameter ($d10 = 27$ µm) are merged with adjacent hill segments.

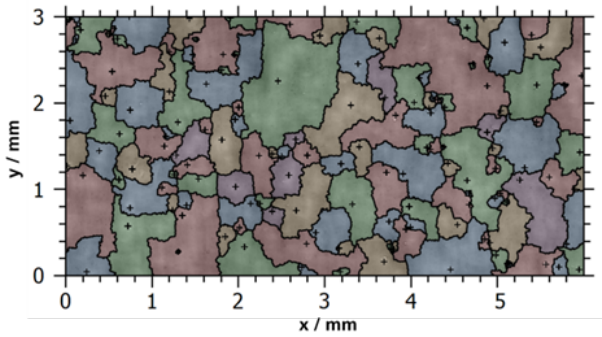

Figure 68.: Example "watershed segmentation" (sample IV) with height pruning 13.5 µm; (+): highest point per segment.

In Table A.32, *Spd* (peak density), *Svd* (valley density) and *Shh* (mean local hill height) are listed. It is notable, that *Svd* is equal for all the considered samples with 13.5 µm height pruning. The value of $Svd = 0.06$ mm-2 originates from the total valley count of one over the entire considered (3×6) mm² area.

Table A.32.: Feature parameters *Spd*, *Svd* and *Shh*; Height pruning 13.5 µm.

$N = 8$	Spd/mm^{-2}	Svd/mm^{-2}	$Shh/\mu m$
Mean	10.10	0.06	22.39
SD	3.48	0.00	1.42

3.3. Process-specific Areal Surface Features

The values presented in Table A.33 were obtained from the MountainsMap® V9.2 particle analysis circle detection module. A variety of characteristic values on feature size, shape, distribution and quantity can be generated. The presented initial selection was based on possible relation to powder particle size and potential relevance for fatigue performance, which will be subject of future work.

For clarity, the chosen parameters are explained in a bit more detail. d_{max} is the largest diameter of a detected particle, meaning, for a (near-) spherical agglomerated particle, and represents the

Table A.33.: Process-specific feature characteristics, Height pruning 13.5 µm.

$N = 8$	d_{max}/µm	z_{max}/µm	area covered /%	particle density $/mm^{-2}$
Mean	27.74	33.64	1.35	21.80
SD	1.87	4.19	0.28	5.68

(partial) sphere diameter. The z_{max} value gives the average of maximum particle z-heights with respect to the lowest point on the surface of all detected particles on the surface. Finally, the percentage of area covered by detected particles and the number of detected particles per unit area (particle density) are given.

Figure 69 shows an area portion on sample IV with circular and near-circular shaped features that could be detected. The top image is the S-L surface with an L-filter of 0.0055 mm. This very low value was chosen to only keep particle attachments and cut out other surface irregularities and waviness. In the bottom image, detected circular particles are marked. The (+) sign again, denotes the highest point on each individual particle.

4. Discussion

From visual inspection, it is confirmed that the dominant process-specific feature on the considered surface condition is agglomeration of powder particles. Examining Table A.31, it is clear from the material ratio curve that the peak portion represented by *Spk*, is considerably larger than the valley population on the surface. The core part of the sample IV curve (Figure 67) is fairly flat and exhibits a steep slope toward the peaks and valleys, where the maximum peak size (e.g., Figure 67: above 75 µm) is significantly larger than the maximum valley size, which is related to attached particles on an otherwise presumably flat surface.

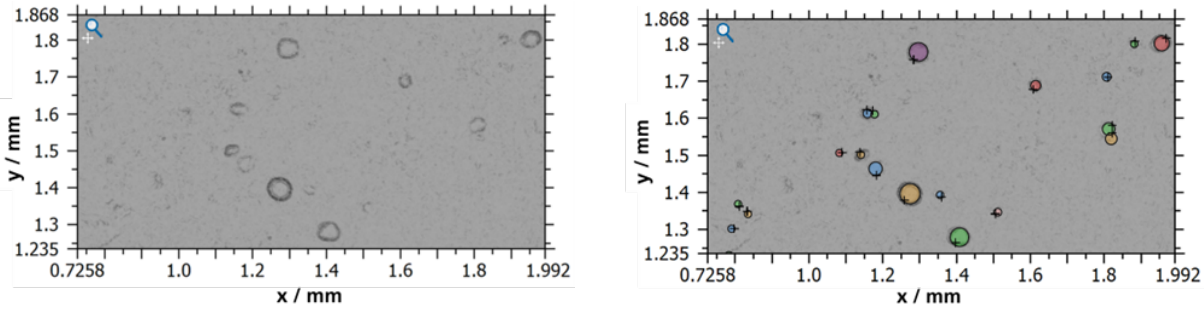

Figure 69.: Example "circle detection" (sample IV), min. diameter 20 µm, max. diameter 200 µm; Extracted area with (near) circular features *(left)*, (b) Detected circular features (same area, *right*).

Using *Sa* as a common and widely known parameter, the surface condition can be considered to be comparatively smooth to other PBF-LB parts (as-built PBF-LB parts can easily exceed an Sa/Ra of 20 µm under similar filtering conditions, depending on material and processing [14, 64]. Correspondingly, the *Svd* value of 0.06 mm-2 (see Table A.32) over the extracted area on each of the considered samples (N = 8) counts one single dale, meaning, there are no significant dales present with a height pruning value of 13.5 µm on the studied surface condition. Considering the peak density *Spd*, there can be significant hills identified on the surface, which is again in agreement with the material ratio curve results (see Figure 67, Table A.31). The mean local hill height *Shh* with 22.39 µm matches the order of magnitude of the $d10$ of 27 µm and is hence representative of the expected feature size.

Moving on toward the discussion of the process-specific feature characteristics, d_{max} and z_{max} are with 28 µm and 34 µm on average similarly close to the $d10$ size. Considering respective standard deviations (Table A.33), it can be concluded that this is equally applying to all evaluated specimens. This suggests that the strategy of using a small L-filter value to only retain sharp edges (i.e., particle boundaries) seems to have been effective. At this point it is emphasised that the generated mean values are based on averages per sample and given standard deviations represent the difference in mean value among the eight assessed specimens. The area of less than 2% covered with particles will supposedly be of interest in comparison with other as-built surfaces (e.g. those introduced in [138]) and in regard to correlation with mechanical properties.

The final feature characteristic value to be discussed is the particle density. While the description itself may suggest similarities to the peak density Spd, the mean value is more than twice as high. This considerable deviation is owing to differences in the detection/segmentation methods and reference surfaces. Firstly, the circle detection is based on an S-L surface with small bandwidth to reliably filter smooth height variations with continuous slopes (waviness or similar) and particles are detected based on their shape rather than height. The peaks are counted based on the original surface (levelled and S-filtered) after watershed segmentation, where it is likely that two adjacent particles are part of the same segment and due to height pruning (combination of smaller features), only the highest of both is counted as segment peak. Secondly, even though identical height pruning values are applied, the pruning is performed with respect to different reference points. While for the ISO 25178 parameters, the height of a hill feature is defined with respect to the highest saddle point on its course line [82] and is merged with the adjacent taller hill if below the threshold value, detected circular particles will only be merged when overlapping. This being addressed, Figure 68 and 69 clarify the large difference in particle and peak density.

5. Conclusions and Future Prospects

This work provides an insight into the opportunities for novel approaches to quality assurance concepts using feature parameters and process-specific surface features for surface texture characterisation of metal additive parts, specifically of AlSi7Mg0.6 specimens from PBF-LB.

In summary, for the examined surface type with the selected measurement method, configuration and software tool settings, the following conclusions are drawn:

- Evaluated feature parameters correspond with the (qualitative) implications of height-based parameters from the material ratio curve (hills/dales, peak/valley portion).
- Mean values of the surface feature characteristics and parameters can be linked with particle size of the powder used in the manufacturing process.

In comparison to common height variation-based parameters such as Sa and Sz, feature parameters and characteristics describe properties of physical topography elements rather than being based on deviation from a mean line or individual extreme values. The material ratio curve parameters on the other hand, could provide an insight on the height distribution, identifying a smaller valley than peak portion, which matched well with the feature parameter results. However, the material ratio curve only provides information about the height distribution, while the characterisation of surface features can provide an understanding of present feature shapes, size distribution or quantity. This approach can be of interest when trying to understand relationships between surface quality and mechanical performance (e.g. fatigue), corrosion or adhesion. The presented results give a first idea of the prospects of quantifying the PBF-LB-specific powder

particle agglomeration features based on mean values per specimen. Ongoing work includes more detailed examinations of distribution and frequency of detected particle sizes on individual samples. Additional aspects to be considered in future work are the challenges imposed on optical metrology systems regarding the accurate representation of surface features and on evaluation software concerning their comprehensive detection.

B. Author Contributions and Selection of Publication Media for Publications 1 to 6

Author Contributions

This chapter includes the author contributions according to CRediT (Contributor Roles Taxonomy)* for Publications 1 to 6.

Publication 1 (Chapter 4)

Buchenau, Theresa; Mertens, Tobias; Lohner, Hubertus; Brüning, Hauke; Amkreutz, Marc (2023): Comparison of Optical and Stylus Methods for Surface Texture Characterisation in Industrial Quality Assurance of Post-processed Laser Metal Additive Ti-6Al-4V. In: Materials 16 (13), S. 4815. DOI: 10.3390/ma16134815

Theresa Buchenau	Conceptualisation (lead), Data curation (lead), Formal analysis (lead), Investigation (lead), Methodology (lead), Visualisation (lead), Writing – original draft preparation (lead), Writing – review and editing (equal)
Tobias Mertens	Conceptualisation (support), Funding acquisition (equal), Resources (equal), Writing – review and editing (equal)
Hubertus Lohner	Conceptualisation (support), Funding acquisition (equal), Resources (equal)
Hauke Brüning	Investigation (support), Funding acquisition (equal), Resources (equal), Writing – review and editing (equal)
Marc Amkreutz	Investigation (support), Funding acquisition (equal), Resources (equal), Writing – review and editing (equal)

Publication 2 (Chapter 4)

Buchenau, Theresa; Brüning, Hauke; Amkreutz, Marc (2022): Post-processing of Surface Topography Data for As-built Metal Additive Surface Texture Characterisation. In: Journal of Additive Manufacturing Technologies 2 (2), S. 697. DOI: 10.18416/JAMTECH.2212697

Theresa Buchenau	Conceptualisation (lead), Data curation (lead), Formal analysis (lead), Investigation (lead), Methodology (lead), Visualisation (lead), Writing – original draft preparation (lead), Writing – review and editing (equal)
Hauke Brüning	Investigation (support), Writing – review and editing (equal), Funding acquisition (equal)
Marc Amkreutz	Investigation (support), Writing – review and editing (equal), Funding acquisition (equal)

*For a description of contributor roles, see *https://credit.niso.org/* (visited 27.02.2024)

Publication 3 (Chapter 5)

Buchenau, Theresa; Amkreutz, Marc; Bruening, Hauke; Mayer, Bernd (2023): Influence of Contour Scan Variation on Surface, Bulk and Mechanical Properties of LPBF-Processed AlSi7Mg0.6. In: Materials 16 (8), S. 3169. DOI: 10.3390/ma16083169

Theresa Buchenau	Conceptualisation (lead), Data curation (lead), Formal analysis (lead), Investigation (lead), Methodology (lead), Visualisation (lead), Writing – original draft preparation (lead), Writing – review and editing (equal)
Hauke Brüning	Methodology (support), Resources (equal), Writing – review and editing (support), Funding acquisition (equal)
Marc Amkreutz	Methodology (support), Resources (equal), Writing – review and editing (equal), Funding acquisition (equal)
Bernd Mayer	Resources (equal), Writing – review and editing (support), Funding acquisition (equal)

Publication 4 (Chapter 5)

Buchenau, Theresa; Amkreutz, Marc; Brüning, Hauke (2021): Surface Texture and High Cycle Fatigue of As-built Metal Additive AlSi7Mg0.6. In: Journal of Additive Manufacturing Technologies 1 (2), S. 531. DOI: 10.18416/JAMTECH.2111531

Theresa Buchenau	Conceptualisation (lead), Data curation (lead), Formal analysis (lead), Investigation (lead), Methodology (lead), Visualisation (lead), Writing – original draft preparation (lead), Writing – review and editing (lead)
Marc Amkreutz	Conceptualisation(support), Investigation (support), Methodology (support), Funding acquisition (equal)
Hauke Brüning	Conceptualisation(support), Investigation (support), Methodology (support), Funding acquisition (equal)

Publication 5 (Chapter 6)

Buchenau, Theresa; Brüning, Hauke; Amkreutz, Marc (2022): Elementparameter zur Oberflächencharakterisierung additiv gefertigter Metallkomponenten. Feature Parameters for Metal Additive Surface Texture Characterisation. In: Martina Zimmermann (Hg.): Werkstoffe und Bauteile auf dem Prüfstand. Prüftechnik - Kennwertermittlung - Schadensvermeidung. S. 117–123. ISBN: 978-3-88355-430-3; DGM 40. Vortrags- und Diskussionstagung Werkstoffprüfung. Dresden (Germany) & Online, October 2022.

Theresa Buchenau	Conceptualisation (lead), Data curation (lead), Formal analysis (lead), Funding acquisition (equal), Investigation (lead), Methodology (lead), Project administration (lead), Visualisation (lead), Writing – original draft preparation (lead), Writing – review and editing (lead)
Marc Amkreutz	Investigation (support), Methodology (support), Funding acquisition (equal), Writing – review and editing (support)
Hauke Brüning	Investigation (support), Methodology (support), Funding acquisition (equal), Writing – review and editing (support)

Publication 6 (Chapter 6)

Buchenau, Theresa; Thompson, Adam; Brüning, Hauke; Amkreutz, Marc; Mayer, Bernd; Piano, Samanta (2023): Surface Features of As-built Metal Additive AlSi7Mg0.6. In: Preprints, 2023030174. DOI: 10.20944/preprints202303.0174.v2; 17th European Conference on Spacecraft Structures, Materials and Environmental Testing. Toulouse (France), March 2023.

Theresa Buchenau	Conceptualisation (lead), Data curation (lead), Formal analysis (lead), Funding acquisition (equal), Investigation (lead), Methodology (lead), Project administration (lead), Visualisation (lead), Writing – original draft preparation (lead)
Adam Thompson	Methodology (support), Investigation (support), Resources (equal), Writing – review and editing (lead)
Hauke Brüning	Conceptualisation (support), Writing – review and editing (support), Funding acquisition (equal)
Marc Amkreutz	Conceptualisation (support), Writing – review and editing (support), Funding acquisition (equal)
Bernd Mayer	Funding acquisition (equal), Resources (equal), Writing – review and editing (support)
Samantha Piano	Methodology (support), Resources (equal), Writing – review and editing (support)

Selection of Publication Media

Two publications were published in the journal *Materials*: Publication 1 in the special issue *Material Surface Topography Measurement, Analysis and Characterisation* and Publication 3 in the special issue *Additive Manufacturing of Aluminum Alloys and Aluminum Matrix Composites*. The journal was selected as it is a respected publication medium in the field of materials science and engineering with a rigorous though fairly fast peer review process. The submission to the respective special issues ensured that the peer review was carried out by experts in the specialised fields addressed in the publications.

Two publications were published in the *Journal of Additive Manufacturing Technologies*. The published results were presented to the public at two different editions of the *Additive Manufacturing Conference Turkey* (2021 & 2022) and were selected for journal publication by the program committee. The peer-reviewed journal is relatively new, but covers a wide range of topics in the subject area of additive manufacturing. It was decided to publish the full articles with this journal to introduce the importance of surface texture characterisation to the general additive manufacturing community.

The peer-reviewed conference paper, Publication 5, was presented at a conference on materials testing and characterisation with experts in the field from across Germany and was organised by the *German Society for Materials Science (DGM)*. The conference was selected to introduce novel approaches to surface texture characterisation to the German expert community.

Publication 6 was presented at the *17th European Conference on Spacecraft Structures, Material and Environmental Testing* and is currently available as preprint. The conference was selected to introduce novel approaches to surface texture characterisation to potential users in the aerospace field. The extension of the preprint for submission to a peer-reviewed journal is currently ongoing. The submission is currently planned for June to *The International Journal of Advanced Manufacturing Technology*, which is a highly respected journal in the field of materials and manufacturing engineering and is part of *Springer Nature*.

C. List of Publications and Public Presentations

Journal Article (peer-reviewed)

Buchenau, Theresa; Mertens, Tobias; Lohner, Hubertus; Brüning, Hauke; Amkreutz, Marc (2023):

Comparison of Optical and Stylus Methods for Surface Texture Characterisation in Industrial Quality Assurance of Post-processed Laser Metal Additive Ti-6Al-4V.

In: Materials 16 (13), S. 4815. DOI: 10.3390/ma16134815

Journal Article (peer-reviewed)

Buchenau, Theresa; Amkreutz, Marc; Brüning, Hauke; Mayer, Bernd (2023):

Influence of Contour Scan Variation on Surface, Bulk and Mechanical Properties of LPBF-Processed AlSi7Mg0.6.

In: Materials 16 (8), S. 3169. DOI: 10.3390/ma16083169

Journal Article (peer-reviewed)

Buchenau, Theresa; Brüning, Hauke; Amkreutz, Marc (2022):

Post-processing of Surface Topography Data for As-built Metal Additive Surface Texture Characterisation.

In: Journal of Additive Manufacturing Technologies 2 (2), S. 697. DOI: 10.18416/JAMTECH.2212697

Journal Article (peer-reviewed)

Buchenau, Theresa; Amkreutz, Marc; Brüning, Hauke (2021):

Surface Texture and High Cycle Fatigue of As-built Metal Additive AlSi7Mg0.6.

In: Journal of Additive Manufacturing Technologies 1 (2), S. 531. DOI: 10.18416/JAMTECH.2111531

Journal Article (peer-reviewed)

Navickaitė, Kristina; Liang, Jierong; Bahl, Christian; Wieland, Sandra; Buchenau, Theresa; Engelbrecht, Kurt (2020):

Experimental Characterization of Active Magnetic Regenerators Constructed Using Laser Beam Melting Technique.

In: Applied Thermal Engineering 174, S. 115297. DOI: 10.1016/j.applthermaleng.2020.115297

Project Report

Amkreutz, Marc; Aumund-Kopp, Claus; Brüning, Hauke; Buchenau, Theresa; Norda, Michael; Sukowski, Frank; Suth, Daniel (2021):

APOLLO – Additive Teilefertigung, -prüfung und Oberflächenbehandlung für Aluminiumkomponenten; Teilvorhaben PROMOTIVE – Prozessoptimierung, Materialcharakterisierung und Oberflächenschutz additiv gefertigter Aluminiumbauteile: Schlussbericht, Laufzeit 01.01.2018 bis 30.06.2021.

TIB - Technische Informationsbibliothek Universitätsbibliothek Hannover. DOI: 10.2314/KXP:1828117579

Conference Paper & Presentation

Buchenau, Theresa; Thompson, Adam; Brüning, Hauke; Amkreutz, Marc; Mayer, Bernd; Piano, Samanta (2023):

Surface Features of As-built Metal Additive AlSi7Mg0.6.

In: Preprints, 2023030174. DOI: 10.20944/preprints202303.0174.v2; 17th European Conference on Spacecraft Structures, Materials and Environmental Testing. Toulouse (France), March 2023.

Conference Paper & Presentation

Buchenau, Theresa; Cersullo, Nicola; Mardaras, Jon; Emile, Philippe; Lafue, Victor; Brüning, Hauke; Amkreutz, Marc; Hühne, Christian (2023):

Fatigue and Surface Texture of Post-processed Metal Additive Ti-6Al-4V.

17th European Conference on Spacecraft Structures, Materials and Environmental Testing. Toulouse (France), March 2023.

Conference Paper (peer-reviewed) & Presentation

Buchenau, Theresa; Brüning, Hauke; Amkreutz, Marc (2022):

Elementparameter zur Oberflächencharakterisierung additiv gefertigter Metallkomponenten. Feature parameters for Metal Additive Surface Texture Characterisation.

In: Martina Zimmermann (Hg.): Werkstoffe und Bauteile auf dem Prüfstand. Prüftechnik – Kennwertermittlung – Schadensvermeidung. Sankt Augustin: Deutsche Gesellschaft für Materialkunde e.V, S. 117–123. ISBN: 978-3-88355-430-3;DGM 40. Vortrags- und Diskussionstagung Werkstoffprüfung. Dresden (Germany) & Online, October 2022.

Conference Presentation

Buchenau, Theresa; Brüning, Hauke; Amkreutz, Marc (2022):

Post-processing of Surface Topography Data for As-built Metal Additive Surface Texture Characterisation.

Additive Manufacturing Conference Turkey. Izmir (Turkey), October 2022.

Conference Presentation

Buchenau, Theresa; Amkreutz, Marc; Brüning, Hauke (2021):

Surface Texture and High Cycle Fatigue of As-built Metal Additive AlSi7Mg0.6.

Additive Manufacturing Conference Turkey. Istanbul (Turkey) & Online, September 2021.

Conference Paper & Presentation

Buchenau, Theresa; Amkreutz, Marc; Brüning, Hauke; Norda, Michael (2019):

Evaluation of Alternative Parameters to Describe the Quality of Additively Manufactured Aluminium Alloy Surfaces.

Additive Manufacturing Conference Turkey. Istanbul (Turkey), Oktober 2019.

Presentation

Theresa Buchenau (2022):

Bulk Quality, Surface Texture and Mechanical Properties of LPBF Al Alloy Parts. Webinar "Aluminium: Processing with Sinter-based and PBF AM Processes".

Webinar Series "AM@IFAM" 2022. Fraunhofer-Institut für Fertigungstechnik und Angewandte Materialforschung. Online, 14.06.2022.

Presentation

Theresa Buchenau (2021):

Surface Texture Analysis for Metal AM.

Unique Materials for Advanced Aerospace Applications. UMA3 Training: Local Individual Scientific Training. Session: Modelling and simulation, testing of materials. Online, 13.12.2021.

Presentation

Theresa Buchenau (2020):

Description of Surface Quality for Metal Additive Manufacturing by Means of Optical Methods.

Guest Seminar. University of Nottingham. Manufacturing Metrology Team. Nottingham (UK), 28.01.2020.

Workshop

Buchenau, Theresa; Derksen, Johannes; Brüning, Hauke; Amkreutz, Marc; Dieckhoff, Stefan (2019):

Oberflächentechnik für additiv gefertigte Metallbauteile. Workshop "Optische Messtechnik" (BDLI AG Oberflächentechnologie).

Fraunhofer IFAM. Workshop for Members of Bundesverband der Deutschen Luft- und Raumfahrtindustrie BDLI - AG Oberflächentechnologie. Bremen, 28.03.2019.

D. Acknowledgements

I thank Prof. Bernd Mayer for the opportunity to work on this doctoral research project, his support, recommendations and for reviewing and evaluating this thesis.

Thanks to Prof. Richard Bibb for agreeing to act as external reviewer and examiner of my work and for the constructive commentary on my thesis prior to the submission.

I thank my topical advisors, Dr. Marc Amkreutz and Dr. Hauke Brüning, for offering me a doctoral research position, for countless inspirational discussions, the exhaustive review of this thesis and our shared publications and for creating a very pleasant working environment. Thank you for your spontaneous availability whenever I had urgent questions. Thank you for including me in projects with external customers and partners and giving me insights into management tasks. I want to thank you especially for providing the space I needed to complete my doctoral research alongside other interesting project work.

A very special additional thanks goes out to Marc. Thank you for listening to all of my doubts and complaints and for rebuilding my confidence when needed. It's a pleasure sharing an office with you!

I thank Dr. Stefan Dieckhoff, Head of the Adhesion and Interfaces Department, for his interest in my work, for all the support, for the freedom I had in selecting topics and projects and the space to develop creative ideas and solutions.

I thank our project partners and co-authors, who supported my work with productive discussions, specifically the Airbus colleagues Nicola Cersullo, Dr.-Ing. Tobias Mertens and Dr.-Ing. Hubertus Lohner.

I am very grateful to the University of Nottingham's Manufacturing Metrology Team for hosting me for several weeks. Particularly, I thank Prof. Samanta Piano and Dr. Adam Thompson for the collaboration and the encouraging exchanges on measurement and characterisation of surface texture. I had an amazing time with your team and very much appreciate everything I got to learn. The visit provided great motivation for the continuation of my work and I look forward to future cooperations.

I thank Michael Norda from the Powder Metallurgy department at IFAM for the initial discussions on processing parameters and for providing me with countless cubes and bars. Thanks to the Functional Printing group for letting me use their fatigue testing equipment. Thanks to Annette Schwingen for many tensile tests and to our former students Sara Theimann and Inga Meyenborg for many, many density measurements. Thanks to all of the colleagues at IFAM who contributed to the great time I had in the last few years.

Inga, I also thank you for the interesting discussions on LPBF processing and material properties, for your great work as a student at IFAM and for all the writing and working session we had afterwards. It was always fun and productive working (and not working) with you. I am grateful you were a part of this journey!

Boudewien, I thank you so much for our "daily writing hours" and all of our co-working sessions and digital coffees during our PhD time and for our student years in- and outside the library. I am so happy we managed to keep in touch over the years. You have always been a great motivation and a wonderful friend to me!

I thank my wonderful friends and family, who accompanied (not only) my PhD journey. Thank you for all the love and support, and for providing distractions. Thanks for all the coffees, the beers, the days and nights, the walks, the talks, the dinners and lunches, the sports sessions, the music, the dancing, and for not forgetting about me whenever I was buried in work for a while. Special thanks to Jule for proof-reading this thesis and moving my commas to the places they belong (and also for all of the above). Big thanks to my cousin Karsten for inspiring me to become an engineer. Thanks to all my grandparents for everything. Thanks to Lissy and the little "Survivor", for the fresh air and the much needed breaks and distractions.

I thank my amazing parents and siblings. Marthi, Heni, you are the best! I am very proud and incredibly lucky to have you as my sister and brother. Thank you for being the inspirational, smart and good people

you are. Extra thanks to Marthi for the correction of the German version of the Abstract (from English-ish with German words to a real German text). Mama, Papa, I don't know where to begin thanking you, so: thanks for everything. Thanks for providing me with the education and experiences that made me the person I am today. Thank you for teaching me to be critical, to question existing structures and hierarchies and to form my own opinions. Thank you for loving and supporting me for longer than I can remember.

And finally, I thank my wonderful partner Guillaume. Thanks for coping with my chaos, the mood swings and my short fuse during the last few months, and thank you for the detailed correction of my bibliography. Thank you for the music, the food, the adventures, the love, our life together. I feel unbelievably lucky we found each other.

Funding

Parts of this presented thesis received external funding:

I thank the *German Federal Ministry of Economics and Energy (BMWi)* for supporting the work on Chapter 4 as part of the LuFo project APOLLO (sub-project PROMOTIVE, funding code 20W1701B, duration 01.01.2018 to 30.06.2021).

I further thank the *Fraunhofer Association* for the financial support of my work and my personal and professional qualification within the *TALENTA start* scholarship program between 01.01.2019 and 31.12.2020.

Moreover, I thank the *German Academic Exchange Service (DAAD)* for partially funding my research visit to the University of Nottingham, UK, for three months starting in fall 2022. The corresponding outcomes are presented in Chapter 6. I received a short-term research scholarship (funding program ID 57556282, personal funding code 91790340).

Bibliography

[1] Nesma T. Aboulkhair, Marco Simonelli, Luke Parry, Ian Ashcroft, Christopher Tuck, and Richard Hague. 3D Printing of Aluminium Alloys: Additive Manufacturing of Aluminium Alloys Using Selective Laser Melting. *Progress in Materials science*, 106:100578, 2019.

[2] Adrián Uriondo, Manuel Esperon-Miguez, and Suresh Perinpanayagam. The Present and Future of Additive Manufacturing in the Aerospace Sector: A Review of Important Aspects. *Proceedings of the Institution of Mechanical Engineers, Part G: Journal of Aerospace Engineering*, 229(11):2132–2147, 2015.

[3] Leendert A. Verhoef, Bart W. Budde, Cindhuja Chockalingam, Brais García Nodar, and Ad J.M. van Wijk. The Effect of Additive Manufacturing on Global Energy Demand: An Assessment Using a Bottom-up Approach. *Energy Policy*, 112:349–360, 2018.

[4] Richard K. Leach. Metrology for Additive Manufacturing. *Measurement and Control*, 49(4):132–135, 2016.

[5] Ian Gibson, David W. Rosen, Brent Stucker, and Mahyar Khorasani. *Additive Manufacturing Technologies*. Springer, 2014.

[6] Andrew Townsend, Nicola Senin, Liam Blunt, Richard K. Leach, and John S. Taylor. Surface Texture Metrology for Metal Additive Manufacturing: A Review. *Precision Engineering*, 46:34–47, 2016.

[7] Shahir Mohd Yusuf, Samuel Cutler, and Nong Gao. The Impact of Metal Additive Manufacturing on the Aerospace Industry. *Metals*, 9(12):1286, 2019.

[8] Gianni Nicoletto, Radomila Konečná, Martin Frkáň, and Enrica Riva. Surface Roughness and Directional Fatigue Behavior of As-built EBM and DMLS Ti6Al4V. *International Journal of Fatigue*, 116:140–148, 2018.

[9] Timothy B. Sercombe and Xiaopeng Li. Selective Laser Melting of Aluminium and Aluminium Metal matrix Composites. *Materials Technology*, 31(2):77–85, 2016.

[10] Cassiopée Galy, Emilie Le Guen, Eric Lacoste, and Corinne Arvieu. Main Defects Observed in Aluminum Alloy Parts Produced by SLM: From Causes to Consequences. *Additive Manufacturing*, 22:165–175, 2018.

[11] Manuela Galati, Giovanni Rizza, Silvio Defanti, and Lucia Denti. Surface Roughness Prediction Model for Electron Beam Melting (EBM) Processing Ti6Al4V. *Precision Engineering*, 69:19–28, 2021.

[12] Grzegorz Pyka, Greet Kerckhofs, Ioannis Papantoniou, Mathew Speirs, Jan Schrooten, and Martine Wevers. Surface Roughness and Morphology Customization of Additive Manufactured Open Porous Ti6Al4V Structures. *Materials*, 6(10):4737–4757, 2013.

[13] Michael O'Brien. Existing standards as the Framework to Qualify Additive Manufacturing of Metals. In *2018 IEEE Aerospace Conference*, pages 1–10, 2018.

[14] Uwe Zerbst, Giovanni Bruno, Jean-Yves Buffiere, Thomas Wegener, Thomas Niendorf, Tao Wu, Xiangqian Zhang, Nikolai Kashaev, Giovanni Meneghetti, Nik Hrabe, et al. Damage Tolerant Design of Additively Manufactured Metallic Components Subjected to Cyclic Loading: State of the Art and Challenges. *Progress in Materials science*, 121:100786, 2021.

[15] Sarah Reichelt. *Einfluss chemischer Oberflächennachbehandlungen auf Additiv gefertigtes Ti-6Al-4V*. Berichte aus dem IW. TEWISS Verlag, 2018.

[16] ISO 25178: Geometric Product Specifications (GPS) - Surface Texture: Areal - Part 2: Terms, Definitions and Surface Texture Parameters, 2022.

[17] Waldemar Steinhilper, Bernd Sauer, and Jörg Feldhusen. *Konstruktionselemente des Maschinenbaus 1: Grundlagen der Berechnung und Gestaltung von Maschinenelementen*. Springer-Verlag, 2008.

[18] Xiangqian Jiang, Nicola Senin, Paul J. Scott, and François Blateyron. Feature-Based Characterisation of Surface Topography and its Application. *CIRP Annals*, 70(2):681–702, 2021.

[19] Shan Lou, Xiangqian Jiang, Wenjuan Sun, Wenhan Zeng, Luca Pagani, and Paul J. Scott. Characterisation Methods for Powder Bed Fusion Processed Surface Topography. *Precision Engineering*, 57:1–15, 2019.

[20] Nesma T. Aboulkhair, Nicola M. Everitt, Ian Maskery, Ian Ashcroft, and Chris Tuck. Selective Laser Melting of Aluminum Alloys. *MRS Bulletin*, 42(4):311–319, 2017.

[21] Paul A. Hooper. Swiss Cheese: A Practical Tutorial on Assessing AM Build Quality. In *Joint Special Interest Group Meeting Between EUSPEN and ASPE: Advancing Precision in Additive Manufacturing*. American Society for Precision Engineering (ASPE), 2020.

[22] Joy Gockel, Luke Sheridan, Brittanie Koerper, and Bo Whip. The Influence of Additive Manufacturing Processing Parameters on Surface Roughness and Fatigue Life. *International Journal of Fatigue*, 124:380–388, 2019.

[23] Jean-Pierre Kruth, Jan Deckers, and Evren Yasa. Experimental Investigation of Laser Surface Remelting for the Improvement of Selective Laser Melting Process. In *2008 International Solid Freeform Fabrication Symposium*, 2008.

[24] Quanquan Han and Yang Jiao. Effect of Heat Treatment and Laser Surface Remelting on AlSi10Mg Alloy Fabricated by Selective Laser Melting. *The International Journal of Advanced Manufacturing Technology*, 102:3315–3324, 2019.

[25] Ahmed S.B. Tawfik, Christopher Jackson, O. Armitage, R. Cawley, Paul Bills, and Liam Blunt. Improving Surface Finish in SLM Additive Manufacturing Components by Implementing Remelting Techniques. In *Joint Special Interest Group Meeting Between EUSPEN and ASPE: Advancing Precision in Additive Manufacturing*. European Society for Precision Engineering and Nanotechnology (euspen), 2023.

[26] Jeremy H. Rao, Yong Zhang, Xiya Fang, Yu Chen, Xinhua Wu, and Chris H. J. Davies. The Origins for Tensile Properties of Selective Laser Melted Aluminium Alloy A357. *Additive Manufacturing*, 17:113–122, 2017.

[27] Naor Elad Uzan, Roni Shneck, Ori Yeheskel, and Nachum Frage. Fatigue of AlSi10Mg Specimens Fabricated by Additive Manufacturing Selective Laser Melting (AM-SLM). *Materials Science and Engineering: A*, 704:229–237, 2017.

[28] Changchun Zhang, Haihong Zhu, Hailong Liao, Yong Cheng, Zhiheng Hu, and Xiaoyan Zeng. Effect of Heat Treatments on Fatigue Property of Selective Laser Melting AlSi10Mg. *International Journal of Fatigue*, 116:513–522, 2018.

[29] Kun V. Yang, Paul Rometsch, Chris H.J. Davies, Aijun Huang, and Xinhua Wu. Effect of Heat Treatment on the Microstructure and anisotropy in Mechanical Properties of A357 Alloy Produced by Selective Laser Melting. *Materials & Design*, 154:275–290, 2018.

[30] Arnold Mauduit, Hervé Gransac, Pierre Auguste, and Sébastien Pillot. Study of AlSi7Mg0.6 Alloy by Selective Laser Melting: Mechanical Properties Microstructure Heat Treatment. *Journal of Casting & Materials Engineering*, 3(1):1, 2019.

[31] Juan Carlos Pereira, Emma Gil, Leire Solaberrieta, María San Sebastián, Yoana Bilbao, and Pedro Pablo Rodríguez. Comparison of AlSi7Mg0.6 Alloy Obtained by Selective Laser Melting and Investment Casting Processes: Microstructure and Mechanical Properties in As-built/As-cast and Heat-Treated Conditions. *Materials Science and Engineering: A*, 778:139124, 2020.

[32] Bo Zhang, Wu Wei, Wei Shi, Yanwu Guo, Shengping Wen, Xiaolan Wu, Kunyuan Gao, Li Rong, Hui Huang, and Zuoren Nie. Effect of Heat Treatment on the Microstructure and Mechanical Properties of Er-containing Al–7Si–0.6 Mg Alloy by Laser Powder Bed Fusion. *Journal of Materials Research and Technology*, 18:3073–3084, 2022.

[33] Nesma T. Aboulkhair, Ian Maskery, Chris Tuck, Ian Ashcroft, and Nicola M. Everitt. Improving the Fatigue Behaviour of a Selectively Laser Melted Aluminium Alloy: Influence of Heat Treatment and Surface Quality. *Materials & Design*, 104:174–182, 2016.

[34] Lucia Denti and Antonella Sola. On the Effectiveness of Different Surface Finishing Techniques on A357.0 Parts Produced by Laser-Based Powder Bed Fusion: Surface Roughness and Fatigue Strength. *Metals*, 9(12):1284, 2019.

[35] Milad Hamidi Nasab, Alessandro Giussani, Dario Gastaldi, Valeria Tirelli, and Maurizio Vedani. Effect of Surface and Subsurface Defects on Fatigue Behavior of AlSi10Mg Alloy Processed by Laser Powder Bed Fusion (L-PBF). *Metals*, 9(10):1063, 2019.

[36] Andrea Gatto, Elena Bassoli, Lucia Denti, Antonella Sola, Emanuele Tognoli, Andrea Comin, Juan Antonio Porro, Francisco Cordovilla, Ignacio Angulo, and Jose Luis Ocaña. Effect of Three Different Finishing Processes on the Surface Morphology and Fatigue Life of A357.0 Parts Produced by Laser-based Powder Bed Fusion. *Advanced Engineering Materials*, 21(7):1801357, 2019.

[37] Antonio Grande, Stefania Cacace, Ali Gökhan Demir, and Giuseppe Sala. Fracture and Fatigue Behaviour of AlSi7Mg0.6 Produced by Selective Laser Melting: Effects of Thermal-Treatments. In *25th International Congress*, Rome, Italy, 2019. Italian Association of Aeronautics and Astronautics.

[38] Stefania Cacace, Ali Gökhan Demir, Giuseppe Sala, and Antonio Mattia Grande. Influence of Production Batch Related Parameters on Static and Fatigue Resistance of LPBF Produced AlSi7Mg0.6. *International Journal of Fatigue*, 165:107227, 2022.

[39] Sarah Bagehorn, Jürgen Wehr, and Hans-Jürgen Maier. Application of Mechanical Surface Finishing Processes for Roughness Reduction and Fatigue Improvement of Additively Manufactured Ti-6Al-4V Parts. *International Journal of Fatigue*, 102:135–142, 2017.

[40] Martin Frkáň, Radomila Konečná, Gianni Nicoletto, and Ludvik Kunz. Microstructure and Fatigue Performance of SLM-fabricated Ti6Al4V Alloy after Different Stress-relief Heat Treatments. *Transportation Research Procedia*, 40:24–29, 2019.

[41] Magnus Kahlin, Hans Ansell, Dejan Basu, Annie Kerwin, Lewis Newton, Bethan Smith, and Johan J. Moverare. Improved Fatigue Strength of Additively Manufactured Ti6Al4V by Surface Post Processing. *International Journal of Fatigue*, 134:105497, 2020.

[42] Gianni Nicoletto. Smooth and Notch Fatigue Behavior of Selectively Laser Melted Inconel 718 with As-built Surfaces. *International Journal of Fatigue*, 128:105211, 2019.

[43] Federico Uriati and Gianni Nicoletto. A Comparison of Inconel 718 Obtained with Three L-PBF Production Systems in Terms of Process Parameters, As-built Surface Quality, and Fatigue Performance. *International Journal of Fatigue*, 162:107004, 2022.

[44] Shahriar Afkhami, Mohammad Dabiri, Heidi Piili, and Timo Björk. Effects of Manufacturing Parameters and Mechanical Post-Processing on Stainless Steel 316L Processed by Laser Powder Bed Fusion. *Materials Science and Engineering: A*, 802:140660, 2021.

[45] Muhannad Ahmed Obeidi, Sinéad Uí Mhurchadha, Ramesh Raghavendra, Alex Conway, Carlos Souto, David Tormey, Inam Ul Ahad, and Dermot Brabazon. Comparison of the porosity and Mechanical Performance of 316L Stainless Steel Manufactured on Different Laser Powder Bed Fusion Metal Additive Manufacturing Machines. *Journal of Materials Research and Technology*, 13:2361–2374, 2021.

[46] Gianluca Alaimo, Massimo Carraturo, Nina Korshunova, and Stefan Kollmannsberger. Numerical Evaluation of High Cycle Fatigue Life for Additively Manufactured Stainless Steel 316L Lattice Structures: Preliminary Considerations. *Material Design & Processing Communications*, 3(4):e249, 2021.

[47] Nina Korshunova, Gianluca Alaimo, Seyyed Bahram Hosseini, Massimo Carraturo, Alessandro Reali, Jarkko Niiranen, Ferdinando Auricchio, Ernst Rank, and Stefan Kollmannsberger. Image-Based Numerical Characterization and Experimental Validation of Tensile Behavior of Octet-Truss Lattice Structures. *Additive Manufacturing*, 41:101949, 2021.

[48] David Bourell, Jean Pierre Kruth, Ming Leu, Gideon Levy, David Rosen, Allison M. Beese, and Adam T. Clare. Materials for Additive Manufacturing. *CIRP annals*, 66(2):659–681, 2017.

[49] Tarasankar Debroy, Huiliang Wei, James Zuback, Tuhin Mukherjee, J. W. Elmer, J. O. Milewski, Allison M. Beese, Alexander Wilson-Heid, Amitava De, and Wei Zhang. Additive Manufacturing of Metallic Components–Process, Structure and Properties. *Progress in Materials science*, 92:112–224, 2018.

[50] Ihsan Murat Kusoglu, Bilal Gökce, and Stephan Barcikowski. Research Trends in Laser Powder Bed Fusion of Al Alloys within the Last Decade. *Additive Manufacturing*, 36:101489, 2020.

[51] Paul A. Rometsch, Yuman Zhu, Xinhua Wu, and Aijun Huang. Review of High-Strength Aluminium Alloys for Additive Manufacturing by Laser Powder Bed Fusion. *Materials & Design*, page 110779, 2022.

[52] Hiren R. Kotadia, Greg Gibbons, Amit Das, and Philip D. Howes. A Review of Laser Powder Bed Fusion Additive Manufacturing of Aluminium Alloys: Microstructure and Properties. *Additive Manufacturing*, 46:102155, 2021.

[53] Sri Lathabai. Additive Manufacturing of Aluminium-Based Alloys and Composites. *Fundamentals of Aluminium Metallurgy*, pages 47–92, 2018.

[54] Daniel Knoop, Andreas Lutz, Bernhard Mais, and Axel von Hehl. A Tailored AlSiMg Alloy for Laser Powder Bed Fusion. *Metals*, 10(4), 2020.

[55] Adam T. Clare, Rajiv S. Mishra, Marion Merklein, Hua Tan, Iain Todd, Lova Chechik, Jingjing Li, and Markus Bambach. Alloy Design and Adaptation for Additive Manufacture. *Journal of Materials Processing Technology*, 299:117358, 2022.

[56] David Schimbäck, Philipp Mair, Marko Bärtl, Frank Palm, Gerhard Leichtfried, Svea Mayer, Peter J. Uggowitzer, and Stefan Pogatscher. Alloy Design Strategy for Microstructural-Tailored Scandium-Modified Aluminium Alloys for Additive Manufacturing. *Scripta Materialia*, 207:114277, 2022.

[57] Tobias Grimm, Georg Wiora, and Gerd Witt. Characterization of Typical Surface Effects in Additive Manufacturing with Confocal Microscopy. *Surface Topography: Metrology and Properties*, 3(1):014001, 2015.

[58] Wilson Tato, Liam Blunt, Iñigo Llavori, Andrea Aginagalde, Andrew Townsend, and Alaitz Zabala. Surface Integrity of Additive Manufacturing Parts: A Comparison Between Optical Topography Measuring Techniques. *Procedia CIRP*, 87:403–408, 2020.

[59] Adam Thompson, Nicola Senin, Claudiu L. Giusca, and Richard K. Leach. Topography of Selectively Laser Melted Surfaces: a Comparison of Different Measurement Methods. *CIRP Annals*, 66(1):543–546, 2017.

[60] Nicola Senin, Adam Thompson, and Richard K. Leach. Characterisation of the Topography of Metal Additive Surface Features with Different Measurement Technologies. *Measurement Science and Technology*, 28(9):095003, 2017.

[61] Lewis Newton, Aditi Thanki, Carlos Bermudez, Roger Artigas, Adam Thompson, Han Haitjema, and Richard K. Leach. Optimisation of Imaging Confocal Microscopy for Topography Measurements of Metal Additive Surfaces. *Metrology*, 3(2):186–221, 2023.

[62] Bo Whip, Luke Sheridan, and Joy Gockel. The Effect of Primary Processing Parameters on Surface Roughness in Laser Powder Bed Additive Manufacturing. *The International Journal of Advanced Manufacturing Technology*, 103:4411–4422, 2019.

[63] Yi Zheng, Xiao Zhang, Shaodong Wang, Qing Li, Hantang Qin, and Beiwen Li. Similarity Evaluation of Topography Measurement results by Different Optical Metrology Technologies for Additive Manufactured Parts. *Optics and Lasers in Engineering*, 126:105920, 2020.

[64] Lewis Newton, Nicola Senin, Carlos Gomez, Reinhard Danzl, Franz Helmli, Liam Blunt, and Richard K. Leach. Areal Topography Measurement of Metal Additive Surfaces Using Focus Variation Microscopy. *Additive Manufacturing*, 25:365–389, 2019.

[65] Lewis Newton, Nicola Senin, Evangelos Chatzivagiannis, Bethan Smith, and Richard K. Leach. Feature-Based Characterisation of Ti6Al4V Electron Beam Powder Bed Fusion Surfaces Fabricated at Different Surface Orientations. *Additive Manufacturing*, 35:101273, 2020.

[66] Carlos Gomez, Rong Su, Adam Thompson, Jack DiSciacca, Simon Lawes, and Richard K. Leach. Optimization of Surface Measurement for Metal Additive Manufacturing Using Coherence Scanning Interferometry. *Optical Engineering*, 56(11):111714–111714, 2017.

[67] Adam Thompson, Lars Körner, Nicola Senin, Simon Lawes, Ian Maskery, and Richard K. Leach. Measurement of Internal Surfaces of Additively Manufactured Parts by X-ray Computed Tomography. In *7th Conference on Industrial Computed Tomography*, Leuven, Belgium, 2017.

[68] Adam Thompson. *Surface Texture Measurement of Metal Additively Manufactured Parts by X-ray Computed Tomography*. PhD thesis, University of Nottingham, 2019.

[69] Sirichanok Chanbai, Mark A. Weber, and Georg Wiora. On the theory of resolution in Conventional and Confocal Microscopes Photogrammetrie, Laserscanning, Optische 3D-Messtechnik: Beiträge der Oldenburger 3D-Tage 2008, 2008.

[70] Richard K. Leach. *Optical Measurement of Surface Topography*. Springer Berlin Heidelberg, Berlin, Heidelberg, 2011.

[71] Federico Sciammarella. An Optical Approach to Accurately Determine Surface Finish for Additive Manufacturing. *Rapid Prototyping Journal*, 2018.

[72] Richard K. Leach, David Bourell, Simone Carmignato, Alkan Donmez, Nicola Senin, and Wim Dewulf. Geometrical Metrology for Metal Additive Manufacturing. *CIRP Annals*, 68(2):677–700, 2019.

[73] Xavier Schwab, Christian Kohler, Klaus Körner, N. Eichhorn, and Wolfgang Osten. Improved Micro Topography Measurement by LCoS-Based Fringe Projection and z-stitching - art. no. 69950Q. *Proc SPIE*, 6995, 2008.

[74] Cheng-Yang Liu, Tzu-Ping Yen, and Chien-Wen Chen. High-resolution Three-dimensional Surface Imaging Microscope Based on Digital Fringe Projection Technique. *Measurement Science Review*, 20(3):139–144, 01 Jun. 2020.

[75] Nicholas Southon, Petros Stavroulakis, Ruth Goodridge, and Richard K. Leach. In-Process Measurement and Monitoring of a Polymer Laser Sintering Powder Bed with Fringe Projection. *Materials & Design*, 157:227–234, 2018.

[76] Andrew Dickins, Taufiq Widjanarko, Danny Sims-Waterhouse, Adam Thompson, Simon Lawes, Nicola Senin, and Richard K. Leach. Multi-View Fringe Projection System for Surface Topography Measurement During Metal Powder Bed Fusion. *J. Opt. Soc. Am. A*, 37(9):B93–B105, 2020.

[77] Xiao Zhang, Yi Zheng, Vignesh Suresh, Shaodong Wang, Qing Li, Beiwen Li, and Hantang Qin. Correlation Approach for Quality Assurance of Additive Manufactured Parts Based on Optical Metrology. *Journal of Manufacturing Processes*, 53:310–317, 2020.

[78] Yue Liu, Liam Blunt, Zonghua Zhang, Hussein Abdul Rahman, Feng Gao, and Xiangqian Jiang. In-situ Areal Inspection of Powder Bed for Electron Beam Fusion System Based on Fringe Projection Profilometry. *Additive Manufacturing*, 31:100940, 2020.

[79] Miroslav Piska, Pavlina Trubacova, Jana Hornikova, and I. Deblir. Analysis of Powder Steel Material, Laser Sintering Technology and Machining on Surface Parameters and Fatigue: Analyse von Stahlpulver, Lasersinter-Verfahren und Bearbeitung auf Oberflächenbeschaffenheit und Ermüdung. *Materialwissenschaft und Werkstofftechnik*, 48(8):820–830, 2017.

[80] Adam Thompson, Lewis Newton, and Richard K. Leach. New Standard for Metal Powder Bed Fusion Surface Texture Measurement and Characterisation. *Metrology*, 3(2):237–245, 2023.

[81] Luke D. Todhunter, Richard K. Leach, Simon Lawes, and François Blateyron. Industrial Survey of ISO Surface Texture Parameters. *CIRP Journal of Manufacturing Science and Technology*, 19:84–92, 2017.

[82] Richard K. Leach. *Characterisation of Areal Surface Texture*. Springer Berlin Heidelberg, Berlin, Heidelberg, 2013.

[83] Emilie Beevers, Ana D. Brandão, Johannes Gumpinger, Michael Gschweitl, Christoph Seyfert, Peter Hofbauer, Thomas Rohr, and Tommaso Ghidini. Fatigue Properties and Material Characteristics of Additively Manufactured AlSi10Mg–Effect of the Contour Parameter on the Microstructure, Density, Residual Stress, Roughness and Mechanical Properties. *International Journal of Fatigue*, 117:148–162, 2018.

[84] Niloofar Sanaei and Ali Fatemi. Analysis of the Effect of Surface Roughness on Fatigue Performance of Powder Bed Fusion Additive Manufactured Metals. *Theoretical and Applied Fracture Mechanics*, 108:102638, 2020.

[85] Stefano Beretta, Mostafa Gargourimotlagh, Stefano Foletti, Antoine Du Plessis, and Martina Riccio. Fatigue Strength Assessment of "As-built" AlSi10Mg Manufactured by SLM with Different Build Orientations. *International Journal of Fatigue*, 139:105737, 2020.

[86] Arun Prasanth Nagalingam, Moiz Sabbir Vohra, Pulkit Kapur, and Swee Hock Yeo. Effect of Cut-off, Evaluation Length, and Measurement Area in Profile and Areal Surface Texture Characterization of As-built Metal Additive Manufactured Components. *Applied Sciences*, 11(11):5089, 2021.

[87] Olena Flys, Johan C. Berglund, and Bengt-Göran Rosen. Using Confocal Fusion for Measurement of Metal AM Surface Texture. *Surface Topography: Metrology and Properties*, 8(2):024003, 2020.

[88] Adam Thompson, Nicola Senin, Ian Maskery, Lars Körner, Simon Lawes, and Richard K. Leach. Internal Surface Measurement of Metal Powder Bed Fusion Parts. *Additive Manufacturing*, 20:126–133, 2018.

[89] Andrew Townsend, Radu Racasan, Richard K. Leach, Nicola Senin, Adam Thompson, Andrew Ramsey, David Bate, Peter Woolliams, Stephen Brown, and Liam Blunt. An Interlaboratory Comparison of X-ray Computed Tomography Measurement for Texture and Dimensional Characterisation of Additively Manufactured Parts. *Additive Manufacturing*, 23:422–432, 2018.

[90] Luca Pagani, Qunfen Qi, Xiangqian Jiang, and Paul J. Scott. Towards a New Definition of Areal Surface Texture Parameters on Freeform Surface. *Measurement*, 109:281–291, 2017.

[91] Andrew Triantaphyllou, Claudiu L. Giusca, Gavin D. Macaulay, Felix Roerig, Matthias Hoebel, Richard K. Leach, Ben Tomita, and Katherine A. Milne. Surface Texture Measurement for Additive Manufacturing. *Surface Topography: Metrology and Properties*, 3(2):024002, 2015.

[92] Gavin D. MacAulay, Nicola Senin, Claudiu L. Giusca, Richard K. Leach, and Atanas Ivanov. Review of Feature Boundary Identification Techniques for the Characterization of Tessellated Surfaces. *Surface Topography: Metrology and Properties*, 3(1):013002, 2015.

[93] Shaojun Xiao, F. Xie, Liam Blunt, Paul J. Scott, and Xiangqian Jiang. Feature Extraction for Structured Surface Based on Surface Networks and Edge Detection. *Materials science in semiconductor Processing*, 9(1-3):210–214, 2006.

[94] Jian Wang, Xiangqian Jiang, Elzbieta Gurdak, Paul Scott, Richard K. Leach, Paul Tomlins, and Liam Blunt. Numerical Characterisation of Biomedical Titanium Surface Texture Using Novel Feature Parameters. *Wear*, 271(7-8):1059–1065, 2011.

[95] Yuan Tian, Jian Wang, Zhongxiao Peng, and Xiangqian Jiang. A New Approach to Numerical Characterisation of Wear Particle Surfaces in Three-Dimensions for Wear Study. *Wear*, 282:59–68, 2012.

[96] Ruifang Ye, Xiangqian Jiang, Liam Blunt, Changcai Cui, and Qing Yu. The Application of 3D-Motif Analysis to Characterize Diamond Grinding Wheel Topography. *Measurement*, 77:73–79, 2016.

[97] Yibo Zou, Shui Cao, Jiaqiang Li, and Yusheng Ju. Multiscale Characterization and Analysis of Additive Manufacturing Surfaces Based on Confocal Laser Scanning Microscopy. *The International Journal of Advanced Manufacturing Technology*, 122(5-6):2475–2491, 2022.

[98] Lewis Newton, Nicola Senin, Bethan Smith, Evangelos Chatzivagiannis, and Richard K. Leach. Comparison and Validation of Surface Topography Segmentation Methods for Feature-Based Characterisation of Metal Powder Bed Fusion Surfaces. *Surface Topography: Metrology and Properties*, 7(4):045020, 2019.

[99] Lewis Newton, Nicola Senin, Bethan Smith, and Richard K. Leach. Feature-Based Characterisation of Evolving Surface Topographies in Finishing Operations for Additive Manufacturing. In *Joint Special Interest Group Meeting Between euspen and ASPE: Advancing Precision in Additive Manufacturing*. American Society for Precision Engineering (ASPE), 2018.

[100] Nicola Senin, Adam Thompson, and Richard K. Leach. Feature-Based Characterisation of Signature Topography in Laser Powder Bed Fusion of Metals. *Measurement Science and Technology*, 29(4):045009, 2018.

[101] Grzegorz Struzikiewicz and Andrzej Sioma. Surface Topographic Features after Milling of Additively Manufactured AlSi10Mg Aluminum Alloy. *Materials*, 15(10):3604, 2022.

[102] Adam Thompson, Sam Tammas-Williams, Nicola Senin, Iain Todd, and Richard K. Leach. Correlating volume and Surface Features in Additively Manufactured Metal Parts. In *Joint Special Interest Group Meeting Between EUSPEN and ASPE: Advancing Precision in Additive Manufacturing*. American Society for Precision Engineering (ASPE), 2018.

[103] Shan Lou, Luca Pagani, Wenhan Zeng, Xiangqian Jiang, and Paul J. Scott. Watershed Segmentation of Topographical Features on freeform Surfaces and its Application to Additively Manufactured Surfaces. *precision engineering*, 63:177–186, 2020.

[104] Nicola Senin and Richard K. Leach. Information-rich Surface Metrology. *Procedia CIRP*, 75:19–26, 2018.

[105] Konda Gokuldoss Prashanth, Sergio Scudino, Hansjörg J. Klauss, Kumar Babu Surreddi, Lukas Löber, Zhi Wang, Anil Kumar Chaubey, Uta Kühn, and Jürgen Eckert. Microstructure and Mechanical Properties of Al-12Si Produced by Selective Laser Melting: Effect of Heat Treatment. *Materials Science and Engineering: A*, 590:153–160, 2014.

[106] Takahiro Kimura and Takayuki Nakamoto. Microstructures and Mechanical Properties of A356 (AlSi7Mg0. 3) Aluminum Alloy Fabricated by Selective Laser Melting. *Materials & Design*, 89:1294–1301, 2016.

[107] Biao Chen, Seung Ki Moon, Xiling Yao, Guijun Bi, Jianghua Shen, Junko Umeda, and Katsuyoshi Kondoh. Strength and Strain Hardening of a Selective Laser Melted AlSi10Mg Alloy. *Scripta Materialia*, 141:45–49, 2017.

[108] Naoki Takata, Mulin Liu, Hirohisa Kodaira, Asuka Suzuki, and Makoto Kobashi. Anomalous Strengthening by Supersaturated Solid Solutions of Selectively Laser Melted Al–Si-Based Alloys. *Additive Manufacturing*, 33:101152, 2020.

[109] Adib Salandari-Rabori, Pusong Wang, Qingshan Dong, and Vahid Fallah. Enhancing As-built Microstructural Integrity and Tensile Properties in Laser Powder Bed Fusion of AlSi10Mg Alloy Using a comprehensive Parameter optimization Procedure. *Materials Science and Engineering: A*, 805:140620, 2021.

[110] Mulin Liu, Naoki Takata, Asuka Suzuki, Makoto Kobashi, and Masaki Kato. Enhancement in Strength and Ductility of Laser Powder Bed fused Al–12Si Alloy by Introducing Nanoscale Precipitates. *Additive Manufacturing Letters*, 1:100008, 2021.

[111] William D. Callister and David G. Rethwisch. *Materials Science and Engineering*. Wiley, 2011.

[112] Daniel Greitemeier, Claudio Dalle Donne, Freerk Syassen, Jens Eufinger, and Tobias Melz. Effect of Surface Roughness on Fatigue Performance of Additive Manufactured Ti-6Al-4V. *Materials Science and Technology*, 32(7):629–634, 2016.

[113] Maximilian Raab and Markus Bambach. Fatigue Properties of Scalmalloy Processed by Laser Powder Bed Fusion in As-built, Chemically and Conventionally Machined Surface Condition. *Journal of Materials Processing Technology*, 311:117811, 2023.

[114] Theresa Buchenau, Nicola Cersullo, Jon Mardaras, Philippe Emile, Victor Lafue, Hauke Brüning, Marc Amkreutz, and Christian Hühne. Fatigue and Surface Texture of Post-Processed Metal Additive Ti-6Al-4V. In *17th European Conference on Spacecraft Structures, Materials and Environmental Testing*, Toulouse, France, 2023. CNES.

[115] Elena Bassoli, Lucia Denti, Andrea Comin, Antonella Sola, and Emanuele Tognoli. Fatigue Behavior of As-built L-PBF A357.0 Parts. *Metals*, 8(8), 2018.

[116] Stefan Einbock. *Statistics of Metal Fatigue in Engineering: Planning and Analysis of Metal Fatigue Tests*. BoD–Books on Demand, 2018.

[117] Sebastien Dezecot and Myriam Brochu. Microstructural Characterization and High Cycle Fatigue Behavior of Investment cast A357 Aluminum Alloy. *International Journal of Fatigue*, 77:154–159, 2015.

[118] ASTM F3624-23: Standard Guide for Additive Manufacturing of Metals—Powder Bed Fusion—Measurement and Characterization of Surface Texture, 2023.

[119] Roland Lachmayer, Philipp Gottwald, and Rene B. Lippert. Approach for a Comparatively Evaluation of the Sustainability for Additive Manufactured Aluminum Components. In *DS 80-4 Proceedings of the 20th International Conference on Engineering Design (ICED 15) Vol 4: Design for X, Design to X, Milan, Italy, 27-30.07. 15*, pages 215–224, 2015.

[120] Dirk Herzog, Vanessa Seyda, Eric Wycisk, and Claus Emmelmann. Additive Manufacturing of Metals. *Acta Materialia*, 117:371–392, 2016.

[121] D. Askeland. *Materialwissenschaften*. Spektrum, Heidelberg, 1996.

[122] I. Inagaki, Y Shirai, T. Takechi, and N. Ariyasu. Application and Features of Titanium for the Aerospace Industry: Technical Report.

[123] Rodney R. Boyer. An Overview on the Use of Titanium in the Aerospace Industry. *Materials Science and Engineering: A*, 213(1):103–114, 1996.

[124] Ares Gomez, Paranjayee Mandal, Diego Gonzalez, Nicola Zuelli, and Paul Blackwell. Studies on Titanium Alloys for Aerospace Application. In *Defect and Diffusion Forum*, volume 385, pages 419–423. Trans Tech Publ, 2018.

[125] Adnan Safdar, H. Z. He, Liu-Ying Wei, A. Snis, and Luis E. Chavez de Paz. Effect of Process Parameters Settings and Thickness on Surface Roughness of EBM Produced Ti-6Al-4V. *Rapid Prototyping Journal*, 2012.

[126] Marc-Antoine de Pastre, Adam Thompson, Yann Quinsat, José A. Albajez García, Nicola Senin, and Richard K. Leach. Polymer Powder Bed Fusion Surface Texture Measurement. *Measurement Science and Technology*, 31(5):055002, jan 2020.

[127] Sarah Bagehorn, Tobias Mertens, Oliver Seack, and Hans-Jürgen Maier, editors. *Reduction of the Surface Roughness of Additively Manufactured Metallic Parts by Enhanced Electrolytic Smoothening*, 2016.

[128] Yifei Zhang, Li Jianzhong, and Che Shuanghang. Electropolishing Mechanism of Ti-6Al-4V Alloy Fabricated by Selective Laser Melting. *International Journal of Electrochemical Science*, 13(5):4792–4807, 2018.

[129] Sarah Bagehorn, Jürgen Wehr, Sonja Nixon, A. Balastrier, Tobias Mertens, and Hans-Jürgen Maier, editors. *Electrochemical Enhancement of the Surface Morphology and the Fatigue Performance of Ti-6Al-4V Parts Manufactured by Laser Beam Melting*, 2017.

[130] ASTM B600-11(2017), Standard Guide for Descaling and Cleaning Titanium and Titanium Alloy Surfaces, 2017.

[131] Donald M. Brunette, Pentti Tengvall, Marcus Textor, and Peter Thomsen. *Titanium in Medicine: Material Science, Surface Science, Engineering, Biological Responses and Medical Applications*. Springer, 2001.

[132] Gianni Nicoletto. Directional and Notch Effects on the Fatigue Behavior of As-built DMLS Ti6Al4V. *International Journal of Fatigue*, 106:124–131, 2018.

[133] ISO 25178: Geometric Product Specifications (GPS) - Surface Texture: Areal - Part 6: Classification of Methods for Measuring Surface Texture, 2010.

[134] Tobias Grimm, Georg Wiora, and Gerd Witt. Quality Control of Laser-Beam-Melted Parts by a Correlation Between Their Mechanical Properties and a Three-Dimensional Surface Analysis. *JOM*, 69(3):544–550, 2017.

[135] *Surface Finishing of Additive Manufactured Ti-6Al-4V – a Comparison of Electrochemical and Mechanical Treatments*, 2015.

[136] Geometrical Product Specifications (GPS) — Surface Texture: Profile — Part 2: Terms, Definitions and Surface Texture Parameters, 2021.

[137] Theresa Buchenau, Marc Amkreutz, and Hauke Bruening. Surface Texture and High Cycle Fatigue of As-built Metal Additive AlSi7Mg0.6. *Journal of Additive Manufacturing Technologies*, 1(2):531, 2021.

[138] Theresa Buchenau, Marc Amkreutz, Hauke Bruening, and Bernd Mayer. Influence of Contour Scan Variation on Surface, Bulk and Mechanical Properties of LPBF-Processed AlSi7Mg0.6. *Materials*, 16(8):3169, 2023.

[139] ISO 21920-3:2021: Geometrical Product Specifications (GPS) — Surface Texture: Profile — Part 3: Specification Operators, 2021.

[140] ISO 3274: Geometric Product Specifications (GPS) - Surface Texture: Profile Method - Nominal Characteristics of Contact (Stylus) Instruments, 1996.

[141] Richard K. Leach. Good Practice Guide No. 37 - The Measurement of Surface Texture Using Stylus Instruments.

[142] Han Haitjema and Richard K. Leach. Surface Texture Metrological Characteristics. In *CIRP Encyclopedia of Production Engineering*, pages 1–5. Springer Berlin Heidelberg, Berlin, Heidelberg, 2018.

[143] Giovanni Strano, Liang Hao, Richard M. Everson, and Kenneth E. Evans. Surface Roughness Analysis, Modelling and Prediction in Selective Laser Melting. *Journal of Materials Processing Technology*, 213(4):589–597, 2013.

[144] Kamran Mumtaz and Neil Hopkinson. Top Surface and Side Roughness of Inconel 625 Parts Processed Using Selective Laser Melting. *Rapid Prototyping Journal*, 2009.

[145] Flaviana Calignano, Diego Manfredi, Elisa Paola Ambrosio, Luca Iuliano, and Paolo Fino. Influence of Process Parameters on Surface Roughness of Aluminum Parts Produced by DMLS. *The International Journal of Advanced Manufacturing Technology*, 67(9-12):2743–2751, 2013.

[146] Evren Yasa and Jean-Pierre Kruth. Application of Laser Re-melting on Selective Laser Melting Parts. *Advances in Production engineering and Management*, 6(4):259–270, 2011.

[147] Amogh Vedantha Krishna. *Towards Topography Characterization of Additive Manufacturing Surfaces*. Licentiate Engineering Thesis, Chalmers University of Technology, Gothenburg, Sweden, 2020.

[148] Hirotoshi Sasaki, Fuimo Takeo, and Hitoshi Soyama. Cavitation Erosion Resistance of the Titanium Alloy Ti–6Al–4V Manufactured through Additive Manufacturing with Various Peening Methods. *Wear*, page 203518, 2020.

[149] Bharat Bhushan. Surface Roughness Analysis and Measurement Techniques. In *Modern Tribology Handbook, two volume set*, pages 79–150. CRC press, 2000.

[150] ISO 4288: Geometric Product Specifications (GPS) - Surface Texture: Profile Method - Rules and Procedures for the Assessment of Surface Texture, 1996.

[151] ISO 4287: Geometric Product Specifications (GPS) - Surface Texture: Profile Method - Terms, Definitions and Surface Texture Parameters, 1997.

[152] Theresa Buchenau, Hauke Bruening, and Marc Amkreutz. Post-Processing of Surface Topography Data for As-built Metal Additive Surface Texture Characterization. *Journal of Additive Manufacturing Technologies*, 2:697, 2022.

[153] Xiangqian Jiang, Paul J. Scott, David J. Whitehouse, and Liam Blunt. Paradigm Shifts in Surface Metrology. Part II. The Current Shift. *Proceedings of the Royal Society A: Mathematical, Physical and Engineering Sciences*, 463(2085):2071–2099, 2007.

[154] Miroslav Piska and Jitka Metelkova. On The Comparison of Contact and Non-Contact Evaluations of a Machined Surface. *MM Sci. J*, 2:476–480, 2014.

[155] ISO 25178: Geometric Product Specifications (GPS) - Surface Texture: Areal - Part 3: Specification Operators, 2012.

[156] Marc Amkreutz, Claus Aumund-Kopp, Hauke Bruening, Theresa Buchenau, Michael Norda, Frank Sukowski, and Daniel Suth. APOLLO - Additive Teilefertigung, -prüfung und Oberflächenbehandlung für Aluminiumkomponenten; Teilvorhaben PROMOTIVE - Prozessoptimierung, Materialcharakterisierung und Oberflächenschutz Additiv gefertigter Aluminiumbauteile : Schlussbericht : Laufzeit des Vorhabens: 01.01.2018 bis 30.06.2021 : Berichtszeitraum: 01.01.2018 bis 30.06.2021, 2021.

[157] Shan Lou, Xiangqian Jiang, and Paul J. Scott. Correlating Motif Analysis and Morphological Filters for Surface Texture Analysis. *Measurement*, 46(2):993–1001, 2013.

[158] Adam Thompson, Nicola Senin, Claudiu L. Giusca, and Richard K. Leach. Topography of Selectively Laser Melted Surfaces: A Comparison of Different Measurement Methods. *CIRP Annals*, 66(1):543–546, 2017.

[159] Theresa Buchenau, Marc Amkreutz, Hauke Brüning, and Michael Norda. Evaluation of Alternative Parameters to Describe the Quality of Additively Manufactured Aluminium Alloy Surfaces. In *Additive Manufacturing Conference Turkey*, Istanbul, Turkey, 2019.

[160] J. Felix Aguilar, Mario Lera, and Colin J. R. Sheppard. Imaging of Spheres and Surface Profiling by Confocal Microscopy. *Applied Optics*, 39(25):4621–4628, 2000.

[161] Wieland Weise, Pavel Zinin, Tony Wilson, Andrew Briggs, and Siegfried Boseck. Imaging of Spheres with the Confocal Scanning Optical Microscope. *Optics letters*, 21(22):1800–1802, 1996.

[162] Diego Manfredi and Róbert Bidulsky. Laser Powder Bed Fusion of Aluminum Alloys. *Acta Metallurgica Slovaca*, 23(3):276–282, 2017.

[163] Nicola Cersullo, Jon Mardaras, Philippe Emile, Katja Nickel, Vitus Holzinger, and Christian Hühne. Effect of Internal Defects on the Fatigue Behavior of Additive Manufactured Metal Components: A Comparison between Ti6Al4V and Inconel 718. *Materials*, 15(19):6882, 2022.

[164] Pietro Magarò, Gianluca Alaimo, Massimo Carraturo, Emanuele Sgambitterra, and Carmine Maletta. A Novel Methodology for the Prediction of the Stress-strain Response of Laser Powder Bed Fusion Lattice Structure Based on a Multi-scale Approach. *Materials Science and Engineering: A*, 863:144526, 2023.

[165] João Teixeira Oliveira de Menezes, Enrique Mariano Castrodeza, and Riccardo Casati. Effect of Build Orientation on Fracture and Tensile Behavior of A357 Al Alloy Processed by Selective Laser Melting. *Materials Science and Engineering: A*, 766:138392, 2019.

[166] Lucia Denti. Additive Manufactured A357.0 Samples Using the Laser Powder Bed Fusion Technique: Shear and Tensile Performance. *Metals*, 8(9):670, 2018.

[167] Todd M. Mower and Michael J. Long. Mechanical Behavior of Additive Manufactured, Powder-Bed Laser-fused Materials. *Materials Science and Engineering: A*, 651:198–213, 2016.

[168] Milad Hamidi Nasab, Simone Romano, Dario Gastaldi, Stefano Beretta, and Maurizio Vedani. Combined Effect of Surface Anomalies and Volumetric Defects on Fatigue Assessment of AlSi7Mg Fabricated via Laser Powder Bed Fusion. *Additive Manufacturing*, 34:100918, 2020.

[169] ASTM E466-15: Standard Practice for Conducting Force Controlled Constant Amplitude Axial Fatigue Tests of Metallic Materials, 2015.

[170] ISO 3369: Impermeable Sintered Metal Materials and Hardmetals - Determination of Density, 2006.

[171] ASTM E8M: Standard Test Methods for Tension Testing of Metallic Materials, 2016.

[172] Andrew Townsend, Radu Racasan, and Liam Blunt. Surface-Specific Additive Manufacturing Test Artefacts. *Surface Topography: Metrology and Properties*, 6(2):024007, 2018.

[173] Jason C. Fox, Shawn P. Moylan, and Brandon M. Lane. Effect of Process Parameters on the Surface Roughness of Overhanging Structures in Laser Powder Bed Fusion Additive Manufacturing. *Procedia CIRP*, 45:131–134, 2016.

[174] Reinhard Danzl, Franz Helmli, and Stefan Scherer. Focus Variation - A Robust Technology for High Resolution Optical 3D Surface Metrology. *Strojniski Vestnik*, 2011:245–256, 03 2011.

[175] Theresa Buchenau, Hauke Brüning, and Marc Amkreutz. Feature Parameters for Metal Additive Surface Texture Characterization. In *40. Vortrags- und Diskussionstagung Werkstoffprüfung*, Dresden, Germany, 2022. DGM.